Errata

Date:	April 17, 2019
Issuing Office:	Federal Highway Administration—Office of Research, Development, and Technology
Address:	Turner-Fairbank Highway Research Center, 6300 Georgetown Pike, McLean, VA 22101
Name of Document:	Analysis Procedures for Evaluating Superheavy Load Movement on Flexible Pavements, Volume I: Final Report
FHWA Publication No.:	FHWA-HRT-18-049

The following changes were made to the document after publication on the Federal Highway Administration website:

Location	Incorrect Values	Corrected Values
TECHNICAL REPORT DOCUMENTATION PAGE, Box 15	Nadarajah Sivaneswaran (HRDI-20; ORCID: 0000-0002-3525-9165), Office of Infrastructure Research and Development, Turner-Fairbank Highway Research Center, served as the Contracting Officer's Representative.	Nadarajah Sivaneswaran (HRDI-20; ORCID: 0000-0003-0287-664X), Office of Infrastructure Research and Development, Turner-Fairbank Highway Research Center, served as the Contracting Officer's Representative.

Analysis Procedures for Evaluating Superheavy Load Movement on Flexible Pavements, Volume I: Final Report

U.S. Department of Transportation
Federal Highway Administration

FOREWORD

The movement of superheavy loads (SHLs) on the Nation's highways is an increasingly common, vital economic necessity for many important industries, such as chemical, oil, electrical, and defense. Many superheavy components are extremely large and heavy (gross vehicle weights in excess of a few million pounds), and they often require specialized trailers and hauling units. At times, SHL vehicles have been assembled to suit the load being transported, and therefore, the axle configurations have not been standard or consistent. Accommodating SHL movements without undue damage to highway infrastructure requires the determination of whether the pavement is structurally adequate to sustain the SHL movement and protect any underground utilities. Such determination involves analyzing the likelihood of instantaneous or rapid load-induced shear failure of the pavement structure.

The goal of this project was to develop a comprehensive analysis process for evaluating SHL movement on flexible pavements. As part of this project, a comprehensive mechanistic-based analysis approach consisting of several analysis procedures was developed for flexible pavement structures and documented in a 10-volume series of Federal Highway Administration reports—a final report and 9 appendices.[1–9] This is *Analysis Procedures for Evaluating Superheavy Load Movement on Flexible Pavements, Volume I: Final Report*, which presents a summary of the analysis procedures developed to address the critical factors associated with SHL movement on flexible pavements. This report is intended for use by highway agency pavement engineers responsible for assessing the structural adequacy of pavements in the proposed route and identifying mitigation strategies, where warranted, in support of the agency's response to SHL-movement permit requests.

Cheryl Allen Richter, Ph.D., P.E.
Director, Office of Infrastructure
Research and Development

TECHNICAL REPORT DOCUMENTATION PAGE

1. Report No. FHWA-HRT-18-049	2. Government Accession No.	3. Recipient's Catalog No.
4. Title and Subtitle Analysis Procedures for Evaluating Superheavy Load Movement on Flexible Pavements, Volume I: Final Report		5. Report Date October 2018
		6. Performing Organization Code
7. Author(s) Elie Y. Hajj (ORCID: 0000-0001-8568-6360), Raj V. Siddharthan (ORCID: 0000-0002-3847-7934), Hadi Nabizadeh (ORCID: 0000-0001-8215-1299), Sherif Elfass (ORCID: 0000-0003-3401-6513), Mohamed Nimeri (ORCID: 0000-0002-3328-4367), Seyed Farzan Kazemi (ORCID: 0000-0003-2313-4995), Dario Batioja-Alvarez (0000-0002-1094-553X), and Murugaiyah Piratheepan (ORCID: 0000-0002-3302-4856)		8. Performing Organization Report No. WRSC-UNR-201710-01
9. Performing Organization Name and Address Department of Civil and Environmental Engineering University of Nevada 1664 North Virginia Street Reno, NV 89557		10. Work Unit No.
		11. Contract or Grant No. DTFH61-13-C-00014
12. Sponsoring Agency Name and Address Office of Research, Development, and Technology Federal Highway Administration 6300 Georgetown Pike McLean, VA 22101		13. Type of Report and Period Covered Final Report; August 2013–July 2018
		14. Sponsoring Agency Code HRDI-20

16. Abstract
The movement of superheavy loads (SHLs) has become more common over the years, since it is a vital necessity for many important industries, such as chemical, oil, electrical, and defense. SHL hauling units are much larger in size and weight compared to the standard trucks. SHL gross vehicle weights may be in excess of a few million pounds, so they often require specialized trailers and components with nonstandard spacing between tires and axles. Accommodating SHL movements requires the determination of whether the pavement is structurally adequate and involves the analysis of the likelihood of instantaneous or rapid load-induced shear failure. In this study, a comprehensive mechanistic-based methodology consisting of the following procedures was developed: segmentation of an SHL vehicle for analysis, subgrade bearing failure analysis, sloped-shoulder failure analysis, buried utility risk analysis, localized shear failure analysis, deflection-based service limit analysis, and cost allocation analysis. In addition, a comprehensive experimental program that included five full-scale pavement/soil testing experiments performed at a large-scale box facility was designed and carried out for the verification and calibration of a number of theoretically based procedures incorporated in the analysis approach. Supplementary numerical modeling as well as measured data from Accelerated Pavement Testing facilities provided additional verification of the procedures adopted in this study. The analysis procedures developed were then implemented into a user-friendly software package, SuperPACK (Superheavy Load Pavement Analysis PACKage), to evaluate SHL movements on flexible pavements. This report presents a summary of the analysis procedures developed for evaluating SHL movement on flexible pavements. Further details of these procedures are presented in a series of stand-alone appendices (volumes II through X).[1–9]

17. Key Words Superheavy load, flexible pavement, nondestructive testing, ultimate failure, buried utility, service limit, cost allocation	18. Distribution Statement No restrictions. This document is available through the National Technical Information Service, Springfield, VA 22161. http://www.ntis.gov		
19. Security Classif. (of this report) Unclassified	20. Security Classif. (of this page) Unclassified	21. No. of Pages 117	22. Price N/A

Form DOT F 1700.7 (8-72)   Reproduction of completed page authorized.

SI* (MODERN METRIC) CONVERSION FACTORS

APPROXIMATE CONVERSIONS TO SI UNITS

Symbol	When You Know	Multiply By	To Find	Symbol
LENGTH				
in	inches	25.4	millimeters	mm
ft	feet	0.305	meters	m
yd	yards	0.914	meters	m
mi	miles	1.61	kilometers	km
AREA				
in^2	square inches	645.2	square millimeters	mm^2
ft^2	square feet	0.093	square meters	m^2
yd^2	square yard	0.836	square meters	m^2
ac	acres	0.405	hectares	ha
mi^2	square miles	2.59	square kilometers	km^2
VOLUME				
fl oz	fluid ounces	29.57	milliliters	mL
gal	gallons	3.785	liters	L
ft^3	cubic feet	0.028	cubic meters	m^3
yd^3	cubic yards	0.765	cubic meters	m^3
NOTE: volumes greater than 1000 L shall be shown in m^3				
MASS				
oz	ounces	28.35	grams	g
lb	pounds	0.454	kilograms	kg
T	short tons (2000 lb)	0.907	megagrams (or "metric ton")	Mg (or "t")
TEMPERATURE (exact degrees)				
^oF	Fahrenheit	5 (F-32)/9 or (F-32)/1.8	Celsius	^oC
ILLUMINATION				
fc	foot-candles	10.76	lux	lx
fl	foot-Lamberts	3.426	candela/m^2	cd/m^2
FORCE and PRESSURE or STRESS				
lbf	poundforce	4.45	newtons	N
lbf/in^2	poundforce per square inch	6.89	kilopascals	kPa

APPROXIMATE CONVERSIONS FROM SI UNITS

Symbol	When You Know	Multiply By	To Find	Symbol
LENGTH				
mm	millimeters	0.039	inches	in
m	meters	3.28	feet	ft
m	meters	1.09	yards	yd
km	kilometers	0.621	miles	mi
AREA				
mm^2	square millimeters	0.0016	square inches	in^2
m^2	square meters	10.764	square feet	ft^2
m^2	square meters	1.195	square yards	yd^2
ha	hectares	2.47	acres	ac
km^2	square kilometers	0.386	square miles	mi^2
VOLUME				
mL	milliliters	0.034	fluid ounces	fl oz
L	liters	0.264	gallons	gal
m^3	cubic meters	35.314	cubic feet	ft^3
m^3	cubic meters	1.307	cubic yards	yd^3
MASS				
g	grams	0.035	ounces	oz
kg	kilograms	2.202	pounds	lb
Mg (or "t")	megagrams (or "metric ton")	1.103	short tons (2000 lb)	T
TEMPERATURE (exact degrees)				
^oC	Celsius	1.8C+32	Fahrenheit	^oF
ILLUMINATION				
lx	lux	0.0929	foot-candles	fc
cd/m^2	candela/m^2	0.2919	foot-Lamberts	fl
FORCE and PRESSURE or STRESS				
N	newtons	0.225	poundforce	lbf
kPa	kilopascals	0.145	poundforce per square inch	lbf/in^2

ANALYSIS PROCEDURES FOR EVALUATING SUPERHEAVY LOAD MOVEMENT ON FLEXIBLE PAVEMENTS PROJECT REPORT SERIES

This volume is the first of 10 volumes in this research report series. Volume I is the final report, and Volume II through Volume X consist of Appendix A through Appendix I. Any reference to a volume in this series will be referenced in the text as "Volume II: Appendix A," "Volume III Appendix B," and so forth. The following list contains the volumes:

Volume	Title	Report Number
I	Analysis Procedures for Evaluating Superheavy Load Movement on Flexible Pavements, Volume I: Final Report	FHWA-HRT-18-049
II	Analysis Procedures for Evaluating Superheavy Load Movement on Flexible Pavements, Volume II: Appendix A, Experimental Program	FHWA-HRT-18-050
III	Analysis Procedures for Evaluating Superheavy Load Movement on Flexible Pavements, Volume III: Appendix B, Superheavy Load Configurations and Nucleus of Analysis Vehicle	FHWA-HRT-18-051
IV	Analysis Procedures for Evaluating Superheavy Load Movement on Flexible Pavements, Volume IV: Appendix C, Material Characterization for Superheavy Load Movement Analysis	FHWA-HRT-18-052
V	Analysis Procedures for Evaluating Superheavy Load Movement on Flexible Pavements, Volume V: Appendix D, Estimation of Subgrade Shear Strength Parameters Using Falling Weight Deflectometer	FHWA-HRT-18-053
VI	Analysis Procedures for Evaluating Superheavy Load Movement on Flexible Pavements, Volume VI: Appendix E, Ultimate and Service Limit Analyses	FHWA-HRT-18-054
VII	Analysis Procedures for Evaluating Superheavy Load Movement on Flexible Pavements, Volume VII: Appendix F, Failure Analysis of Sloped Pavement Shoulders	FHWA-HRT-18-055
VIII	Analysis Procedures for Evaluating Superheavy Load Movement on Flexible Pavements, Volume VIII: Appendix G, Risk Analysis of Buried Utilities Under Superheavy Load Vehicle Movements	FHWA-HRT-18-056
IX	Analysis Procedures for Evaluating Superheavy Load Movement on Flexible Pavements, Volume IX: Appendix H, Analysis of Cost Allocation Associated with Pavement Damage Under a Superheavy Load Vehicle Movement	FHWA-HRT-18-057
X	Analysis Procedures for Evaluating Superheavy Load Movement on Flexible Pavements, Volume X: Appendix I, Analysis Package for Superheavy Load Vehicle Movement on Flexible Pavement (SuperPACK)	FHWA-HRT-18-058

TABLE OF CONTENTS

LIST OF FIGURES

LIST OF TABLES

LIST OF ABBREVIATIONS AND SYMBOLS

Abbreviations

2D	two dimensional
3D	three dimensional
AASHTO	American Association of State Highway and Transportation Officials
AC	asphalt concrete
ALA	American Lifelines Alliance
APT	Accelerated Pavement Testing
CAB	crushed aggregate base
CEPA	Canadian Energy Pipeline Association
CTB	cement-treated base
FEM	finite element method
FOS	factor of safety
FWD	falling weight deflectometer
GUI	graphical user interface
GVW	gross vehicle weight
LaDOTD	Louisiana Department of Transportation and Development
LRFD	Load and Resistance Factor Design
LVDT	linear variable differential transformer
ME	mechanistic–empirical
MEPDG	*Mechanistic–Empirical Pavement Design Guide*
MLET	Multilayer Linear Elastic Theory
NAPTF	National Airport Pavement Test Facility
No.	number
NPV	net present value
PDAC	pavement damage–associated cost
RSL	remaining service life
SG	subgrade
SHA	State highway agency
SHL	superheavy load
SSR	shear stress ratio
SuperPACK	Superheavy Load Pavement Analysis PACKage
TEPC	total earth pressure cell
UCR	University of Costa Rica
VMT	vehicle miles traveled

Symbols

A	intercept of the viscositytemperature susceptibility relationship
$A_{affected}$	area of the uniform stress distribution induced by the nucleus on top of the SG
B	width of foundation (or diameter)
B_{wedge}	width of wedge
c	cohesion

D_0	center deflection at the center of the FWD plate
E	elastic modulus
E^*	dynamic modulus
E_i	initial tangent modulus
f'_c	compressive strength
Fcd	depth factor with respect to cohesion
Fci	load inclination factor with respect to cohesion
Fcs	shape factor with respect to cohesion
F_D	resultant force from the bottom soil (slip surface)
Fqd	depth factor with respect to overburden
Fqi	load inclination factor with respect to overburden
Fqs	shape factor with respect to overburden
FWD_{allow}	allowable falling weight deflectometer load level
FWD_{equiv}	equivalent falling weight deflectometer load level
$F\gamma d$	depth factor with respect to unit weight
$F\gamma i$	load inclination factor with respect to unit weight
$F\gamma s$	shape factor with respect to unit weight
i	layer number
K_{xx}	slippage stiffness in x-direction
K_{yy}	slippage stiffness in y-direction
l	length of foundation
M_R	resilient modulus
M_u	maximum induced moment
Nc	bearing capacity factor with respect to cohesion
Nq	bearing capacity factor with respect to overburden
$N\gamma$	bearing capacity factor with respect to unit weight
P	resultant horizontal force due to surcharge load
p	Drucker–Prager yield criterion mean normal stress
$p_{applied}$	induced mean normal stress
P_D	resistive force from the side soil that makes an angle the resultant force makes with the normal to the bottom slip surface with the normal to the side surfaces (i.e., front and back)
P_u	maximum axial thrust
Q	lateral earth pressure from adjacent soil
q	deviator stress in Drucker–Prager yield criterion
q'	effective stress at the bottom of the foundation level
$q_{applied}$	induced deviator stress
q_{ave}	average uniform vertical stress
$q_{failure}$	deviator stress at failure in Drucker–Prager yield criterion
q_u	ultimate bearing capacity
q_U	unconfined compressive strength
$SAF_{Flexible}$	stress adjustment factor for flexible utilities
SAF_{Rigid}	stress adjustment factor for rigid utilities
$SAF_{Shoulder}$	stress adjustment factor for sloping shoulder
$SAF_{Utility}$	stress adjustment factor for buried utilities

T'_D	developed resisting cohesion force resulting from mobilized cohesion acting on the side surfaces (i.e., front and back)
T_D	mobilized cohesion acting on the bottom slip surface
$u_1^-(H_i$	displacements in x-direction at the bottom of layer i
$u_2^-(H_i$	displacements in y-direction at the bottom of layer i
$\tilde{u}_1^+(0$	displacements in x-direction on top of layer $i + 1$
$\tilde{u}_2^+(0$	displacements in y-direction on top of layer $i + 1$
V_a	air void
V_{beff}	effective binder content
V_u	maximum induced shear
VTS	slope of the viscosity–temperature susceptibility relationship
W	weight of sliding wedge
γ	unit weight of SG soil
δ_{SHL}	superheavy load vehicle–induced surface deflection
ε_1	axial strain
θ	bulk stress
θ_{wedge}	angle between slip surface and horizontal surface
σ_{ij}	stress tensor
σ_c	confining stress
σ_d	deviator stress
σ_{df}	deviator stress at failure
σ_v	vertical stress
$\sigma_{zz\text{-}3D\text{-}Move}$	3D-Move ENHANCED computed load-induced vertical stresses
τ_{max}	shear strength
$\tau_{mobilized}$	applied (mobilized) shear stress
$\tau_{xz}^i(H_i$	longitudinal shear stress at the interface of layers i and $i + 1$
$\tau_{yz}^i(H_i$	lateral shear stress at the interface of layers i and $i + 1$
ϕ	angle of internal friction
ϕ_D	angle the resultant force makes with the normal to the bottom slip surface
$\phi_a P_n$	factored compressive axial resistance
$\phi_f M_n$	factored flexural resistance
$\phi_s V_n$	force factored shear resistance

CHAPTER 1. INTRODUCTION

The movement of superheavy loads (SHLs) on the Nation's highways is an increasingly common, vital economic necessity for many important industries, such as chemical, oil, electrical, and defense. Many SHL components are very large in size and weight and often require specialized trailers and hauling units. The movements of such loads have become more common over the years. The SHL vehicles are often oversized and exceed legal gross vehicle weight (GVW), axle, and tire load limits. Therefore, they require special permits to operate on U.S. highways.[10] Such vehicles usually operate under single-trip permits that require pavement structural analysis to determine that the pavement is structurally adequate to sustain the SHL movement.

1.1. PROBLEM STATEMENT

SHL hauling units are much larger in size and weight compared to standard trucks, and they travel at much lower speeds. They often require specialized trailers and components that are assembled to suit the SHL vehicle's characteristics. Although the tires used in the transport are often conventional (which enables the use of existing methodologies in addressing critical issues such as pavement–tire interaction stresses), the axle and tire configurations used are variable. This means that the spacing between tires and axles is not standard, and the tire imprints can span more than the entire width of a lane. Two examples of permitted SHL vehicles, LA-8T-14 and LA-12T-16, are illustrated in figure 1 and figure 2. The LA-8T-14 nomenclature refers to a Louisiana-permitted SHL vehicle having 8 tires per axle and an identifier of 14. The LA-12T-16 nomenclature refers to a Louisiana-permitted SHL vehicle having 12 tires per axle and an identifier of 16.

Axle Spacing = 4 ft - 7 inch

Length of Vehicle = 128 ft – 4.8 inch, Width of Vehicle = 17 ft – 5.8 inch, GVW = 3,660,552 lb
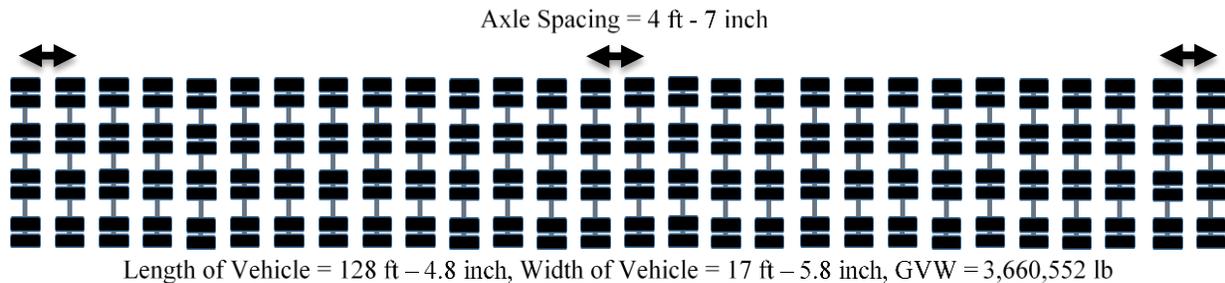
© 2018 UNR.

Figure 1. Illustration. Example configuration (LA-8T-14) of a Louisiana-permitted SHL vehicle (continuous axle configuration).

Spacing between Dollies = 37 ft - 11 inch

Axle Spacing = 4 ft - 7 inch   Axle Spacing = 4 ft - 7 inch   Axle Spacing = 4 ft - 7 inch   Axle Spacing = 4 ft - 7 inch

Length of Vehicle = 205 ft – 4.8 inch, Width of Vehicle = 17 ft – 5.8 inch, GVW = 1,754,220 lb
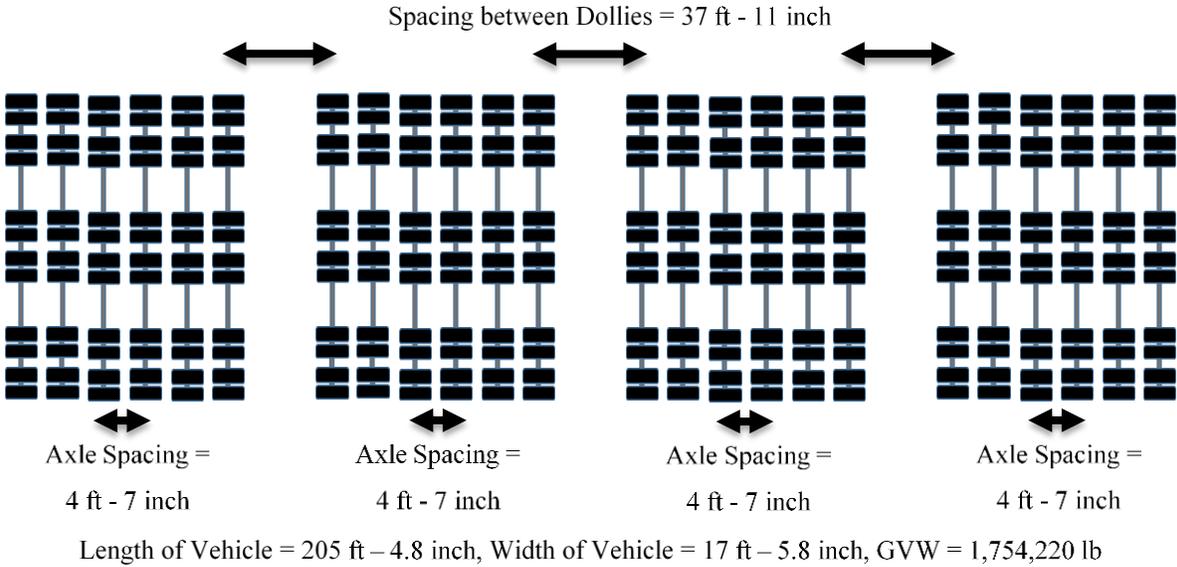
© 2018 UNR.

Figure 2. Illustration. Example configuration (LA-12T-16) of a Louisiana-permitted SHL vehicle (fragmented axle configuration).

Table 1 summarizes examples of axle and tire configurations of SHL vehicles observed from past permits collected from select State highway agencies (SHAs). The axle weights for the SHL vehicles varied from approximately 25,000 to 131,000 lb. An axle can have between 4 and 12 tires with an axle width between approximately 12 and 25 ft. The distance between adjacent axles ranged between 4 ft and 7 inches and 12 ft and 1 inch. Depending on the SHL-vehicle configuration, the tire load was as low as 3,538 lb and as high as 16,341 lb. Efforts to study SHL-vehicle axle and tire configurations revealed that SHL vehicles cannot be categorized into one or more common and generic configurations. Therefore, it is imperative that the nongeneric nature of the axle and tire configurations be considered in a realistic manner when studying pavement distresses under an SHL-vehicle movement.

Table 1. Examples for SHL vehicles' axle and tire configurations from past SHA permits.

SHL-Vehicle Information	Arizona	Louisiana	Nevada	New York
GVW (lb)	647,855–1,180,000	402,240–3,660,551	250,041–6,215,938	200,000–855,000
Axle weight (lb)	46,305–51,687	25,639–130,734	18,000–75,000	28,300–52,600
Number of tires per axle	8	4, 8, or 12	4 or 8	4 or 8
Axle width (out-to-out edges of the outside tires)	18 ft 4 inches to 20 ft 4 inches	17 ft 5 inches to 24 ft 7.3125 inches	–	12 ft 10 inches to 13 ft 6 inches
Center-to-center distance between adjacent axles	6 ft to 12 ft 1 inch	4 ft 7 inches to 11 ft 0.75 inches	–	4 ft 11 inches to 5 ft
Tire load (lb)	5,000–6,460	7,028–16,341	2,580–11,500	3,538–6,575
Tire width	8.25 to 11 inches	1 ft 0.5 inch to 1 ft 2 inches	–	1 ft 0.5 inch to 1 ft 2 inches

–No data.

As a representative example, the case of a five-line load model is shown in figure 3 (plan view) and figure 4 (elevation view). The surface-load configuration consists of a uniform longitudinal (i.e., vehicle direction) spacing between the axles; however, spacing in the transverse direction is not uniform through the entire width. The elevation plot (figure 4) shows the overlapping of vertical stresses (σ_v) at deeper locations within the pavement. These overlapping stresses, at any interior plane, can fall under one of the three cases shown in figure 5 through figure 7. Case 1 represents no overlapping (figure 5), case 2 shows moderate overlapping (figure 6), and case 3 shows substantial overlapping of σ_v (figure 7). The σ_v resulting from surface tire loads of the SHL vehicle is expected to overlap beyond a specific depth within the pavement structure. The extent of overlapping is highly affected by the surface-load magnitude and configuration as well as the pavement-layer properties and thicknesses.
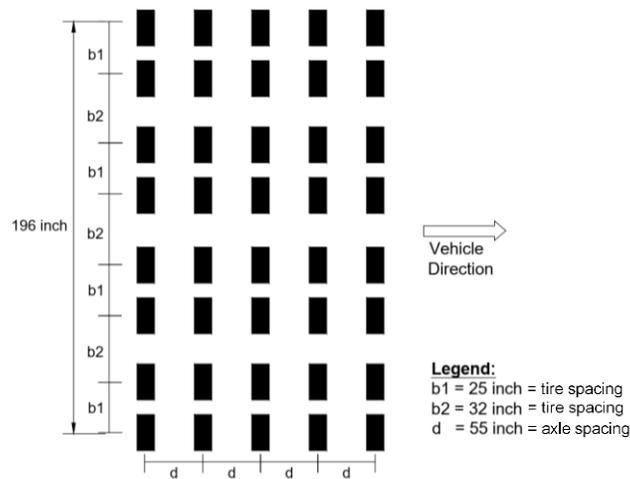
© 2018 UNR.

Figure 3. Illustration. Five-line model for SHL-vehicle simulation—plan view.
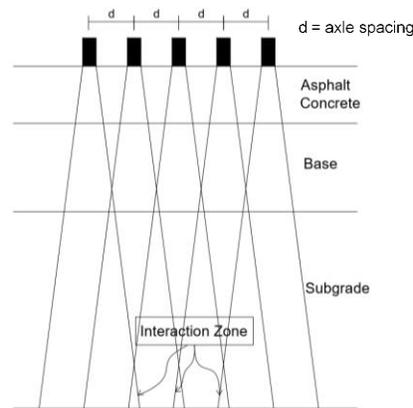
© 2018 UNR.

Figure 4. Illustration. Five-line model for SHL-vehicle simulation—elevation view.
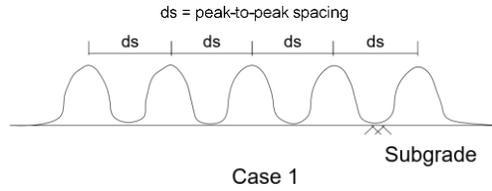
© 2018 UNR.

Figure 5. Illustration. σ_v distribution within pavement—case 1.
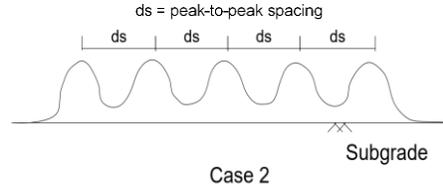
© 2018 UNR.

Figure 6. Illustration. σ_v distribution within pavement—case 2.
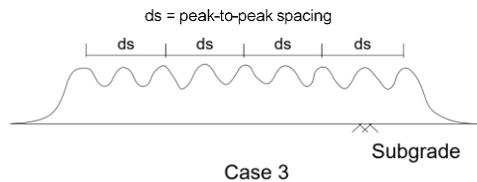
© 2018 UNR.

Figure 7. Illustration. σ_v distribution within pavement—case 3.

The σ_v distribution below the pavement surface under an SHL vehicle can become important because such high tire loads as well as overlapping stress distributions under the tire loads can render a critical condition of instantaneous ultimate (global) or localized shear failure, especially in the influenced zone of the subgrade (SG). It should be noted that the most vulnerable layer for shear failure is likely the SG layer because it is the weakest layer in the pavement structure. Furthermore, unexpected, excessive surface deflections leading to premature pavement distresses (e.g., permanent deformation) need to be considered in the cases of SHL movements. In addition to the likelihood of instantaneous shear failure, critical concerns exist with respect to the stability of sloped pavement shoulders as well as the integrity of existing buried utilities under an SHL-vehicle movement. Last but not least, determination of the pavement damage–associated cost (PDAC) attributable to an SHL movement also needs to be addressed.

To study the aforementioned concerns associated with SHL movements on flexible pavements in a mechanistic manner, the properties of existing pavement layers need to be realistically characterized. The slow-moving SHL vehicle plays a major role in the viscoelastic behavior of the asphalt concrete (AC) layer, whereas the stress-dependent resilient behavior of unbound layers is highly influenced by the nonconventional axle configuration and tire loading of an SHL vehicle. Such aspects should be regarded when determining pavement responses under SHL movements.

In summary, the evaluation of SHL movements on flexible pavements should address the following important factors:

- Nonconventional SHL-vehicle axle and tire loadings and configurations.

- Slow-moving nature of an SHL vehicle in relation to viscoelastic properties of the AC layer.

- Role of higher magnitude stress states induced by an SHL-vehicle movement on stress-dependent behavior of unbound materials.

- Likelihood of ultimate and localized shear failure in the influenced zone of the SG layer.

- Likelihood of excessive pavement surface deflections.

- Role of SHL-vehicle movement on the stability of a sloped pavement shoulder.

- Impact of SHL-vehicle movement on the integrity of existing buried utilities.

- PDACs attributable to SHL-vehicle movement.

1.2.   OBJECTIVES AND SCOPE OF WORK

As part of this Federal Highway Administration project, *Analysis Procedures for Evaluating Superheavy Load Movement on Flexible Pavements*, a comprehensive mechanistic-based analysis approach consisting of several analysis procedures was developed. This report (Volume I) is the first of 10 volumes and presents a summary of the analysis procedures developed to address the critical factors associated with SHL movement on flexible pavements.[1–9] The analysis procedures developed and associated objectives (including related volume numbers) are summarized in table 2.

Table 2. Developed analysis procedures to evaluate SHL movement on flexible pavements.

Procedure	Objective
SHL analysis vehicle	Identify segment(s) of the SHL-vehicle configuration that can be regarded as representative of the entire SHL vehicle (Volume III: Appendix B).[2]
Flexible pavement structure	Characterize representative material properties for existing pavement layers (Volume IV: Appendix C and Volume V: Appendix D).[3,4]
SG bearing failure Analysis	Investigate instantaneous ultimate shear failure in pavement SG (Volume VI: Appendix E).[3]
Sloped-shoulder failure analysis	Examine the stability of sloped pavement shoulder under an SHL-vehicle movement (Volume VII: Appendix F).[6]
Buried utility risk analysis	Perform risk analysis of existing buried utilities (Volume VIII: Appendix G).[7]
Localized shear failure analysis	Inspect the likelihood of localized failure (yield) in the pavement SG (Volume VI: Appendix E).[5]
Deflection-based service limit analysis	Investigate the development of premature surface distresses (Volume VI: Appendix E).[5]
Cost allocation analysis	Determine PDAC attributable to SHL-vehicle movement (Volume IX: Appendix H).[8]

As discussed subsequently in this report, complementary verification and calibration processes of a number of important theoretically based aspects incorporated in the proposed procedures were conducted in this study. To this end, a comprehensive experimental program was designed and carried out. The program included five full-scale pavement/soil testing experiments performed at a large-scale box facility (Volume II: Appendix A).[1] In addition, supplementary numerical modeling as well as measured data from Accelerated Pavement Testing (APT) facilities provided additional verification and validation to the procedures adopted in this study.

The 3D-Move ENHANCED computer program was employed in this study as the computational model to evaluate pavement responses under an SHL-vehicle movement (Volume X: Appendix I).[11,9] The 3D-Move ENHANCED program and its predecessor, 3D-Move, use a finite layer approach and account for viscoelastic material behavior.[12] The family of 3D-Move models is capable of analyzing SHL-vehicle axles moving at constant speed with nonuniform and/or noncircular tire loads. The ability to model SHL-vehicle speed is critical because SHL vehicles normally operate at notably low speeds, which can cause significant pavement damage. Furthermore, surface shear stresses in both longitudinal and transverse directions can be modeled independently with no limitations such as symmetry. This is very important when analysis of interface shear stresses from vehicle braking is to be investigated. 3D-Move ENHANCED, in particular, is capable of providing three-dimensional (3D) surface plots for a specific pavement response at a desired depth where the distribution of a critical pavement response needs to be generated.[11] Additionally, layer interface conditions such as debonding or slippage can be modeled using 3D-Move ENHANCED. These unique features make 3D-Move ENHANCED a robust pavement response analysis model.

As part of this project, a comprehensive user-friendly software package, Superheavy Load Pavement Analysis PACKage (SuperPACK) was developed (Volume X: Appendix I).[9] SuperPACK is the result of incorporating the 3D-Move ENHANCED analysis engine with the implementation of analysis procedures developed and is a comprehensive and user-friendly package to evaluate the impact of SHL movements on flexible pavements.[11]

1.3.   ORGANIZATION OF REPORT

This report presents a summary of the analysis procedures developed to address the critical factors associated with SHL movement on flexible pavements. In chapter 2, the developed methodology and associated analysis procedures are presented. Chapter 3 describes the efforts conducted to verify and calibrate several of the theoretical concepts and procedures developed in this study. Demonstration of the analysis procedures using two distinct permitted SHL vehicles is presented in chapter 4. The implementation of the analysis procedures in SuperPACK as well as its main components and unique features to analyze an SHL movement are described in chapter 5.[9] Chapter 6 summarizes the overall methodology and findings and provides suggested future developments and enhancements.

CHAPTER 2. METHODOLOGY

The goal of this report is to describe the procedures that were developed in this research study to evaluate SHL movements on flexible pavements. Figure 8 shows the flowchart of the overall approach developed as part of this project. In general, the approach consists of the following four major components:

- Ultimate failure analyses.
- Buried utility risk analysis.
- Service limit analyses.
- Cost allocation analysis.

It should be noted that mitigation strategies may be needed at any stage of the evaluation process when the calculated results fail to meet the respective requirements imposed (e.g., when the results indicate high potential of shear failure to pavement or damage to buried utilities).

As shown in figure 8, the first step of the approach involves a risk analysis of instantaneous or rapid load-induced ultimate shear failure. As the SG is generally the weakest layer in the pavement structure, the bearing failure analysis investigates the likelihood of general bearing capacity failure under the SHL vehicle within the influenced zone of the SG layer. Next, the sloped-shoulder failure analysis examines the bearing capacity failure and the edge slope stability associated with the sloping ground under the SHL-vehicle movement. Once the ultimate failure analyses are investigated and ruled out, when applicable, a buried utility risk analysis is conducted. In this analysis, the induced stresses and deflections by the SHL vehicle on existing buried utilities are evaluated and compared to established design criteria. Subsequently, if no mitigation strategies are needed, service limit analyses for localized shear failure and deflection-based service limit are conducted. The localized shear failure analysis investigates the possibility of failure at the critical location on top of the SG layer under the SHL vehicle. The deflection-based service limit analysis assesses the magnitude of the load-induced pavement deflections during the SHL movement. For instance, this analysis may suggest the need for mitigation strategies to meet the imposed acceptable surface deflection limits. After successfully completing all previously described analyses (i.e., ultimate failure analyses, buried utility risk analysis, and service limit analyses), a cost allocation analysis is then conducted.

In this chapter, the aforementioned analysis procedures and corresponding theoretical concepts are briefly described. As depicted in table 3, there are nine stand-alone appendices to this report—Volume II: Appendix A through Volume X: Appendix I—and they elaborate on the various aspects of the developed procedures.[1–9] As mentioned in section 1.2, these analysis procedures were implemented in SuperPACK.[9]
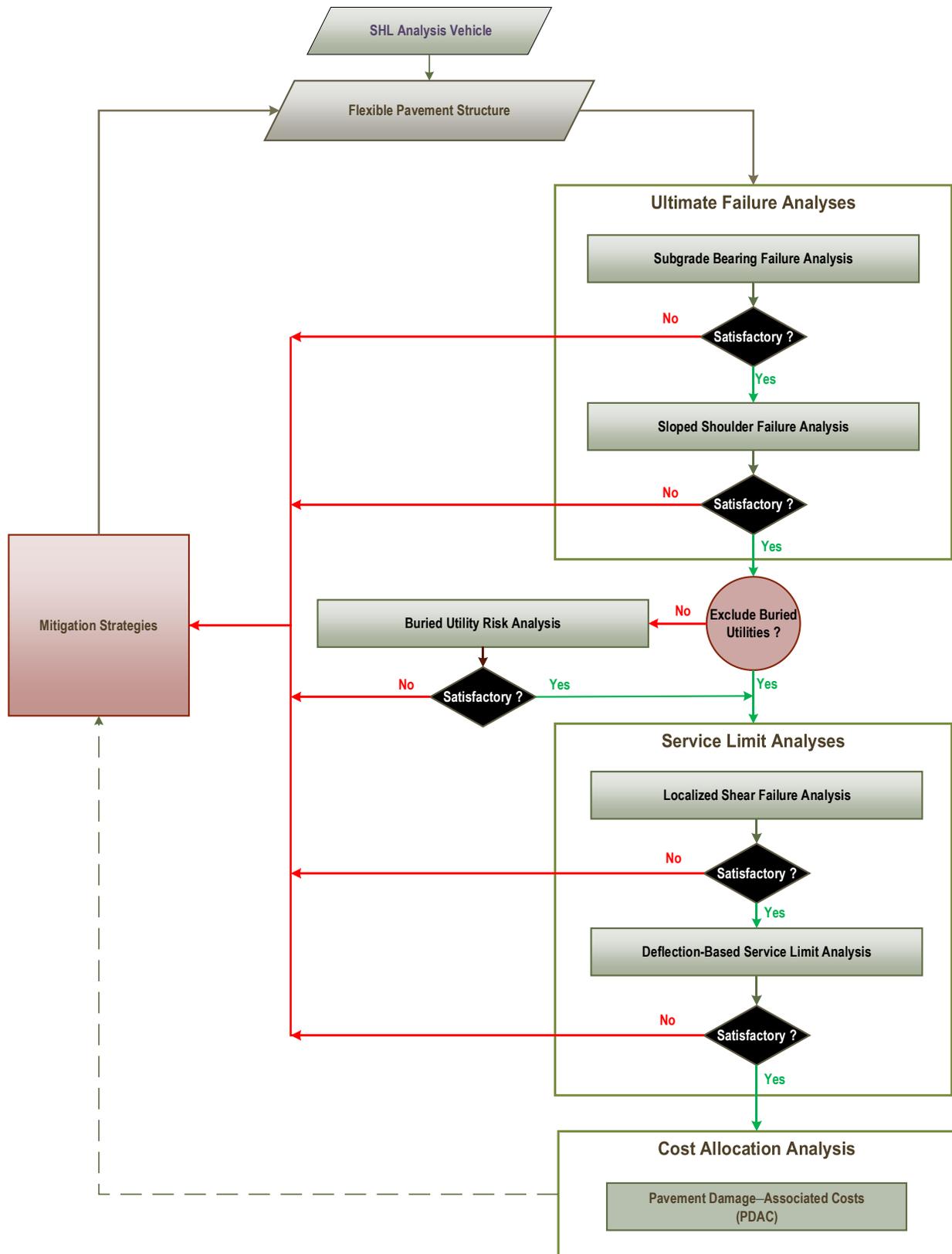
Figure 8. Flowchart. Overall SHL-vehicle analysis methodology.

Table 3. Developed analysis procedures to evaluate SHL movements on flexible pavements.

Title	Overall Description and Components
Appendix A: Experimental Program (Volume II)[1]	• Provides details of large-scale pavement/soil laboratory experiments conducted. 　o Characteristics of five full-scale pavement testing experiments under a variety of loading (dynamic and static).
Appendix B: Superheavy Load Configurations and Nucleus of Analysis Vehicle (Volume III)[2]	• Addresses nonconventional SHL-vehicle axle and tire loadings and configurations. 　o Axle groupings for SHL vehicle. 　o Identification of critical nucleus of analysis vehicle.
Appendix C: Material Characterization for Superheavy Load Movement Analysis (Volume IV)[3]	• Addresses slow-moving nature of SHL vehicle in relation to viscoelastic properties of AC layer. 　o Determination of damaged E^* master curve for AC layer. • Addresses role of higher magnitude stress states induced by SHL-vehicle movement on stress-dependent behavior of unbound materials. 　o Determination of the unbound material M_R as a function of the stress state.
Appendix D: Estimation of Subgrade Shear Strength Parameters Using Falling Weight Deflectometer (Volume V)[4]	• Estimates in situ τ_{max} parameters (ϕ and c of pavement SG layer) using falling weight deflectometer.
Appendix E: Ultimate and Service Limit Analyses (Volume VI)[5]	• Addresses likelihood of ultimate and localized shear failure in the influenced zone of the SG layer. 　o Ultimate shear failure analysis procedure. 　o Localized shear failure analysis procedure. • Addresses likelihood of excessive pavement surface deflections. 　o Deflection-based service limit analysis procedure.
Appendix F: Failure Analysis of Sloped Pavement Shoulders (Volume VII)[6]	• Addresses role of SHL-vehicle movement on the stability of a sloped pavement shoulder. 　o Slope stability analysis procedure. 　o Verification and calibration using the large-scale pavement laboratory experiments.
Appendix G: Risk Analysis of Buried Utilities Under SHL-Vehicle Movements (Volume VIII)[7]	• Addresses impact of SHL vehicle on the integrity of existing buried utilities. 　o Buried utility risk analysis procedure. 　o Verification and calibration using the large-scale pavement laboratory experiments.
Appendix H: Analysis of Cost Allocation Associated With Pavement Damage Under a Superheavy Load Vehicle Movement (Volume IX)[8]	• Addresses PDAC attributable to SHL-vehicle movement. 　o PDAC procedure.
Appendix I: Analysis Package for Superheavy Load Vehicle Movement on Flexible Pavement (SuperPACK) (Volume X)[9]	• Describes the SuperPACK ability and analysis modules. 　o Preanalysis modules. 　o Analysis modules. 　o 3D-Move ENHANCED analysis engine.[11]

E^* = dynamic modulus; M_R = resilient modulus; τ_{max} = shear strength; ϕ = angle of internal friction; c = cohesion.

2.1. SHL ANALYSIS VEHICLE

SHL vehicles consist of specialized trailers and components with nonconventional axle and tire configurations. They normally are much larger than conventional vehicles in size (spanning more than one lane) and weigh more and may involve GVWs in excess of a few million pounds. This study was initially intended to identify some common configurations for SHL vehicles' hauling units. However, examples of SHL-vehicle data collected from select SHAs revealed that SHL vehicles cannot be classified into one or more identical and generic types. Hence, evaluating the SHL-induced pavement distresses requires a realistic simulation of the SHL vehicle considering the nongeneric nature of the axle and tire configurations. To do so, the steps detailed in sections 2.1.1 and 2.1.2 have been followed. Detailed discussion on this matter can be found in Volume III: Appendix B.[2]

2.1.1. Axle Grouping of SHL Vehicle

The axle grouping defines the groups of axles with identical configuration and with spacing less than 60 inches between the adjacent axles within the group. For instance, the axle configuration for the SHL vehicle shown in figure 9 is divided into seven axle groups: the steering single axle, a tridem axle, and five tandem axles. It should be noted that the selected limit of 60 inches is consistent with the routinely used convention to consider tire groups present on only one side of the standard truck. In other words, when the pavement responses from a standard truck are evaluated, the influence of the tire groups in the transverse direction is not included. Furthermore, previous studies revealed that, when the spacing between two adjacent axles of a standard truck is more than 60 inches, generally there is limited interaction between these two axles.[13]
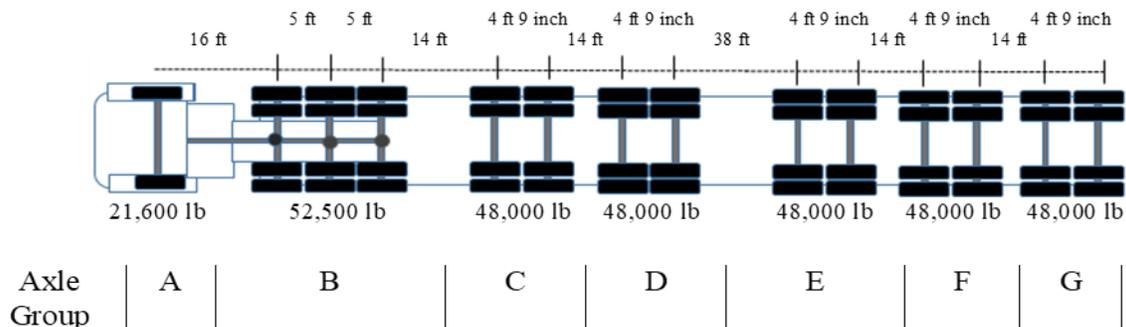
© 2018 UNR.

Figure 9. Illustration. Example configuration of a permitted SHL truck in Nevada.

2.1.2. Nucleus of SHL Analysis Vehicle

SHL vehicles can be of any size, shape, and configuration. Thus, numerical simulation of an entire SHL-vehicle load configuration can lead to substantially higher computational efforts. This is particularly true when viscoelastic behavior of an AC layer under the moving nature of the SHL vehicle is considered. In the case of 3D-Move, the Fourier expansion of the tire contact stress distribution in space is undertaken to simulate the SHL vehicle's axle load.[12] Thus, the

load distribution is harmonic, and therefore, quiet zones need to be defined to avoid the contributions from the adjacent loaded areas. When a large loaded area needs to be considered (e.g., SHL vehicle), the Fourier expansion requires substantially higher computational effort. Hence, the concept of the nucleus developed here leads to considerably less computational effort without jeopardizing the accuracy of the analysis.

Nucleus is defined as a segment (or element) of each axle group configuration that can be regarded as representative of the axle group. Using this element (i.e., nucleus), σ_v, distribution (or any other pavement responses) under the entire SHL configuration can be estimated by superimposing the stresses calculated under the nucleus, eliminating the need to model the entire SHL vehicle.

To identify a representative nucleus, an incremental tire load approach is used. First, a single tire load is applied at the surface of known pavement-layer thicknesses and properties. The σ_v response is then calculated at the point of interest (i.e., centerline of the tire load at the specific depth, which is generally the top of the SG). Additional tire loads in travel direction are applied one at a time, and the pavement σ_v values at the point of interest are monitored. The tire addition process continues until the last added tire load does not influence the response of interest at the point of interest. Similarly, the number of tires in the transverse direction of the nucleus configuration can also be identified. It should be noted that axle configurations, tire loads, vehicle speed, pavement structure, material properties, and AC-layer temperature play major roles in the identification of the nuclei of the SHL vehicle's axle groups. Comprehensive sensitivity analysis to study the impact of these factors is presented in Volume III: Appendix B.[2]

As an example, SHL-vehicle case number (No.) LA-8T-14's axle load configuration is shown in figure 10. The vehicle had 28 line axles and 8 tires per axle. In this case, the GVW was over 3.6 million lb with an average tire load of 16,342 lb. Since the entire SHL vehicle consisted of axles uniformly spaced less than 60 inches apart, there was only one axle group. As illustrated in figure 10, based on the σ_v distributions, two additional tires in each direction were influential, and therefore, to generate the maximum σ_v, the representative nucleus became a group of 5 by 5 tires.

The critical axle group defined by the highest induced σ_v under its nucleus is first determined. This critical axle group is subsequently employed to compute the state of stresses in the unbound layers, leading to the determination of representative material properties for these layers. The nucleus of each axle group is then used to investigate the likelihood of ultimate shear failure in the SG. However, service limit analyses, including localized shear failure analysis and deflection-based service limit analysis, are conducted for the critical axle group, which governs the likelihood of failure, as a conservative measure. In addition, slope stability analysis as well as buried utility risk analysis utilize the stresses induced by the nucleus of the critical axle group. However, in the cost allocation analysis, the nuclei of all axle groups present in the SHL vehicle need to be considered.

Length of Vehicle = 128 ft − 4.8 inch, Width of Vehicle = 17 ft − 5.8 inch, GVW = 3,660,552 lb

Axle Spacing = 4 ft - 7 inch
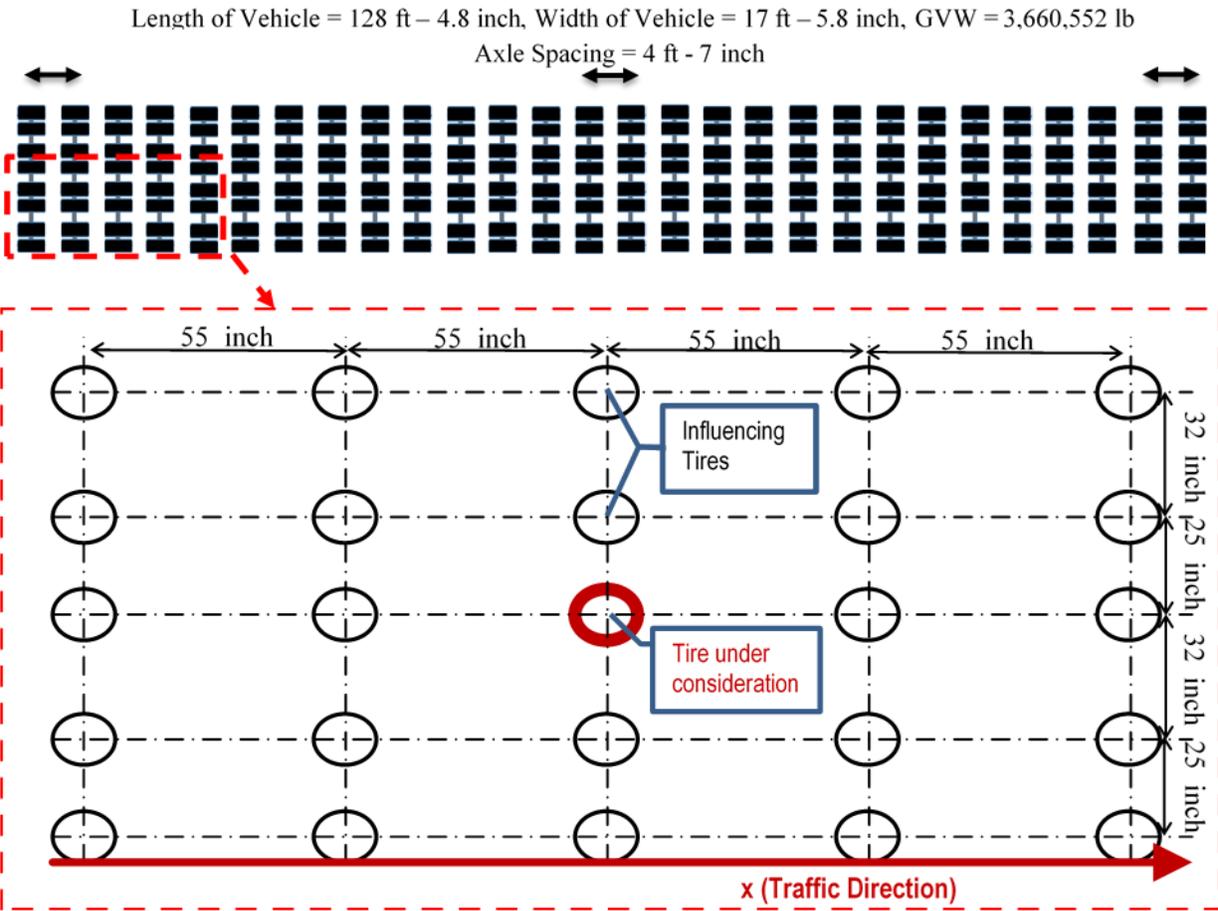
Figure 10. Illustration. Representative nucleus for case No. LA-8T-14.

2.2. FLEXIBLE PAVEMENT STRUCTURE

Critical inputs for the analysis of an SHL-vehicle movement using numerical models (i.e., mechanistic-based pavement analysis) are the thicknesses and the material properties of the existing pavement layers. The thickness of the pavement layers can be determined using either destructive approaches (e.g., taking cores or cutting trenches) or nondestructive testing (e.g., ground penetrating radar). A pavement management system or historical documentation of construction data can also provide this information.

To capture the different behaviors of existing materials in the pavement structures (i.e., viscoelastic, stress dependent), material properties at the time of the SHL movement should be properly characterized. When mechanistic analysis of standard truck loading is undertaken, for computational simplicity, the practice is to assume the pavement layer materials are linear elastic. However, such simplified assumptions may not be valid for the computation of pavement responses under slow-moving SHL vehicles with nonconventional axle configurations and tire loadings.

12

Therefore, viscoelastic behavior of the AC layer is characterized in this study by incorporating dynamic modulus (E^*), which is a function of material temperature and loading frequency. The stress-dependent behavior of unbound layers, such as the crushed aggregate base (CAB) and the SG, are accounted for by using a procedure that characterizes the unbound material resilient modulus (M_R) as a function of the state of stresses based on the results from nondestructive testing (i.e., falling weight deflectometer (FWD)).

In addition to the stiffness properties of pavement layers, shear strength (τ_{max}) characteristics of the SG layer under in situ conditions is a necessary input in the investigation of the likelihood of ultimate and localized shear failures. As part of this research study, an FWD-based procedure to estimate the τ_{max} properties (angle of internal friction (ϕ) and cohesion (c)) of the SG layer was developed. The following section provides a summary of procedures to characterize the stiffness and strength properties of pavement layers.

2.2.1. Stiffness Properties of Pavement Layers

In this section, different approaches to characterizing existing AC materials as well as unbound materials are summarized. A detailed discussion can be found in Volume IV: Appendix C.[3]

Characterization of Existing AC Layer

All existing AC layers need to be characterized (thickness and properties) in the analysis. In the case of multiple AC layers with different properties (e.g., successive AC overlays), layer-specific material characteristics can be individually assigned. However, when appropriate, a user can combine multiple AC layers and assign representative properties to those combined adjacent layers.

E^* is the most important asphalt-mixture material property that is used in mechanistic–empirical (ME) pavement analysis and design procedures such as the *Mechanistic–Empirical Pavement Design Guide* (MEPDG).[14] The E^* measurement considers the frequency and temperature dependency of an asphalt material. By conducting a series of E^* tests at various temperatures and frequencies, the E^* master curve can be developed.

To address the effect of lower SHL-vehicle speed (i.e., role of the SHL-vehicle speed) as well as AC temperature at the time of SHL-vehicle movement, the use of the E^* master curve for the AC layer, which is a readily accepted input for the 3D-Move approach, was considered.[12] In addition, reduction in the AC-layer stiffness due to existing damage (i.e., cracking) is addressed by using the field-damaged E^* master curve.

In this approach, the damaged E^* of the AC layer can be either determined from laboratory testing of core samples collected directly from the pavement where the SHL movement is anticpated to take place or from nondestructive techniques through the use of FWD measurements along with field survey and historical data. Figure 11 summarizes the measurements and properties needed for determining the damaged E^* of the AC layer from testing of core samples or from nondestructive techniques.
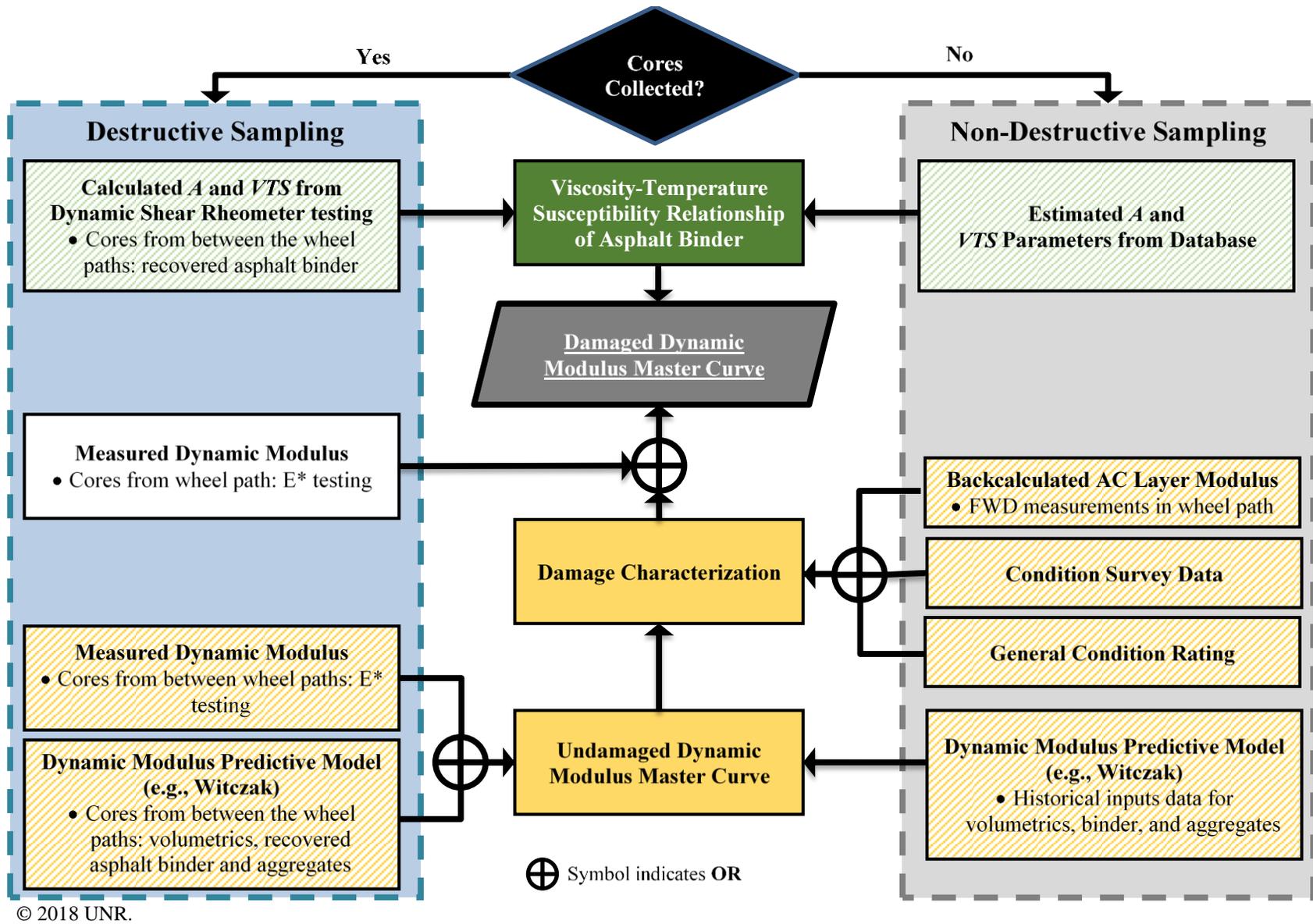
Figure 11. Flowchart. Estimation of damaged *E** for AC layer.

14

As presented in table 4, the approach developed consists of determining the field-damaged E^* master curve of the existing AC layer following two major steps: the determination of the viscosity–temperature susceptibility relationship of the asphalt binder and the construction of the field-damaged E^* master curve.

Step 1 is accomplished by either calculating intercept of the viscosity–temperature susceptibility relationship (A) and slope of the viscosity–temperature susceptibility relationship (VTS) parameters from measured shear modulus and phase angle data in the dynamic shear rheometer (option 1A), or by estimating the A and VTS parameters from a database (option 1B). Step 2 is accomplished by either collecting and conducting E^* testing on cores from the wheel path (option 2A) or by estimating the damaged E^* master curve (option 2B). The latter requires, first, the characterization of the undamaged E^* master curve, which can be undertaken by either collecting and conducting E^* testing on cores from between the wheel paths (option 2B-1A) or by using the Witczak predictive model.[14] The predictive model requires inputs related to asphalt binder properties, aggreagte gradation, and mixture volumetric properties that can be determined from testing on core samples collected from between the wheel paths or estimated from historical data. The final step under option 2B is to characterize the damage due to fatigue cracking in the AC layer. This is done by either conducting FWD testing in the most trafficked wheel path (option 2B-2A) or by estimating the damage from a condition survey (option 2B-2B) or a general condition rating (option 2B-2C).

Table 4. Determination of field damaged E* master curve for an AC layer.

Main Steps	Options	Substeps	Suboptions	Required Inputs
Step 1. Determination of viscosity–temperature susceptibility relationship of asphalt binder	Option 1A: Calculated *A* and *VTS* parameters from measured shear modulus and phase angle.	N/A	N/A	• Recovered asphalt binder according to AASHTO T 319.[15] • Measured asphalt binder shear modulus and phase angle at a minimum of three temperatures according to AASHTO T 315.[16]
Step 1. Determination of viscosity–temperature susceptibility relationship of asphalt binder	Option 1B: Estimated *A* and *VTS* parameters from database.	N/A	N/A	• Asphalt binder performance grade or asphalt binder penetration grade.
Step 2. Construction of damaged *E** master curve	Option 2A: Measured *E** on cores from wheel path.	N/A	N/A	• Measured *E** according to AASHTO T 378 on core from wheel path.[17]
Step 2. Construction of damaged *E** master curve	Option 2B: Estimated damaged *E** master curve.	Step 2B-1: Construction of undamaged *E** master curve	Option 2B-1A: Measured *E** on cores from between wheel paths.	• Measured *E** according to AASHTO T 378 on core from between the wheel paths.[17]
Step 2. Construction of damaged *E** master curve	Option 2B: Estimated damaged *E** master curve.	Step 2B-1: Construction of undamaged *E** master curve	Option 2B-1B: *E** predictive model (e.g., Witczak)	• Asphalt mixture volumetrics, V_a and V_{beff} (AASHTO T 166 and AASHTO T 209 or historical data).[18,19] • Aggregate gradation (AASHTO T 319 and AASHTO T 30 or historical data).[15,20] • Asphalt binder viscosity (AASHTO T 319 and AASHTO T 315 or historical data).[15,16]
Step 2. Construction of damaged *E** master curve	Option 2B: Estimated damaged *E** master curve.	Step 2B-2: Damage characterization	Option 2B-2A: Using backcalculated AC-layer modulus	• Backcalculated modulus of AC layer. • FWD-loading frequency. • Temperature at the mid-depth of AC layer.
Step 2. Construction of damaged *E** master curve	Option 2B: Estimated damaged *E** master curve.	Step 2B-2: Damage characterization	Option 2B-2B: Condition survey data	• Condition survey data (percent bottom–up fatigue cracking). • Bottom–up fatigue cracking calibrated transfer function.
Step 2. Construction of damaged *E** master curve	Option 2B: Estimated damaged *E** master curve.	Step 2B-2: Damage characterization	Option 2B-2C: General condition rating	• Pavement condition rating (excellent, good, fair, poor, very poor).

N/A = not applicable; AASHTO = American Association of State Highway and Transportation Officials; V_a = air void; V_{beff} = effective binder content.

Characterization of Unbound Materials

M_R is an important material property for unbound materials (e.g., CAB and SG). The repeated triaxial M_R test is performed on the unbound materials over a wide range of confining stress (σ_c) and deviator stress (σ_d) to capture the stress dependency (i.e., nonlinearity) of unbound materials.[21,22] It is commonly accepted to treat an unbound layer as linear elastic in the traditional pavement analysis procedures (e.g., standard traffic loading). The FWD backcalculated unbound-layer moduli are seen as appropriate since the stress conditions induced by FWD at load levels of approximately 9,000 to 12,000 lb and standard traffic loading are considered similar.

In the case of SHL-vehicle movement analysis, considering the same FWD backcalculated properties for the unbound layers may lead to improper estimation of pavement responses since different states of stress conditions are induced in the pavement layers. Considering the M_R variability as a function of stress state for unbound materials in a pavement analysis may require a finite element type of analysis. 3D-Move ENHANCED, selected here for response computations, assumes uniform properties that do not vary in the lateral direction. To overcome this concern, an iterative approach incorporating a nonlinear stress-dependent M_R relationship and the existing state of stresses in the unbound layers was employed in this project. As summarized in table 5, the approach consists of two main steps: determination of M_R relationship and determination of representative M_R.

Table 5. Determination of representative M_R for an unbound layer.

Main Steps	Options	Substeps
Step 1. Determination of the M_R relationship	Option 1A: Laboratory measured M_R according to AASHTO T 307[22]	N/A
Step 1. Determination of the M_R relationship	Option 1B: Using FWD data at multiple load levels	• Step 1B-1. Determine the backcalculated modulus at each load level. • Step 1B-2. Compute the σ_{ij} at the representative element of the layer. • Step 1B-3. Calculate the equivalent triaxial confining, deviator, and bulk stresses. • Step 1B-4. Determine the regression constants for the M_R relationship.
Step 2. Determination of representative M_R under an SHL vehicle	N/A	• Step 2-1. Assume seed value for the M_R of the unbound layer. • Step 2-2. Determine the nucleus of the SHL vehicle. • Step 2-3. Compute the σ_{ij} at the representative element of the unbound layer. • Step 2-4. Calculate the equivalent triaxial confining, deviator, and bulk stresses. • Step 2-5. Estimate the M_R using the developed M_R relationship in step 1 in conjunction with calculated deviator and bulk stresses. • Step 2-6. Compare the estimated M_R with the seed value. If the difference is high (say, more than 5 percent), use the estimated value as a new seed value in step 2-2. • Step 2-7. Repeat step 2-2 to step 2-7 until the differences between two consecutive iterations are less than 5 percent.

AASHTO = American Association of State Highway and Transportation Officials; N/A = not applicable; σ_{ij} = stress tensor.

Characterization of Chemically Stabilized Materials

The chemically stabilized materials consist of lean-concrete, cement-stabilized, open-graded-cement-stabilized, soil-cement, and lime-treated materials. These materials are considered linear elastic with constant elastic modulus (E), which can be determined from the existing correlations with compressive strength ($f'c$). For instance, figure 12 and figure 13 present the equations for calculating E for lean concrete and cement-treated base (CTB) as well as soil cement.[14] Then the engineer may apply some reduction factors on the calculated modulus based on the measured or perceived cracking condition of the stabilized layer. Backcalculation using FWD data can also help in determining in situ M_R values.

$$E = 57000\sqrt{f_c'}$$

Figure 12. Equation. Estimation of *E* for lean concrete and CTB.

$$E = 1200q_U$$

Figure 13. Equation. Estimation of *E* for soil cement.

Where q_U is unconfined $f'c$ (psi).

2.2.2. SG τ_{max} Properties

As mentioned in section 2.2, investigating the likelihood of shear failure (i.e., ultimate and localized) in the pavement SG subjected to SHL movement requires the τ_{max} properties for the SG. The τ_{max} parameters (ϕ and c) are not readily available and are not used in routine pavement design processes. Although existing database or engineering judgment can provide information regarding the strength properties of the SG layer, many researchers have questioned the validity of such estimates. In addition, because of the variability of the SG, a realistic estimation under in situ conditions for the influenced zone in the SG (i.e., pavement SG layer) is more appropriate.

Although laboratory testing provides the most reliable measurements for τ_{max} parameters of unbound materials (e.g., base and SG), the time-consuming and destructive process of sample collection, testing, and associated costs is an objectionable limitation. In this study, an FWD-based procedure was developed for estimating in situ τ_{max} parameters of the SG contained within the influenced zone (i.e., pavement SG layer) that impact pavement performance. The concept behind this methodology was to identify an equivalent triaxial condition for the representative element of the SG layer under FWD loading.[23,24] To this end, the nonlinear stress dependency of SG materials under multiple FWD-load levels along with the extension of the commonly accepted hyperbolic stress–strain relationship of unbound materials applied at the lower FWD-induced state of stresses were used (figure 14 and figure 15).[25,26]

In this methodology, the stress tensor (σ_{ij}) at a representative element in the SG is calculated first by using a layered linear elastic program (e.g., 3D-Move ENHANCED using static condition) that simulates each of the applied FWD-load levels.[11] The analysis utilizes the backcalculated modulus at each of the respective FWD-load levels. Such an approach inherently considers the role of stress dependency in an unbound material. The calculated σ_{ij} are transformed to the equivalent stress conditions associated with triaxial compression tests (σ_d and σ_c) for each of the

FWD-load levels using the stress invariants (i.e., octahedral stress components). A hyperbolic relationship (figure 16) is subsequently fitted to the equivalent triaxial test datasets of σ_d and axial strain (ε_1). By rewriting the hyperbolic equation in a linear form in terms of ε_1/σ_d and ε_1 (figure 17), σ_d at failure (σ_{df}) and initial tangent modulus (E_i) can be estimated by inversing the slope and intercept, respectively. Volume V: Appendix D describes in greater detail the FWD-based procedure as well as the verification exercises.[4] The Mohr–Coulomb failure envelope equation is subsequently used in the estimation of the SG c by assuming an acceptable range for the ϕ.
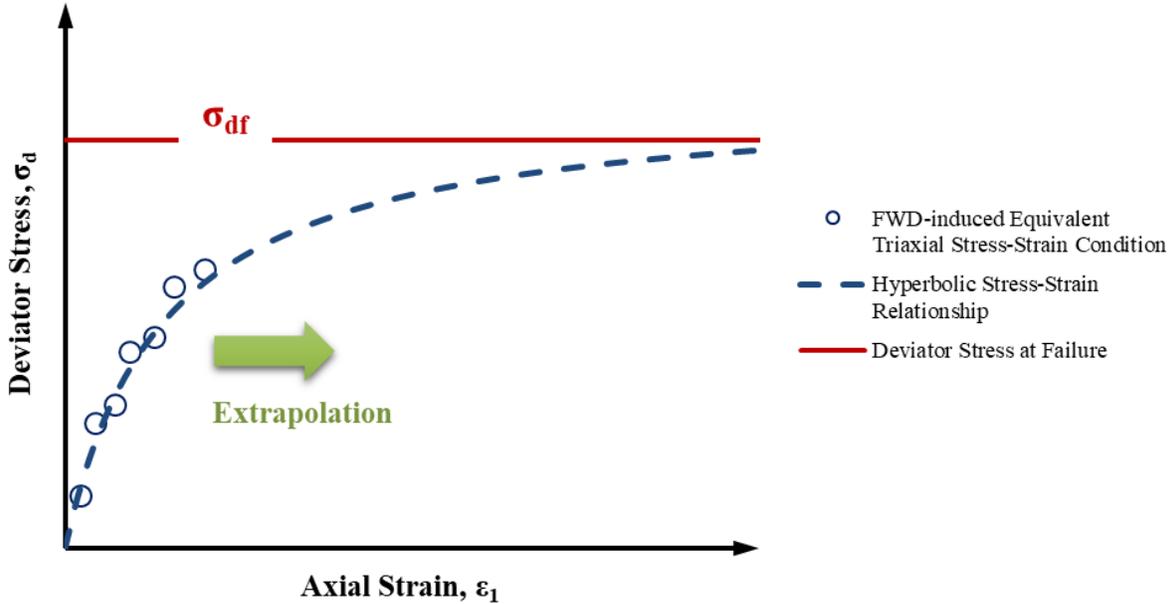
© 2018 UNR.

Figure 14. Graph. Extrapolation of hyperbolic relationship.
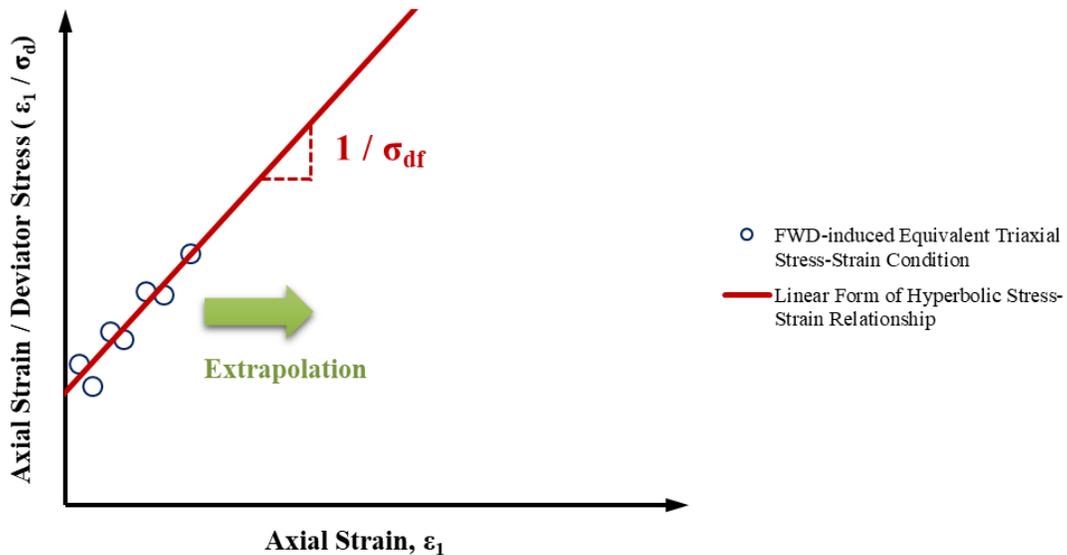
© 2018 UNR.

Figure 15. Graph. Estimation of σ_{df} using linear form of hyperbolic relationship.

19

$$\sigma_d = \frac{\varepsilon_1}{\frac{1}{E_i} + \frac{\varepsilon_1}{\sigma_{df}}}$$

Figure 16. Equation. Nonlinear hyperbolic stress–strain relationship of soils.

$$\frac{\varepsilon_1}{\sigma_d} = \varepsilon_1 \frac{1}{\sigma_{df}} + \frac{1}{E_i}$$

Figure 17. Equation. Hyperbolic relationship in linear form.

2.3. ULTIMATE FAILURE ANALYSES

Ultimate failure analyses include the investigation of the SG bearing failure as well as sloped-shoulder failure. In this section, these two analyses are briefly explained. Volume VI: Appendix E and Volume VII: Appendix F provide detailed discussion regarding these analyses.[5,6]

2.3.1. SG Bearing Failure Analysis

SHL vehicles with nonconventional axle and tire loadings and configurations can render a critical condition of shear failure either in an ultimate or localized manner. Ultimate shear failure is an instantaneous failure and focuses on the SG layer as it is typically the weakest layer in the pavement structure.

To examine the risk of instantaneous shear failure, Meyerhof's general bearing capacity equation (figure 18) is viewed as an ideal selection because it is a well-established and validated foundation design analysis procedure under static or slow-moving vehicle loading conditions.[27] Accordingly, the distributed σ_v induced by the SHL vehicle on top of the influenced SG layer is compared with the bearing capacity of the layer to identify the possibility of ultimate shear failure in the pavement SG layer. It should be noted that a modified bearing capacity equation is applied when a sloping pavement shoulder is present.[27]

$$q_u = cNc\, Fcs\, Fcd\, Fci \ + \ q'Nq\, Fqs\, Fqd\, Fqi \ + \ \frac{1}{2}\gamma\, B\, N\gamma\, F\gamma s\, F\gamma d\, F\gamma i$$

Figure 18. Equation. Meyerhof's general bearing capacity.

Where:
  q' = effective stress at the bottom of the foundation level.
  γ = unit weight of SG soil.
  B = width of the foundation (or diameter).
  Fcs = shape factor with respect to c.
  Fqs = shape factor with respect to overburden.
  $F\gamma s$ = shape factor with respect to unit weight.
  Fcd = depth factor with respect to c.
  Fqd = depth factor with respect to overburden.
  $F\gamma d$ = depth factor with respect to unit weight.
  Fci = load inclination factor with respect to c.

Fqi = load inclination factor with respect to overburden.
$F\gamma i$ = load inclination factor unit weight.
Nc = bearing capacity factor with respect to cohesion.
Nq = bearing capacity factor with respect to overburden.
$N\gamma$ = bearing capacity factor with respect to unit weight.

As mentioned in section 2.1.2, the SHL vehicle may consist of several individual axle groups, and each axle group has a nucleus (figure 10). To identify the possibility of ultimate shear failure in the pavement SG layer, each axle group is individually assumed to be a bearing capacity investigation zone (i.e., loaded area). Accordingly, the distributed σ_v on the top of the SG induced by the nucleus of an axle group is compared against the bearing capacity of the SG layer. It should be noted that the dimension of the bearing capacity investigation zone in Meyerhof's equation is specified as being equal to the length and width of the axle group.

It is expected that the nucleus-induced σ_v on top of the SG represents a nonuniform distribution. As an example, computed σ_v distribution for the nucleus of SHL case No. LA-8T-14 (figure 10) is depicted in figure 19. However, Meyerhof's equation assumes the loaded area to be of a certain fixed shape with a uniform pressure distribution. The average uniform σ_v (q_{ave}) induced by the nucleus can be calculated by first integrating the volume of the nucleus-induced σ_v distribution on top of the SG and then dividing it by the area of the uniform stress distribution induced by the nucleus on top of the SG ($A_{affected}$), as illustrated in figure 20.
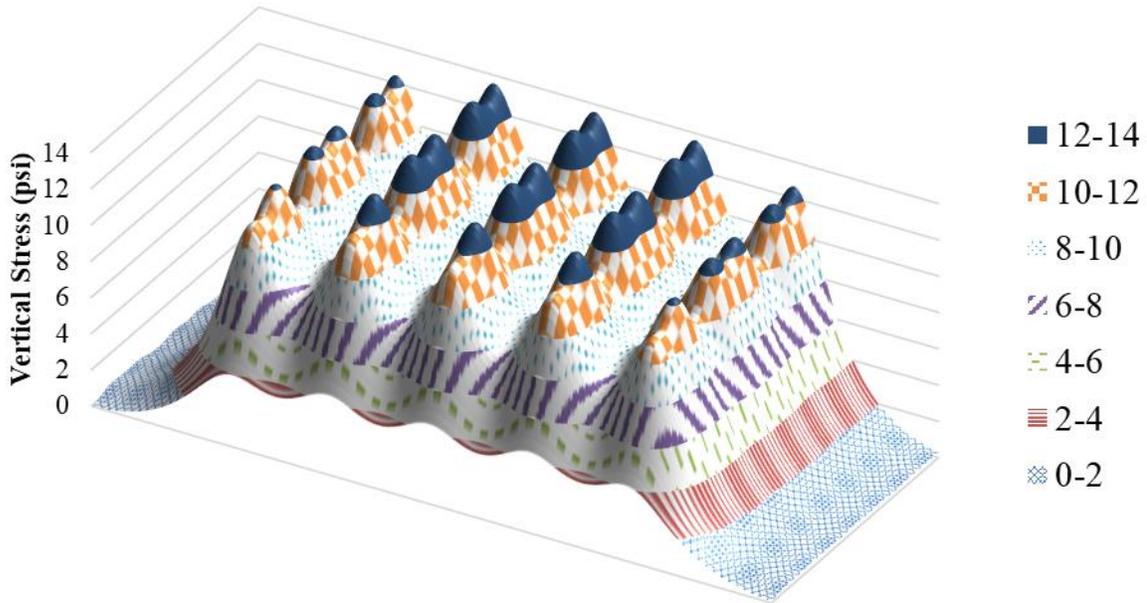
© 2018 UNR.

Figure 19. Chart. σ_v distribution on top of the SG under the nucleus (case No. LA-8T-14).
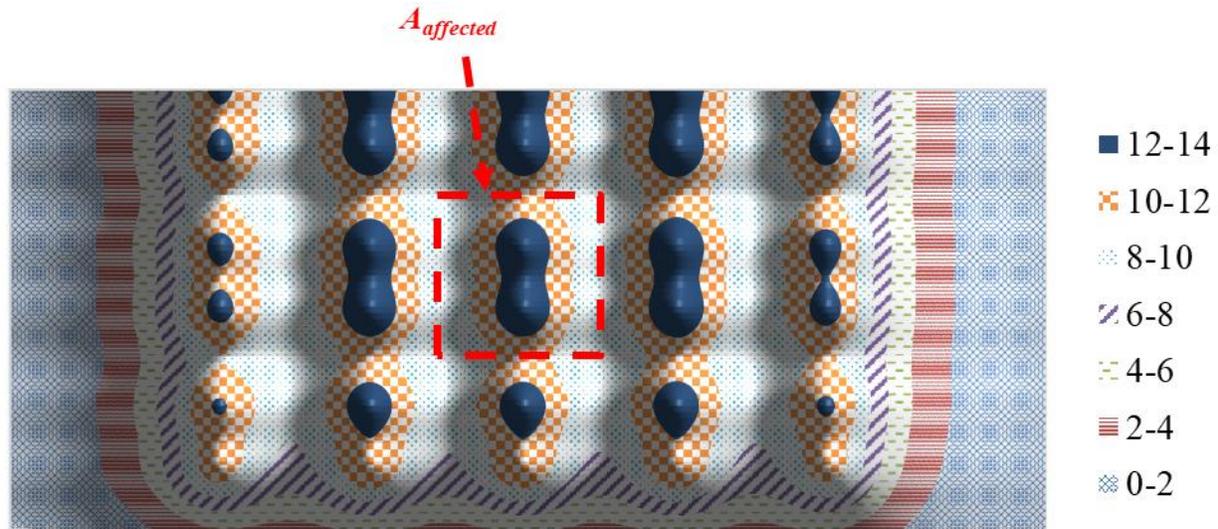
Figure 20. Chart. σ_v distribution on top of the SG under the nucleus and $A_{affected}$ (case No. LA-8T-14).

As a conservative measure, q_{ave} is assumed to cover the entire rectangular area of the axle group. This stress distribution can be considered the most critical possible scenario. It may be noted that a smaller subset of tires or axles within the SHL truck may be assumed to be the bearing capacity investigation zone (i.e., loaded area). However, it is physically impossible, because of the interconnectivity of the axles, to have one part of the vehicle develop a general bearing capacity failure mechanism while the rest does not. The entire axle group, since it is interconnected, will behave as a unit, and therefore, the failure should be undertaken for the entire axle group.

2.3.2. Sloped-Shoulder Failure Analysis

Although slope stability is one of the common problems in geotechnical practice, it has not been a major concern for a pavement shoulder subjected to the standard truck loading. However, substantial higher surcharge load resulting from the SHL movements might lead to a critical condition for failure.

SHL vehicles are usually moved under traffic control, so it is often possible to keep the SHL vehicle far away from the pavement edge and shoulder. It is recommended that the vehicle stay away from the pavement edge, particularly in routes where there is an unpaved shoulder and/or a steep slope. However, it is not always possible to keep the SHL vehicle far from the pavement edge (e.g., narrow lanes and/or a wide SHL vehicle). Therefore, it is necessary to investigate the stability of a sloped pavement shoulder under the SHL-vehicle movement.

The wedge method is a well-accepted slope stability–analysis methodology in geotechnical practice.[28] In this research study, wedge-method slope stability analysis was modified so that stability of a sloping layered medium consisting of pavement layers with distinct properties could be evaluated under SHL movements. The following briefly presents the modified slope stability wedge method; details are presented in Volume VII: Appendix F.[6]

22

Figure 21 illustrates a typical flexible pavement structure with a sloped shoulder. As illustrated in this figure, to investigate the stability of a pavement shoulder subjected to SHL movement, various wedges of failure are selected. This figure shows several slip surfaces passing through point A as solid lines. In all cases, the failure wedge is bounded by a vertical plane, and a horizontal or an inclined slip surface is located in the SG layer. The vertical plane is located to the left of the AC layer as it is assumed that the vertical plane cannot extend through the AC layer. It is also assumed that the slip surface is developed in the SG layer, which is the weakest layer in the pavement structure. Searching for the critical location of the failure wedge involves systematically varying the horizontal boundaries of the wedges until the corresponding minimum factor of safety (FOS) is found.
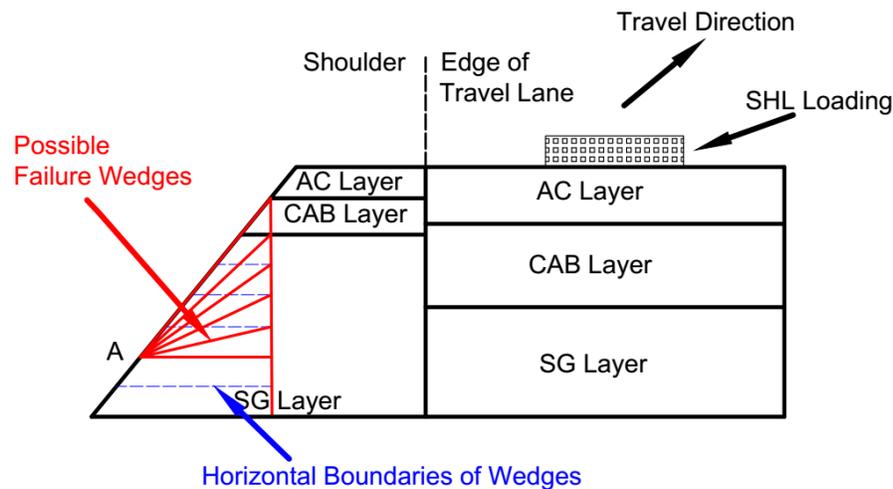
© 2018 UNR.

Figure 21. Illustration. Search schemes for failure wedges.

The stability of each failure wedge is evaluated by considering the wedge as a rigid sliding mass or a gravity-retaining structure. As shown in figure 22 and figure 23, the following five forces acting on the failure wedge can be identified:

- Weight of the sliding wedge (W).

- Developed resisting c force resulting from the mobilized c (T_D) acting on the bottom slip surface.

- Resultant force from the bottom soil (F_D) that makes an angle (ϕ_D) with the normal to the bottom slip surface.

- Two components of horizontal deriving forces acting on the vertical plane: lateral earth pressure from adjacent soil (Q) and resultant horizontal force due to surcharge load (P) (i.e., SHL vehicle).

23
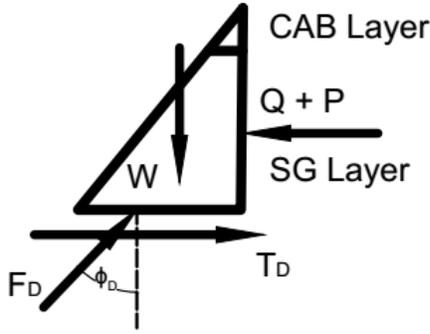
© 2018 UNR.

Figure 22. Illustration. Failure wedge with horizontal slip surface and applied forces.
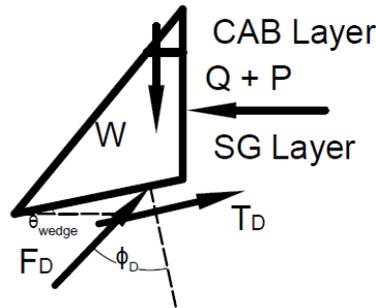
© 2018 UNR.

Figure 23. Illustration. Failure wedge with inclined slip surface and applied forces.

To determine the FOS, the force equilibrium equations in the parallel and perpendicular directions to the slip surface are applied. Consequently, the FOS using the equations presented in figure 24 or figure 25 can be determined. Here, θ_{wedge} is the angle between the slip surface and horizontal surface (figure 23), and l is the length of the bottom slip surface. For the failure wedges with horizontal slip surface where θ_{wedge} is 0, the FOS can be simplified to the equation shown in figure 25.

$$FOS = \frac{(W\cos\theta - (Q + P)\sin\theta_{wedge})\tan\phi + c * l}{(W\sin\theta_{wedge} + (Q + P)\cos\theta_{wedge})}$$

Figure 24. Equation. FOS against failure for the wedges with inclined slip surface.

$$FOS = \frac{W\tan\phi + c * l}{P + Q}$$

Figure 25. Equation. FOS against failure for the wedges with horizontal slip surface.

Q is calculated using the Rankine active earth pressure, which is a well-accepted theory in the design of retaining structures. To estimate the resultant horizontal force due to a surcharge SHL vehicle (P), 3D-Move ENHANCED is utilized so that the role of layered pavement structure with distinctly different material properties is considered.[11]

24

Subsequently, 3D-Move ENHANCED computed horizontal stresses are modified through the application of a stress adjustment factor for sloping shoulder ($SAF_{Shoulder}$) to account for the role of a sloping shoulder near the edge of the pavement since this software assumes that pavement layers extend laterally to infinity. $SAF_{Shoulder}$ equal to 1.5 was determined based on the results obtained from the large-scale experiments conducted.[23] Discussion regarding the determination of $SAF_{Shoulder}$ is presented in chapter 3.

A similar exercise is followed in geotechnical practice when the value of P is calculated based on the Boussinesq theory assuming elastic, homogenous, and isotropic semi-infinite soil medium.[27,28] Subsequently, the calculated horizontal stress using the Boussinesq solution is doubled to account for the yielding soil continuum (i.e., $SAF_{Shoulder}$ equal to 2).

2.4.   BURIED UTILITY RISK ANALYSIS

As part of this project, a study was carried out to assess the risk against failure in existing buried utilities due to SHL movement, which is described in Volume VIII: Appendix G.[7] Review of the existing state-of-practice methods that are employed for the design of buried utilities revealed that every utility has certain specific design considerations that are unique to that particular buried utility. However, two common steps of design are followed by all methods. In the first step, the focus is on the determination of load distribution on the buried utility structure due to the dead (i.e., soil overburden) and live (i.e., standard truck traffic) loads. Once the load distribution is obtained, the structural design is then dictated by specifications for the buried utility type.

Procedures to analyze the risk of failure in flexible and rigid buried structures due to SHL movement were developed in a similar fashion in this study. Reliable assessment of induced stresses due to live load (i.e., SHL-vehicle load) and subsequent investigation of buried utility integrity subjected to the induced stresses are the main components of the developed procedures.

Widely accepted and available buried utility design procedures were adopted in this study to assess the failure risk of existing buried utilities under SHL vehicle–induced stresses.

For flexible pipes, a hybrid step-by-step evaluation procedure provided in American Lifelines Alliance (ALA) and Canadian Energy Pipeline Association (CEPA) reports was implemented in this study.[29,30] The procedure is divided into four general checks:

1. Assess FOS against pipe circumferential stress failure.
2. Check ovality of pipe cross section.
3. Check ring buckling stress.
4. Check wall crushing stress.

In the case of rigid concrete culvert, the stability of a rigid buried utility is investigated by analyzing the flexural strength, τ_{max} , and axial thrust in the culvert members (i.e., top slab, bottom slab, and sidewalls) in accordance with *AASHTO [American Association of Highway and Transportation Officials] LRFD [Load and Resistance Factor Design] Bridge Design Specifications*.[31]

Although the state of practice provides recommendations with respect to the live load distribution, their application is questionable for assessing the risk of buried utilities under an SHL-vehicle movement. Consideration of only a standard truck (mostly HS20) as a live load and simulating it as a point or rectangular load that is statically applied at the surface of unpaved roads (i.e., neglecting the AC and CAB layer) are the significant limitations for the application to SHL-vehicle movement. Therefore, adoption of 3D-Move ENHANCED was seen as more appropriate because of its merits to realistically simulate pavement structure and SHL vehicles. Accordingly, the load-induced σ_v at the location of buried utility is computed using 3D-Move ENHANCED ($\sigma_{zz\text{-}3D\text{-}Move}$) (figure 26).[11] The role of soil–structure interaction and discontinuities within the medium (i.e., existence of buried utilities) is accounted for by using a stress adjustment factor for buried utilities ($SAF_{Utility}$). Therefore, computed σ_v using 3D-Move ENHANCED at the location of the buried utility were modified and utilized in the analysis.[11]
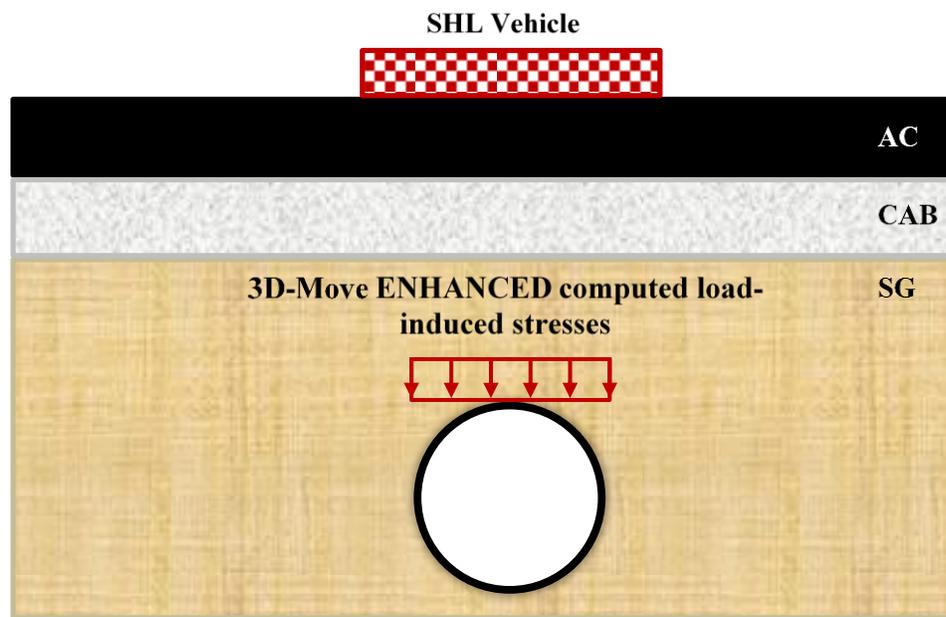
© 2018 UNR.

Figure 26. Illustration. Computation of σ_v at the location of buried utility using 3D-Move ENHANCED.[11]

The behavior of buried utilities observed in the large-scale experiments conducted were employed to determine $SAF_{Utility}$ for flexible steel pipe and rigid concrete box culvert. It was found that the σ_v experienced by the flexible pipe were much lower than those stresses transferred in the continuum medium (i.e., no buried utility). In the case of concrete culvert, substantially higher σ_v were measured on top of concrete culvert when compared with those induced in the soil medium under the control condition (i.e., no buried utility). As a conservative measure, it is recommended to retain $SAF_{Utility}$ for flexible pipes as 1. This recommendation is mainly to be on the conservative side until further experimental testing and numerical investigations are carried out. However, in the case of rigid culverts, $SAF_{Utility}$ equal to 1.5 is recommended.

2.5. SERVICE LIMIT ANALYSES

The service limit analyses include localized shear failure analysis and deflection-based service limit analysis. The localized shear failure analysis investigates the likelihood of localized failure (yield) at the critical location on top of the SG layer under the SHL vehicle. The deflection-based service limit analysis assesses the magnitude of the load-induced pavement deflections during the SHL movement. The following sections describe these procedures; detailed discussions are presented in Volume VI: Appendix E.[5]

2.5.1. Localized Shear Failure Analysis

As mentioned in section 2.2, ultimate failure analysis (SG bearing failure and, when applicable, sloped-shoulder failure) is an essential first step for evaluating the risk of shear failure in the pavement SG subjected to SHL movement. Once this analysis confirms the bearing capacity of the SG is adequate, the likelihood for onset of yielding in the SG layer due to localized shear failure is then examined. It is believed that the substantial SHL vehicle–induced state of stress developed in the pavement structure might reach close to the failure state. Therefore, comparing the load-induced stress level on top of the SG layer with the corresponding yield criterion for this layer is carried out in localized shear failure analysis. It may be noted that the localized shear failure analysis focuses on the SG layer, which typically represents the most vulnerable pavement layer with the lowest strength.

Several failure criteria, such as Mohr–Coulomb, Drucker–Prager, Lade–Duncan, and Matsuoka–Nakai, have been proposed for evaluating the yielding (i.e., failure) of soil materials.[28] The Drucker–Prager yield criterion that involves the τ_{max} parameters (ϕ and c) of material is one of the well-accepted criteria in soil plasticity.[32] As presented in figure 27, the Drucker–Prager yield criterion includes the Mohr–Coulomb criterion for 3D stress states.

Per Drucker and Prager, σ_d is represented as q. The Drucker–Prager failure criterion is a straight line on a q versus mean normal stress (p) plot. Figure 28 demonstrates the Drucker–Prager failure envelope in q–p space. As presented in this figure, at a certain induced mean normal stress ($p_{applied}$), the FOS is defined as the ratio between the Drucker and Prager's deviator stress at failure ($q_{failure}$) and induced deviator stress ($q_{applied}$). FOS is an indication of how far the stress state is from the failure envelope.
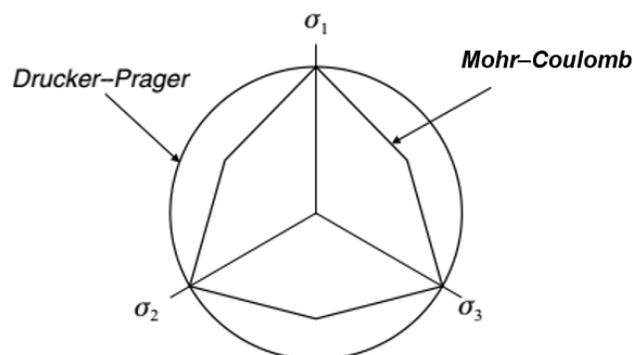
© 2018 UNR.

Figure 27. Illustration. The Drucker–Prager and Mohr–Coulomb yield surfaces.
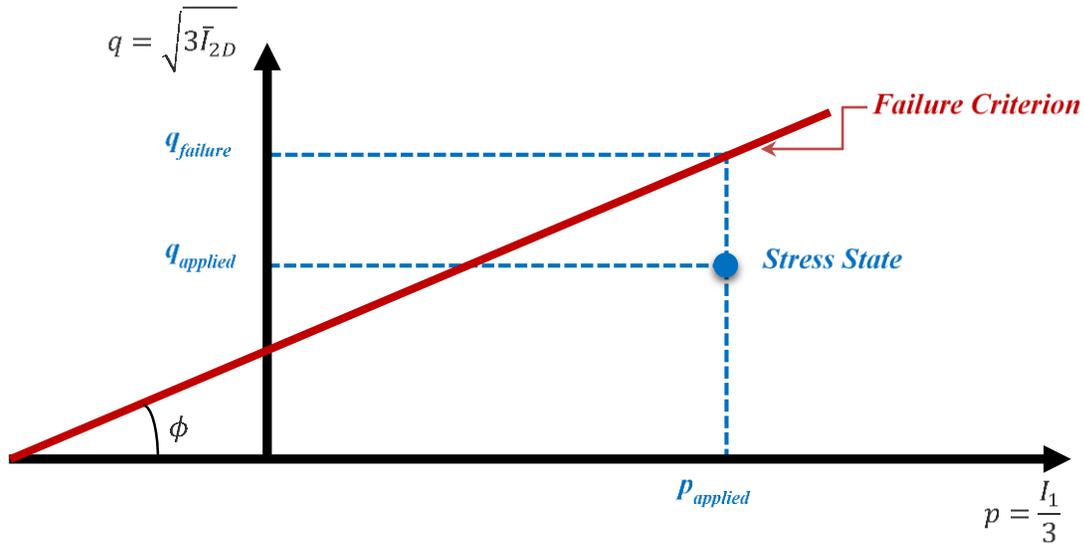
© 2018 UNR.

Figure 28. Graph. Representation of Drucker–Prager failure criterion in the q–p plot.

For the conventional triaxial test, q and p are directly measured. The SHL vehicle's $p_{applied}$ and $q_{applied}$ can be determined by transforming the computed σ_{ij} to the equivalent triaxial testing condition. This can be done since q and p can be written as a function of the stress invariants. Subsequently, FOS against localized shear failure for the pavement structure subjected to the SHL-vehicle movement is determined. It should be noted that the nucleus of the critical axle group and the representative moduli for the pavement layers are used to calculate the σ_{ij} at various locations on top of the SG.

The highest possibility for the localized shear failure (i.e., lowest FOS) is at the locations where the lowest σ_c and highest σ_d are induced. Although the σ_v may reach a maximum at the middle of the nucleus, the locations at the edge of the nucleus may experience the lowest σ_c. For instance, figure 29 shows the 3D surface plot for FOS determined at the SG of pavement structure in case No. LA-8T-14 (figure 10). Figure 29 implies that a minimum FOS (i.e., highest possibility for localized shear failure) is at the edge of the SHL vehicle's nucleus. It should be mentioned that 3D-Move ENHANCED, which is incorporated in SuperPACK, is capable of providing a 3D surface plot at any depth of interest.[11,9] Therefore, the critical location at the top of the SG and subsequent minimum FOS can be readily identified by SuperPACK.[9]
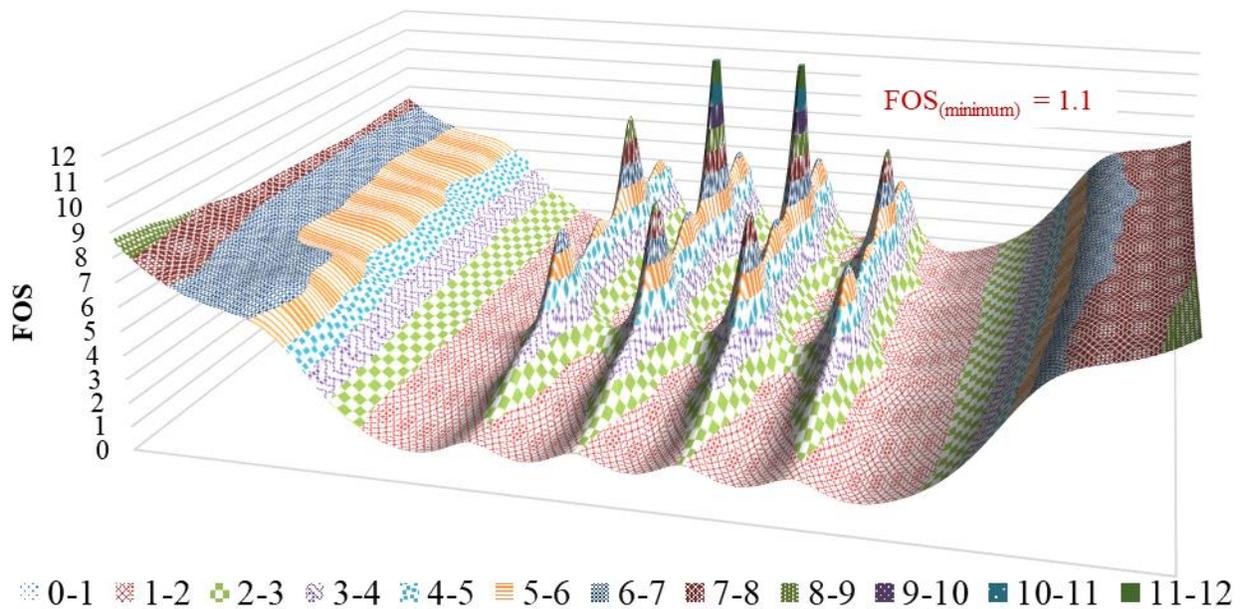
Figure 29. Chart. FOS under SHL-vehicle nucleus.

2.5.2. Deflection-Based Service Limit Analysis

Although the shear failure analyses (i.e., ultimate and localized) may inform that the pavement structure is capable to sustain the SHL movement without experiencing any shear failure, the pavement structure could still be subjected to excessive surface deflection under an SHL vehicle that may eventually lead to the development of premature surface distresses and rapid deterioration. To prevent this, the SHL vehicle–induced surface deflection (δ_{SHL}) should be determined and limited to an allowable surface displacement. It may be noted that the nucleus of the critical axle group and the representative moduli for the pavement layers are used to compute δ_{SHL}.

In the deflection-based service limit analysis, an equivalent FWD-load level (FWD_{equiv}), which generates surface center deflection at the center of the FWD plate (D_0) equal to δ_{SHL}, is determined. In other words, the equivalency is established between the SHL-vehicle load and an FWD-load level (i.e., FWD_{equiv}) based on the same induced surface deflection. Subsequently, FWD_{equiv} is compared to an allowable FWD-load level (FWD_{allow}). An FWD_{equiv} higher than FWD_{allow} indicates a need for mitigation strategies.

To determine the FWD_{equiv}, the FWD load–deflection curve is developed using the load and D_0 measurements at multiple FWD-load levels (figure 30). However, the AC-layer temperature at the time of SHL movement, referred to as analysis temperature, may be different from the time of FWD testing. Therefore, measured D_0 needs to be adjusted based on the analysis temperature. To accomplish this, the AC-layer stiffness at the analysis temperature is determined using the field damaged E^* master curve and knowing the FWD-loading frequency. Accordingly, surface deflections at different FWD-load levels are calculated using the determined AC-layer stiffness (i.e., temperature adjusted) and along with backcalculated resilient moduli of the unbound layers

29

at the corresponding FWD load, using the static loading condition in 3D-Move ENHANCED.[11] Consequently, knowing the calculated δ_{SHL} and developed FWD load–deflection curve, the FWD_{equiv} to the SHL-vehicle load is identified as illustrated in figure 30.
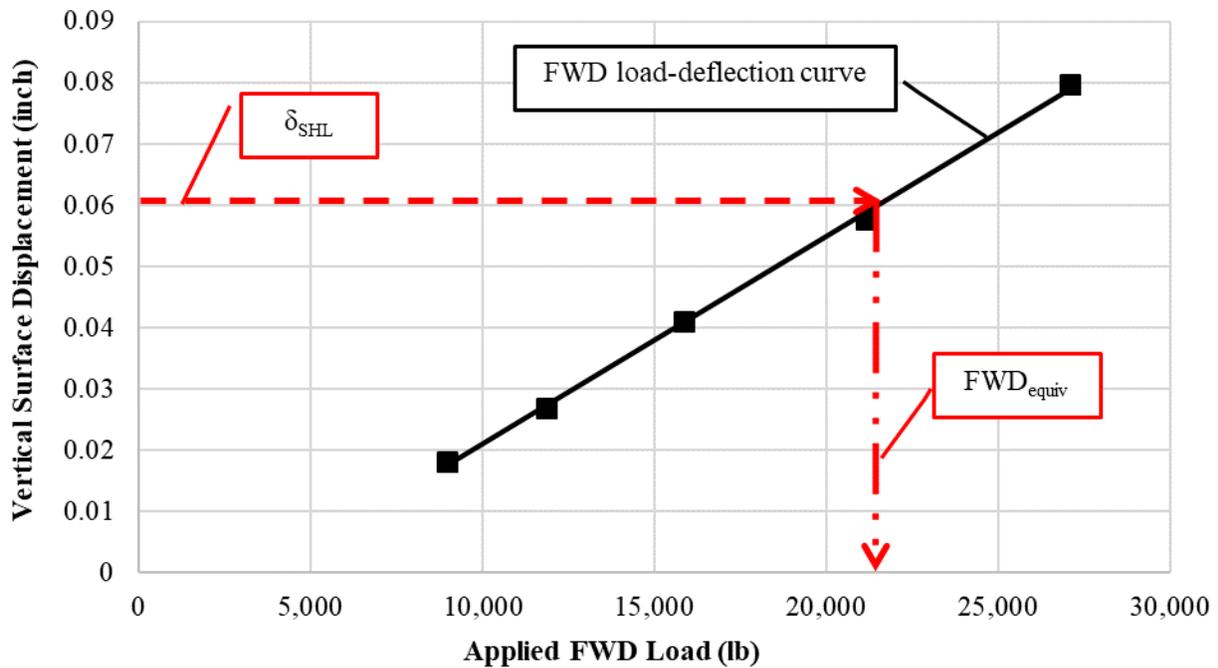
© 2018 UNR.

Figure 30. Chart. FWD load–deflection curve.

The concept of shear stress ratio (SSR) was employed to determine the FWD_{allow}. Previous studies reported that permanent deformation potential of unbound materials (i.e., CAB and SG) could be reasonably assessed by means of the SSR concept.[33–36] As illustrated in figure 31, the SSR is defined as the ratio between applied (mobilized) shear stress ($\tau_{mobilized}$) and the material's τ_{max}. It has been concluded that when unbound materials experience SSR values higher than 0.7, high permanent strain accumulates in the materials, eventually resulting in permanent deformation.[33–36] Accordingly, the FWD-load level that induces an SSR value equal to 0.7 in the pavement SG layer (top of SG) is identified as FWD_{allow}.

The AC-layer stiffness at the analysis temperature predetermined using field damaged E^* master curve along with the backcalculated resilient moduli of the unbound layers at multiple FWD-load levels are employed to calculate the σ_{ij}. Here, the point of interest is located below the center of the simulated FWD-loading plate on top of the SG. Subsequently, σ_{ij} is transformed into equivalent σ_c and σ_d in laboratory triaxial testing conditions by the use of stress invariants. Knowing the FWD-induced σ_d and σ_c, the FWD load–SSR curve representing the SSR values at multiple FWD-load levels is established. As illustrated in figure 32, this can be used to obtain the FWD_{allow} corresponding to an SSR value equal to 0.7.
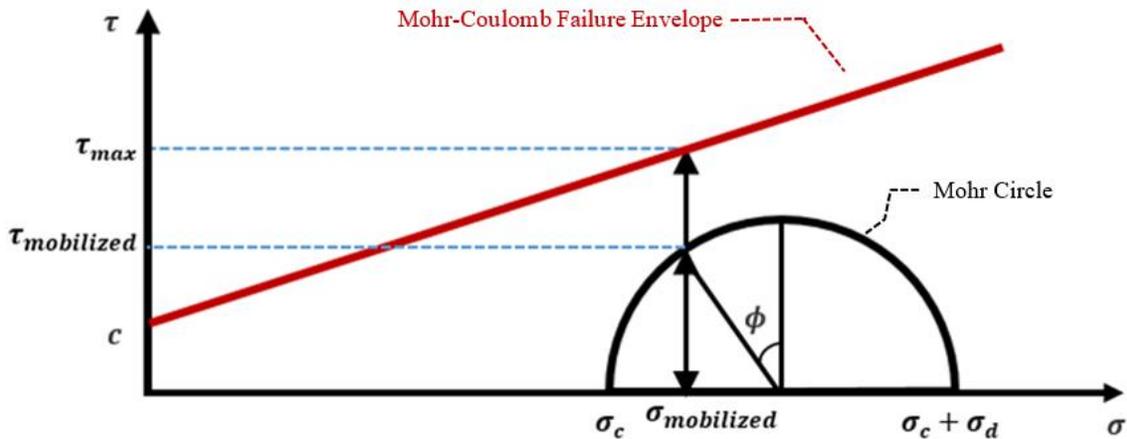
© 2018 UNR.

Figure 31. Chart. Representation of τ_{max} and applied stresses.
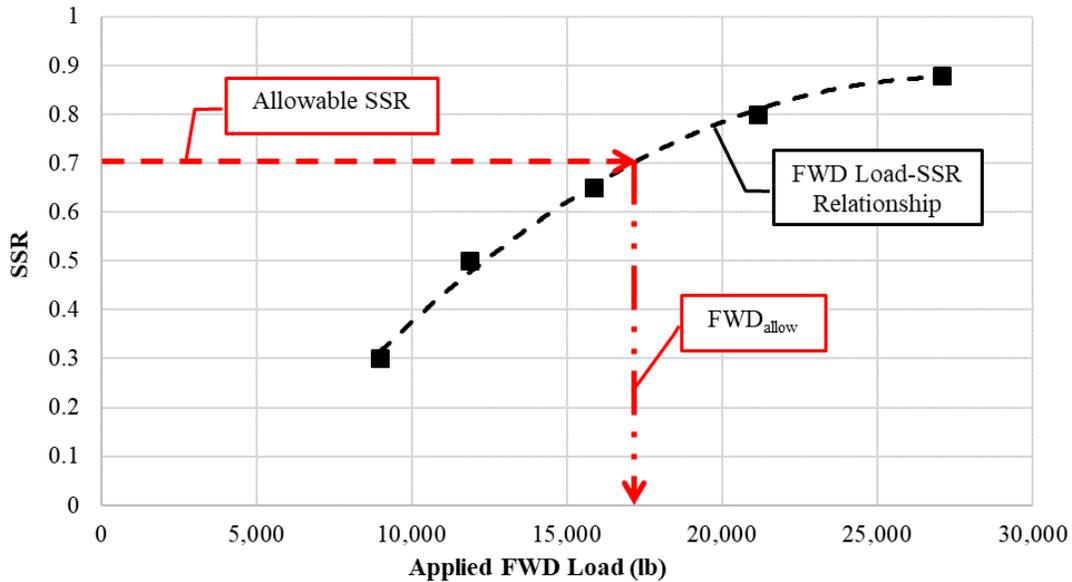
© 2018 UNR.

Figure 32. Chart. FWD load–SSR curve.

2.6. COST ALLOCATION ANALYSIS

SHAs issue special permits for SHL-vehicle movements and collect a nominal fee, making SHL-vehicle operation legal on their highway network. However, quantifying pavement damage attributed to an SHL movement is a challenging task. An array of factors specific to each SHL movement (e.g., axle and tire loadings and configurations, traveling speed, and temperature and properties of existing pavement layers at the time of the movement) influences the magnitude of the load-induced pavement damage.

SHL vehicles generally present a nonstandard axle configuration, and any additional pavement damage caused by their operation is generally not considered in the new and rehabilitation

31

designs of pavements. Since heavier axle loads of SHL vehicles can introduce greater stresses and strains in the pavement compared to those estimated under a traditional truck loading, a single SHL-vehicle pass could induce damage similar to that caused by multiple passes of a standard truck, leading to a faster deterioration rate in the pavement condition.

Another challenge associated with determining pavement damage attributable to an SHL movement is properly accounting for the characteristics of the existing pavement layers at the time of the movement. For instance, the viscoelastic property of the AC layer is critical as it influences the load-induced pavement responses with the SHL movements often being at much lower speeds. For example, pavement damage caused by an SHL vehicle operating during the summer (or even daytime hours) may be significantly different from the damage caused by the same vehicle operating during a different season (or during nighttime hours of the same day).

One of the objectives in this research project was to establish an appropriate mechanistic-based cost allocation methodology for SHL movement on flexible pavements. The procedure developed in this study allows for the estimation of PDACs due to a single pass of an SHL vehicle. The PDAC can be estimated for different SHL-vehicle axle loadings and configurations with due considerations given to locally calibrated pavement distress models, existing pavement condition, different pavement repair options, and vehicle miles traveled (VMT).

The approach suggested by Tirado et al. of using the highway cost-occasioned method to estimate PDACs based on ME analysis was adopted in this project.[37] This cost allocation approach estimates pavement-damage costs considering the predicted pavement life reduction due to a single pass of the SHL vehicle. With this method, different pavement distress models, pavement repair options, and any axle configuration can be implemented. The net present value (NPV) of repair costs and VMT are also needed inputs of the process.

The approach presented by Tirado et al. was revised, in this study, to consider the condition of the pavement at the time of the SHL-vehicle movement. Consequently, lower PDACs have been estimated when an SHL movement occurs on a pavement section with lower remaining life (i.e., a pavement section that has already been subjected to a large percentage of its original design truck traffic).

To estimate PDAC, distress prediction models are needed to predict pavement performance and estimate pavement damage under both SHL vehicles and reference vehicles. The estimated damage is then used to calculate the PDAC due to a single pass of the SHL vehicle. The overall flowchart for the cost allocation analysis method is presented in figure 33. It should be noted that the damage caused by a single pass of the SHL vehicle is compared to that of a reference vehicle. The equivalency concept is used in the determination of cost attributable to SHL-vehicle movement.

There are cases when the SHL-vehicle configuration has several trailers, or dollies, comprising multiple tires and complex and specialized axle arrangements. This type of configuration requires the determination of the nucleus so that the SHL vehicle is divided into one or more numbers of nuclei where the nucleus repeats itself across the SHL-vehicle configuration; therefore, the number of nucleus repetitions within the SHL truck domain is considered for pavement damage costs calculation instead of individual axle repetitions. It should be noted that

this approach is consistent with the pavement response analysis and estimation of pavement damage using MEPDG methodology for different axle types (i.e., single, tandem, tridem, and quad axles).[14] In cases when the spacing between two trailers is greater than 60 inches, they are treated as independent groups by defining a separate nucleus for each group.
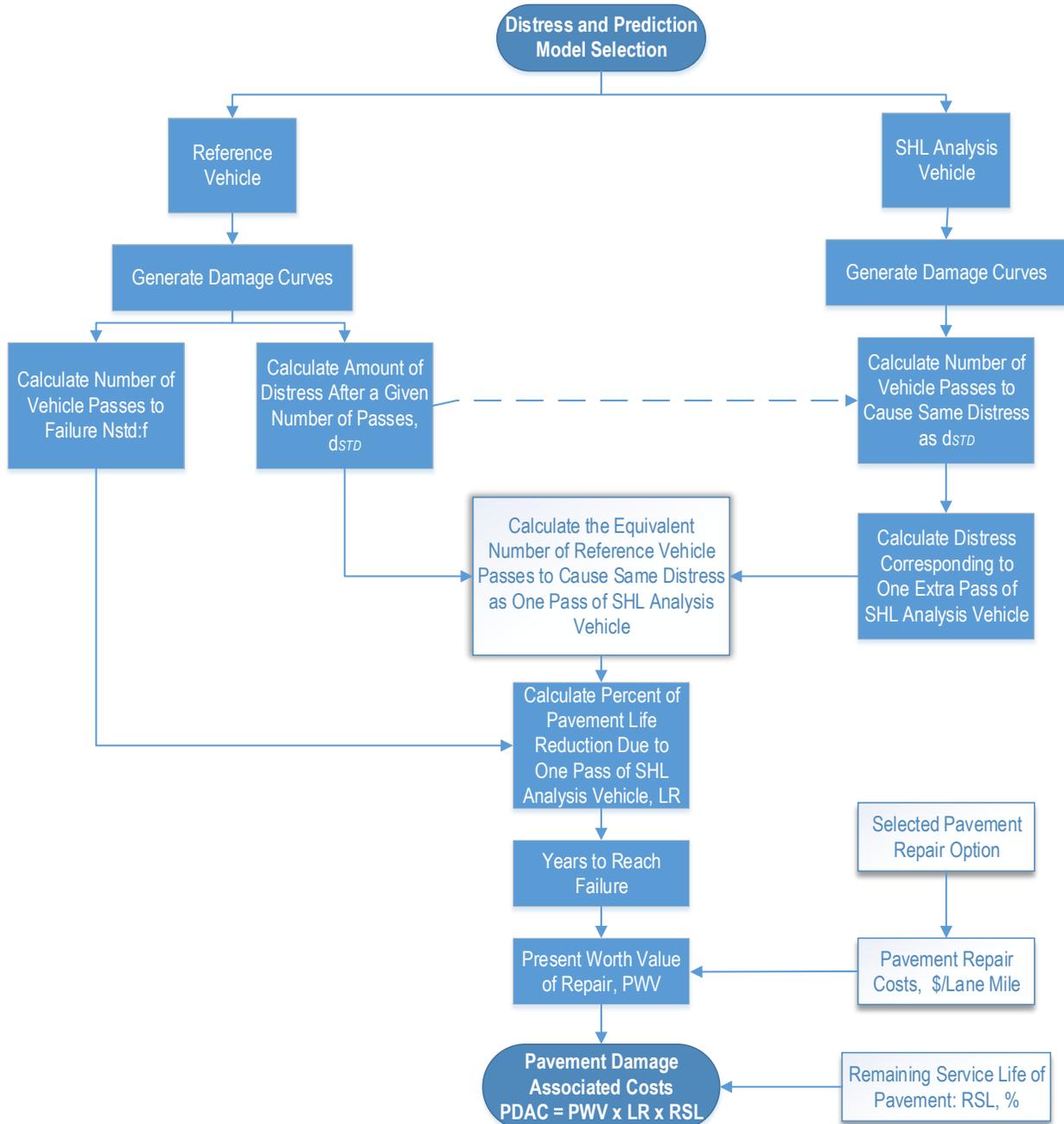
Modified from © 2010 Tirado et al. Reprinted by permission from SAGE Publications, Inc.

Figure 33. Flowchart. Overall approach for the estimation of pavement damage and allocated cost.[37]

2.7. MITIGATION STRATEGIES

The analysis procedures for evaluating SHL movement on flexible pavements that are developed in this study consisted of the following four major components: ultimate failure analyses, buried utility risk analysis, service limit analyses, and cost allocation analysis.

Prior to the conducting of cost allocation analysis and determination of PDAC, ultimate failure analyses, buried utility risk analysis, and service limit analyses need to be completed to assess the potential impact of SHL movement on flexible pavements. It should be noted that mitigation strategies may be needed at any stage of the evaluation process when the calculated results fail to meet the imposed respective requirements.

Table 6 presents mitigation strategies that can attenuate the SHL vehicle–induced distresses and damages, whereas some of the strategies are limited to only one type of distress (or failure). It is also noted that 3D-Move ENHANCED, which is the analysis engine of SuperPACK, is capable of modeling the layer interface conditions, such as debonding or slippage.[11,9] Therefore, simulation of debonded layers or mat (e.g., steel plate, aggregate base cover) can be conducted whenever the analyses procedures indicate the need for application of mitigation strategies. These remedial strategies should be considered on an individual basis using SuperPACK.[9]

Table 6. Select mitigation strategies applicable to SHL movement.

Mitigation Strategy	Advantages	Additional Considerations
Surface protection and load dispersion: Deploy steel plate.	• Spreads the load over a larger area. • Easy to deploy. • Applicable for ultimate failure, buried utility failure, and service limit failure.	• Cost (e.g., heavy hauling equipment and supervision). • Safety.
Surface protection and load dispersion: Deploy timber mat.	• Spreads the load over a larger area. • Easy to deploy. • Applicable for ultimate failure, buried utility failure, and service limit failure.	• Efficiency (e.g., labor intensive).
Surface protection and load dispersion: Deploy concrete slab.	• Spreads the load over a larger area. • Applicable for ultimate failure, buried utility failure, and service limit failure.	• Cost (e.g., design, materials, and placement). • Time consuming.
Surface protection and load dispersion: Provide aggregate base cover.	• Spreads the load over a larger area. • Applicable for ultimate failure, buried utility failure, and service limit failure.	• Cost (e.g., relatively lower cost for design, materials, and placement). • Time consuming.
Increase the clearance from the sloped edge.	• Easy to apply.	• Applicable only for sloped-shoulder failure.
Reduce the operating pressure in the pipe.	• Easy to apply.	• Applicable only for flexible buried utility failure.
Reassemble SHL-vehicle configuration.	• Applicable for ultimate failure, buried utility failure, and service limit failure.	• Cost. • Constraints related to axle spacing and capacity.
Reroute.	• Applicable for ultimate failure, buried utility failure, and service limit failure.	• Traffic control. • Longer hauling distances.

CHAPTER 3. VERIFICATION AND CALIBRATION

As part of this project, a comprehensive experimental program was carried out to verify and calibrate multiple theoretical approaches that were developed in this study. This program utilized a full-scale pavement/soil testing facility (large-scale box). A total of five large-scale box experiments were performed, and they all represent typical pavement structures. Specific characteristics of the experiments are presented in table 7. All experiments had, whenever applicable, the same layer thicknesses for AC, CAB, and SG.

Table 7. Large-scale box experiments.

Experiment No.	Description	Loading Protocol
1	• SG only (no AC or CAB). • Apply loads on top of the SG.	• Apply dynamic loads of different amplitudes simulating the FWD loading for low number of cycles. • Apply increasing static load until failure using 11.9-inch circular steel plate.
2	• Unbound materials only (CAB and SG). • Apply loads on top of the CAB.	• Apply dynamic loads of different amplitudes simulating the FWD loading for low number of cycles. • Apply increasing static load until failure using 11.9-inch circular steel plate.
3	• Control section (full pavement structure: AC, CAB, and SG). • Apply loads on top of the AC layer.	• Apply dynamic loads of different amplitudes simulating the FWD loading for low number of cycles. • Apply increasing static load until failure using 11.9-inch circular steel plate.
4	• Impact of sloped shoulder (full pavement structure: AC, CAB, and SG with 1:1.5 side slope). • Apply loads on top of the AC layer.	• Apply dynamic loads of different amplitudes simulating the FWD loading at three locations: 12, 24, and 36 inches from the edge of the slope. • Apply increasing static load until failure using 11.9-inch circular steel plate.
5	• Impact of loading on two buried utilities (full pavement structure: AC, CAB, and SG). • Apply loads on top of the AC layer at three different locations.	• Apply dynamic loads of different amplitudes simulating the FWD loading for low number of cycles. • Apply increasing static load until failure using 11.9-inch circular steel plate.

Each experiment was extensively instrumented to provide a comprehensive database of the system response. In all cases, the vehicular loading was simulated by applying hydraulically the FWD type of loading on an 11.9-inch diameter circular plate. Each load pulse duration was 0.1 s with 0.9 s of rest period. Linear variable differential transformers (LVDTs) were used to record pavement surface deformations up to 60 inches from the center of the surface load. Surface and embedded accelerometers were installed to measure accelerations at various locations that in turn can be used to estimate the displacements at the same locations. Total earth pressure cells (TEPCs) were used to capture the stresses induced in the CAB and SG layers due to surface

loading. Strain gauges were attached to the AC layer as well as the utility pipe to provide the strain distribution resulting from the surface loading.

At different stages of the verification and calibration process, as needed, numerical modeling using 3D-Move ENHANCED, ILLI-PAVE, and BAKFAA software was employed.[11,38,39] In addition, FWD measurements as well as laboratory material testing were obtained from the National Airport Pavement Test Facility (NAPTF) of the Federal Aviation Administration and from the APT at the University of Costa Rica (UCR), known as LanammeUCR. In this chapter, brief descriptions of the large-scale box experiments, recorded measurements, and observations are presented first, followed by details on the verification and calibration exercises.

3.1. LARGE-SCALE BOX DESCRIPTION

The experimental program of this project required a large container to achieve the program's objectives. Thus, the research team designed, fabricated, and built a large-scale box with internal dimensions of 124 by 124 by 72 inches. Figure 34 shows the drawing of the large-scale box. The large-scale box consisted of a steel base plate, vertical H-shaped steel columns infilled with 4- by 6-inch wood beams and braced at two levels with steel beams and tension rods to act as a lateral bracing system.

The steel base plate was grouted to the laboratory floor, followed by 20 steel columns appropriately aligned and welded to the base plate. After the assembly of the steel columns, a total of 224 wood beams of 4 by 6 by 120 inches were fitted between the columns. Polyvinyl chloride foam boards were used as filler between the gap inside the web of the columns and the wood beams. A screw/nut fastening method was used to install the bracing system that consisted of eight steel beams and four tension rods.

The experimental setup, characterization of material used in the experiments, construction practice, and instrumentation plans for each experiment are explained in detail in Volume II: Appendix A.[1]
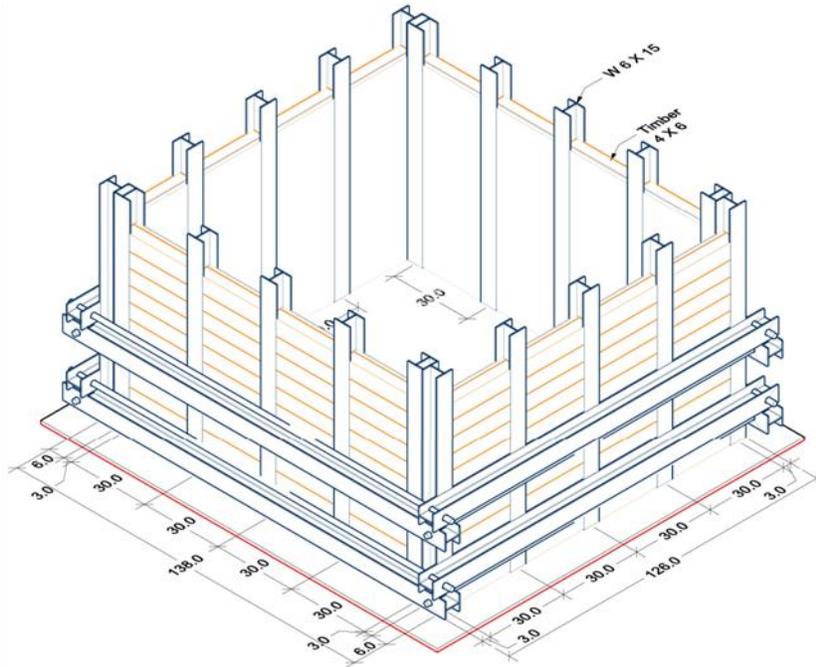
Note: All dimensions are in inches.

Figure 34. Illustration. 3D schematic of large-scale box.

3.2. VERIFICATION AND CALIBRATION EXERCISE

As presented in table 8, multiple theoretical procedures developed in this study were verified or calibrated using experimental testing and numerical modeling. The processes associated with the verification and calibration exercises are described in this section.

Table 8. Elements of verification and calibration exercise.

Objective	Large-Scale Experiments Exercise	Numerical Modeling Exercise	APTs Data Exercise
Verification of 3D-Move ENHANCED	• Experiment No. 1. • Experiment No. 2. • Experiment No. 3.	• BAKFAA.[39] • 3D-Move ENHANCED.[11]	N/A
Verification of SG τ_{max} parameters estimation procedure	• Experiment No. 1. • Experiment No. 2. • Experiment No. 3.	• ILLI-PAVE.[38] • BAKFAA.[39] • 3D-Move ENHANCED.[11]	• NAPTF. • LanammeUCR.
Determination (calibration) of $SAF_{Shoulder}$	• Experiment No. 3. • Experiment No. 4.	• BAKFAA.[39] • 3D-Move ENHANCED.[11]	N/A
Verification of sloped-shoulder failure analysis procedure	• Experiment No. 3. • Experiment No. 4.	• BAKFAA.[39] • 3D-Move ENHANCED.[11]	N/A
Determination (calibration) of $SAF_{Utility}$	• Experiment No. 3. • Experiment No. 5.	• BAKFAA.[39] • 3D-Move ENHANCED.[11]	N/A
Verification of buried utility risk analysis procedure	• Experiment No. 3. • Experiment No. 5.	• BAKFAA.[39] • 3D-Move ENHANCED.[11]	N/A

N/A = not applicable.

3.2.1. Verification of 3D-Move ENHANCED

As previously stated, the analysis procedures developed and implemented in SuperPACK require the pavement responses that are computed by 3D-Move ENHANCED analysis engine incorporated in SuperPACK.[9,11] Therefore, verification and validation of 3D-Move ENHANCED computed responses was seen as important. To do so, the measurements recorded in experiment Nos. 1, 2, and 3 were employed.

Although experiment No. 1 consisted of 66 inches of SG layer, no AC or CAB layers were present (figure 35). In experiment No. 2, an SG layer with similar thickness and materials was paved with 6 inches of CAB (figure 36). As illustrated in figure 37, a full pavement structure was constructed in experiment No. 3 with a total thickness of 77 inches (i.e., 5 inches of AC layer, 6 inches of CAB, and 66 inches of SG). In all three experiments, the loads at different intensities were applied to the circular plate to simulate FWD-loading and -load levels at the surface (figure 38 to figure 40). Meanwhile, pavement response in terms of surface deflection and induced σ_v was monitored. As a representative example, measured pavement responses recorded from experiment No. 3 are presented in figure 41 and figure 42.
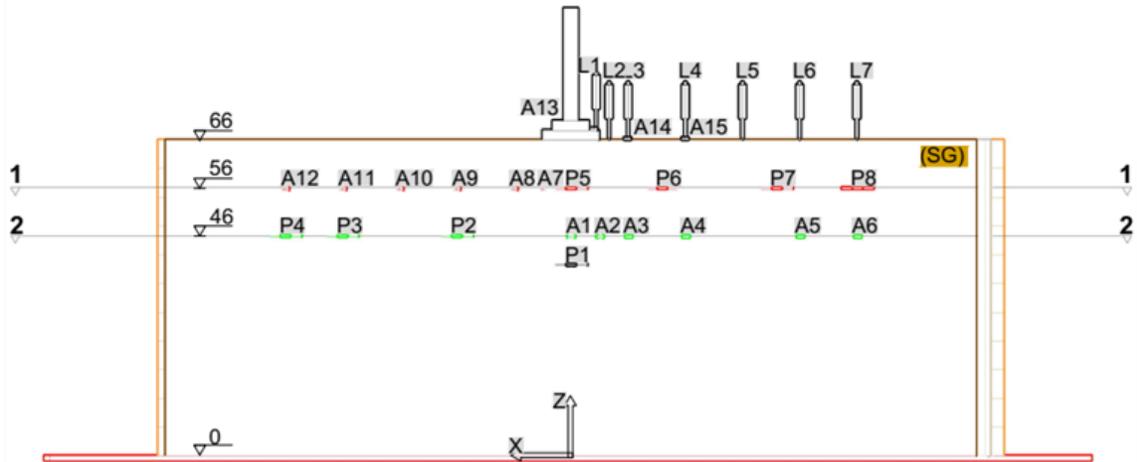
© 2018 UNR.
All dimensions are in inches; L = LVDT; P = total earth pressure cell; A = accelerometer;
S = strain gauge.

Figure 35. Illustration. Large-scale box experiment No. 1.
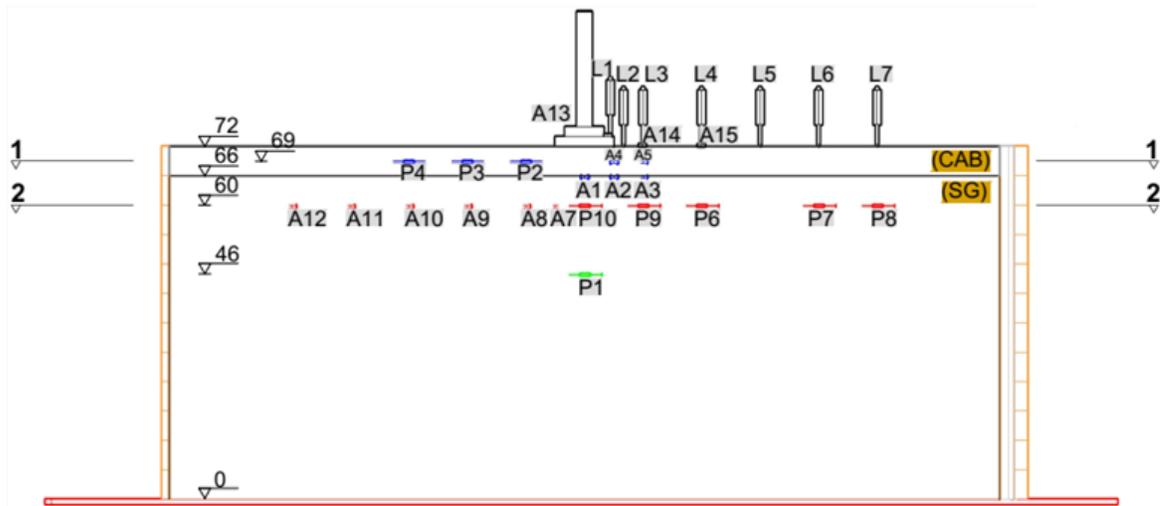
© 2018 UNR.
All dimensions are in inches; L = LVDT; P = total earth pressure cell; A = accelerometer;
S = strain gauge.

Figure 36. Illustration. Large-scale box experiment No. 2.
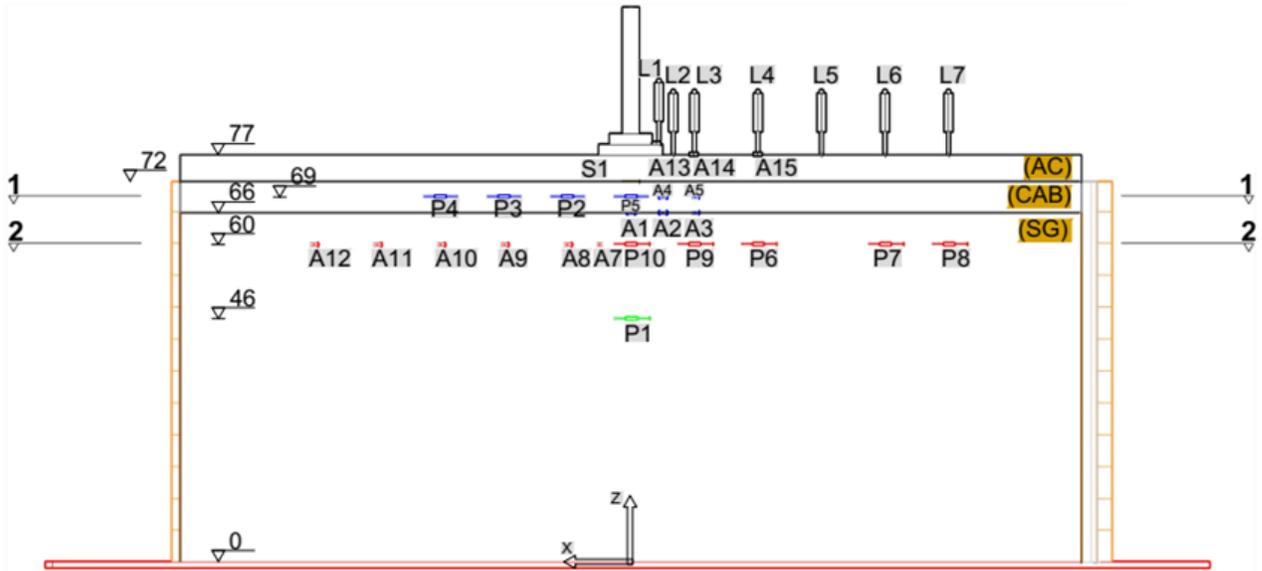
© 2018 UNR.
All dimensions are in inches; L = LVDT; P = total earth pressure cell; A = accelerometer;
S = strain gauge.

Figure 37. Illustration. Large-scale box experiment No. 3.

© 2018 UNR.

Figure 38. Photo. Completed large-scale box test setup for experiment No. 1.

Figure 39. Photo. Completed large-scale box test setup for experiment No. 2.
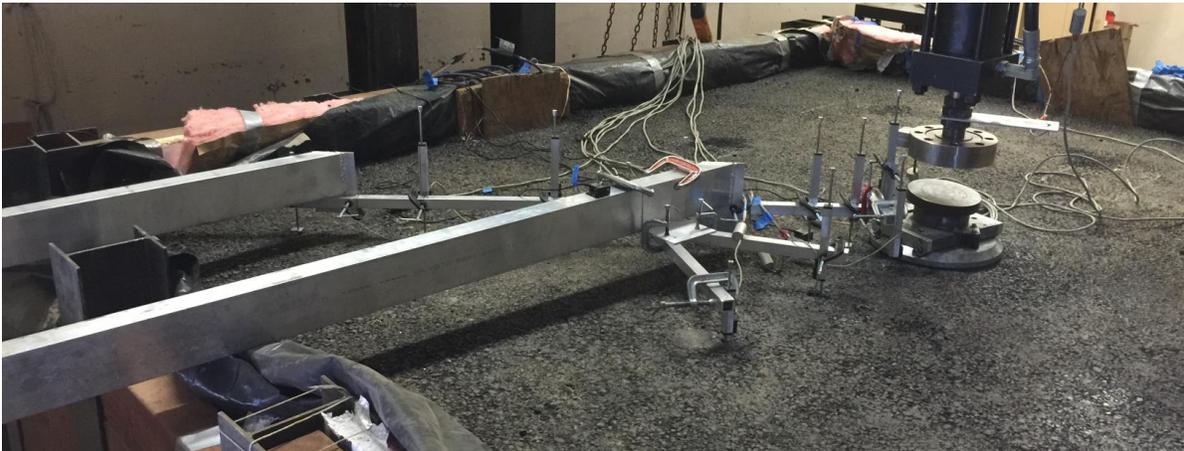
Figure 40. Photo. Completed large-scale box test setup for experiment No. 3.
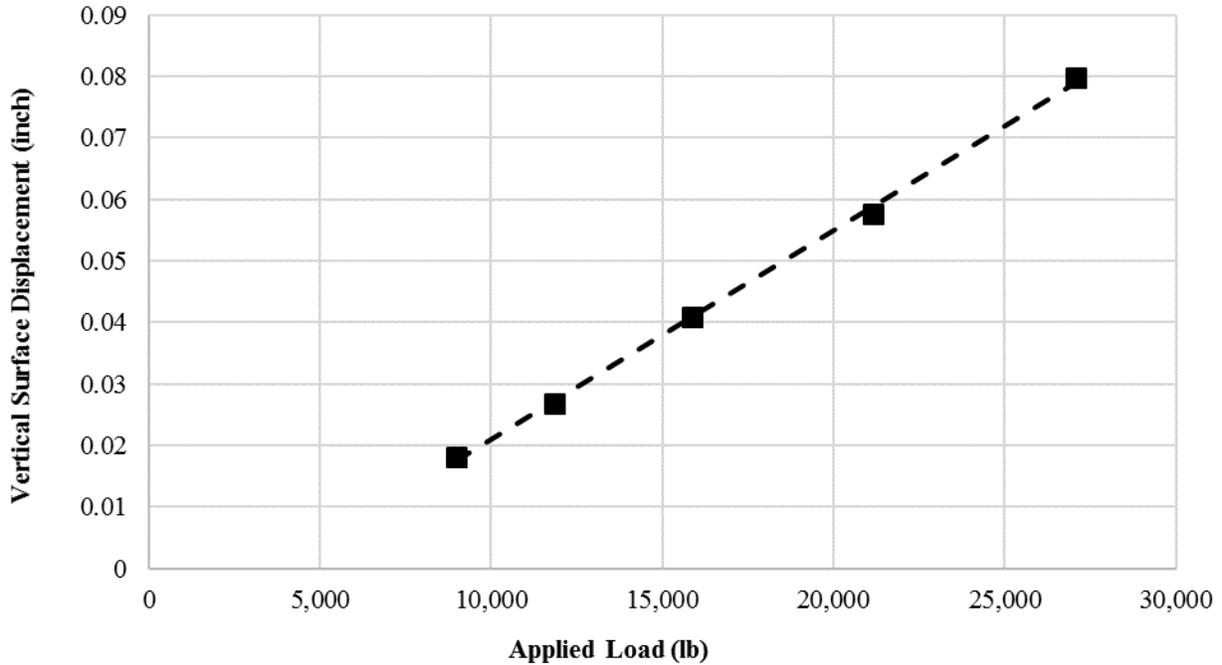
© 2018 UNR.

Figure 41. Graph. Vertical surface displacements measured by LVDT1 in experiment No. 3 at different load levels.
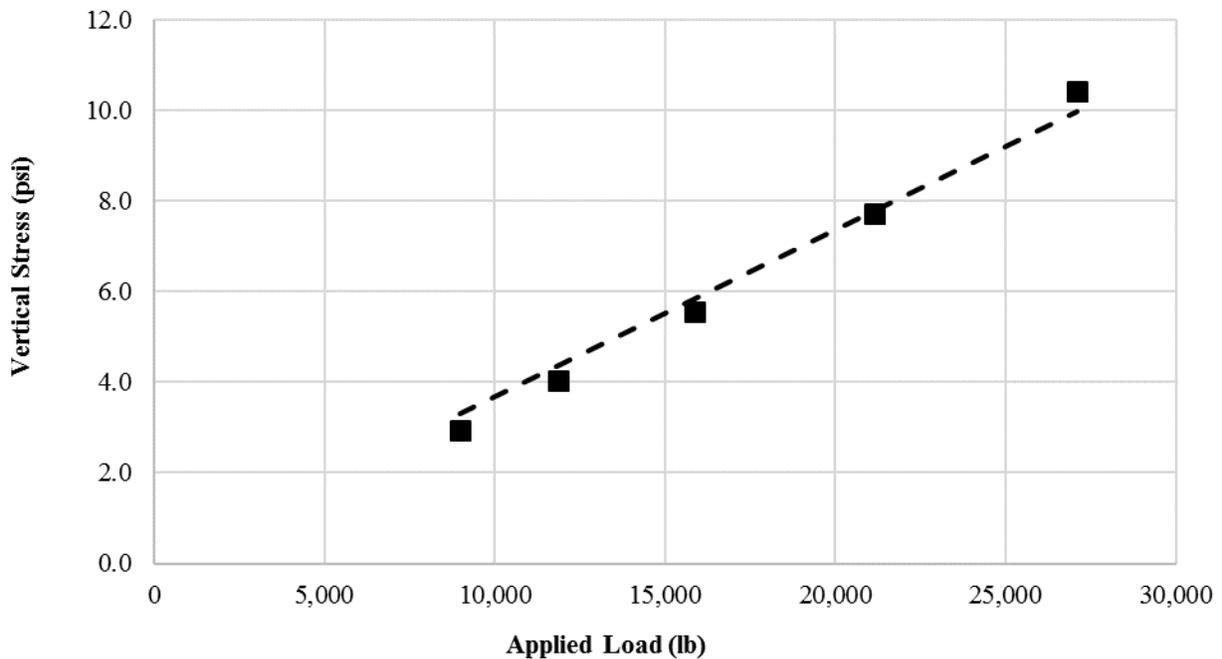
© 2018 UNR.

Figure 42. Graph. σ_v measured by TEPC1 in experiment No. 3 at different load levels.

The surface deflection basins at different load levels measured in these three experiments (experiment Nos. 1, 2, and 3) were individually employed in the backcalculation process using the program BAKFAA.[39] Subsequently, 3D-Move ENHANCED and the backcalculated layer

moduli were utilized to compute the pavement surface deflections and σ_v at the locations of LVDTs and TEPCs, respectively.[11]

Figure 43 presents the deflection basins at each of the applied load levels in experiment No. 3. Figure 44 and figure 45 depict the comparison of measured and calculated responses (i.e., surface deflection and σ_v, respectively) by 3D-Move ENHANCED using associated backcalculated moduli.[11] These figures reveal the capability of this software to estimate the load-induced surface deflections and stresses at interior locations. It should be noted that similar conclusions are presented in Volume IV: Appendix C with the measurements from experiment Nos. 1 and 2.[3]
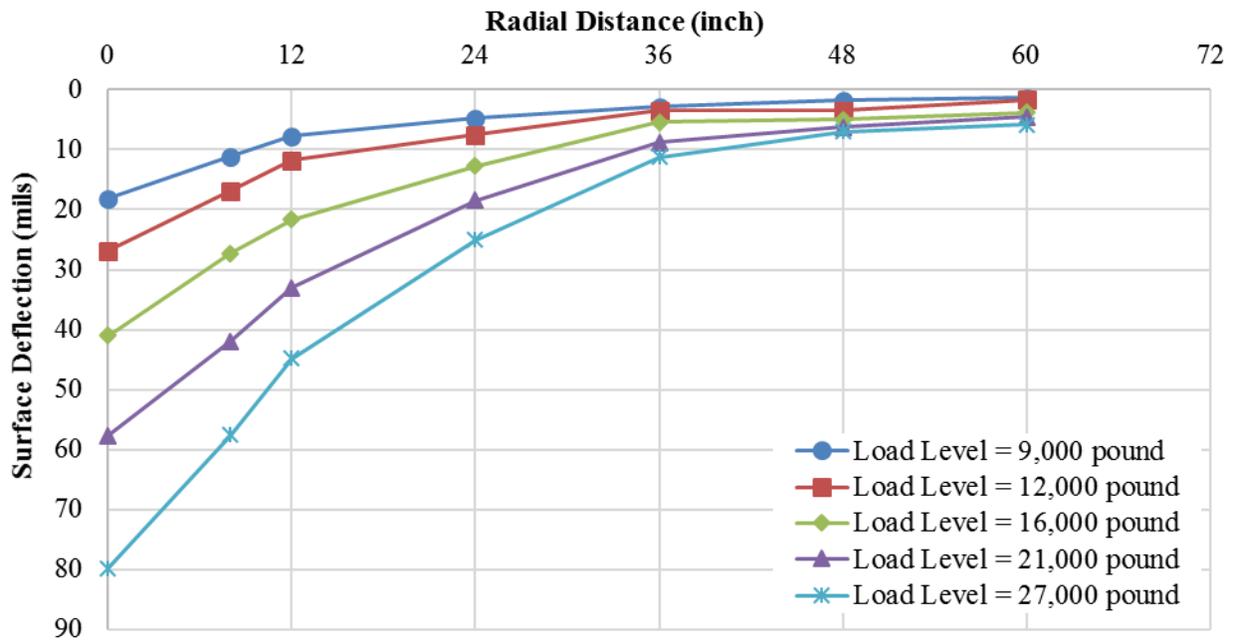
© 2018 UNR.

Figure 43. Graph. Measured deflection basin in experiment No. 3.
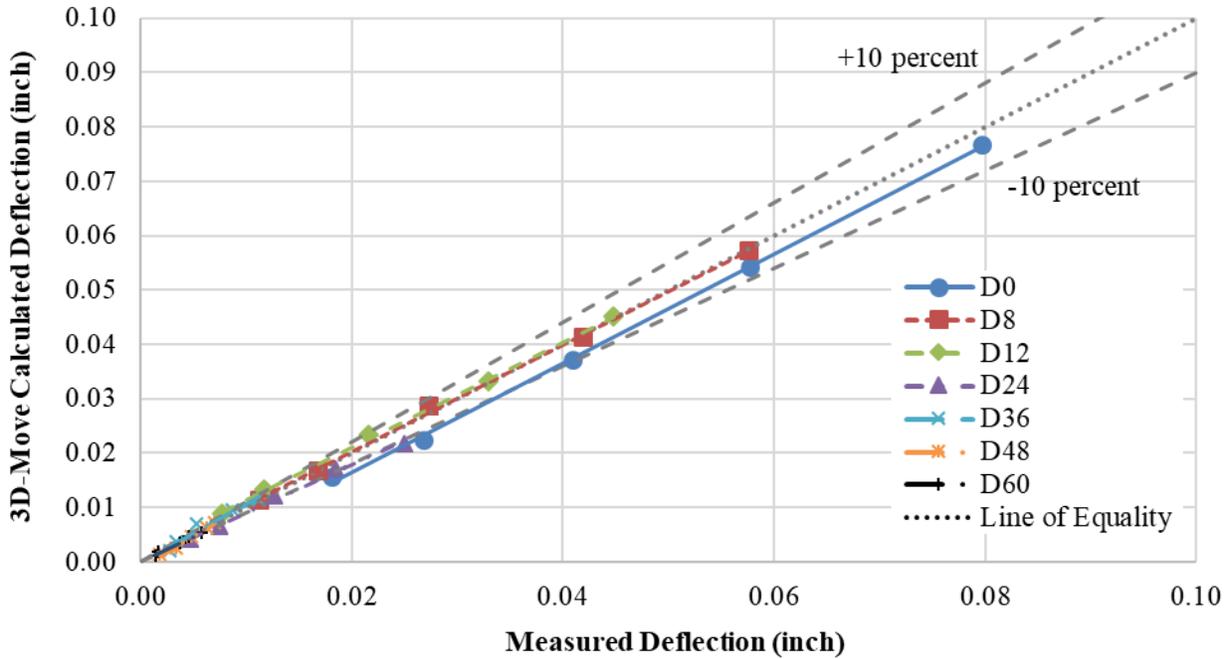
© 2018 UNR.
D = deflection.

Figure 44. Graph. Comparison between 3D-Move calculated deflections and measured surface deflections in experiment No. 3.
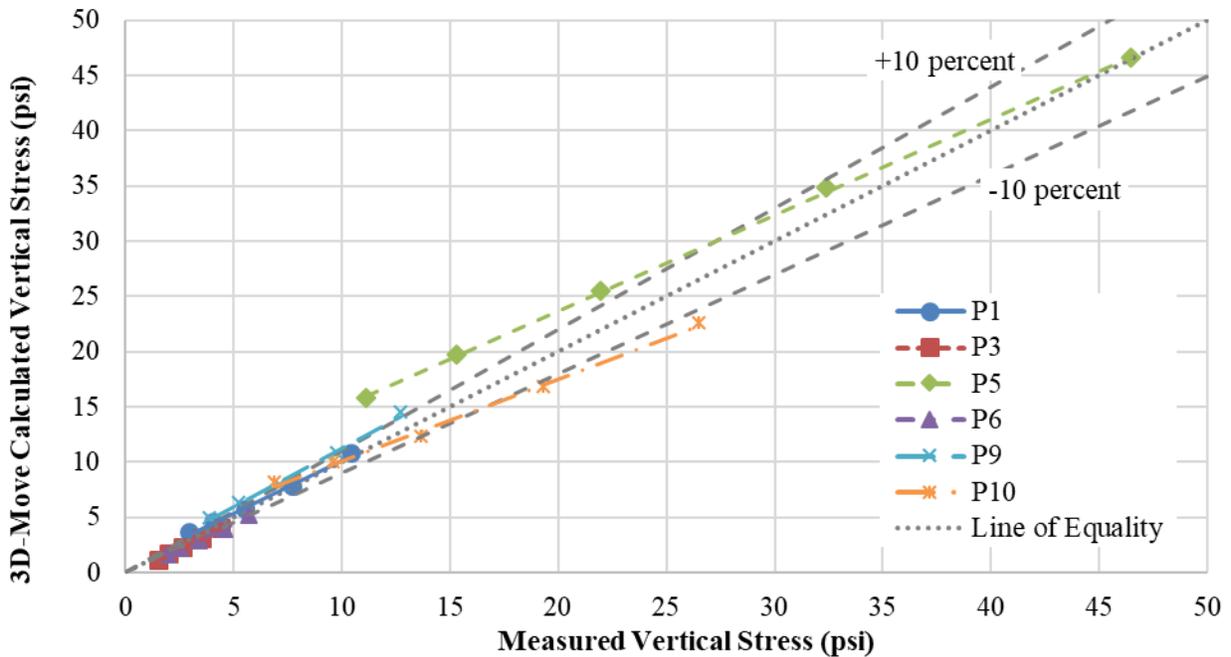
© 2018 UNR.
P = total earth pressure cell.

Figure 45. Graph. Comparison between 3D-Move calculated σ_v and measured σ_v in experiment No. 3.

3.2.2. Verification of SG τ_{max} Parameters Estimation Procedure

The SG layer ϕ and c are necessary inputs for investigating the likelihood of ultimate and localized shear failure as well as pavement shoulder slope stability under SHL movement. In this study, an FWD-based procedure for estimating in situ τ_{max} parameters of the SG was developed. Detailed description of the procedure as well as verification using numerical modeling, large-scale box experiments, and measurements from APTs are provided in Volume V: Appendix D.[4] In this section, a summary of the verification process undertaken is presented.

It is known that FWD-load levels and the associated state of stresses in the SG layer do not reach the failure state of the materials. The main concept behind this FWD-based procedure is to extend the data obtained at lower stress levels to the failure state by implementing the nonlinear hyperbolic stress–strain relationship of unbound material. This enables the estimation of σ_{df} (asymptotic value) and subsequent estimation of τ_{max} parameters.

In this study, an extrapolation of the hyperbolic relationship using measured data at a lower state of stresses was examined first by means of measured triaxial test results. To this end, the available results of consolidated undrained triaxial tests without pore-water measurements conducted on two different types of soils (i.e., clayey sand with gravel and Dupont clay) were employed. For each set of triaxial test results, σ_d up to the cutoff levels of 20, 30, 40, and 50 percent of σ_{df} and corresponding ε_l were individually used to develop the linear form of the hyperbolic relationship. Consequently, the estimated σ_{df} using many sets of truncated data was determined.

Figure 46 and figure 47 depict the estimated σ_{df} normalized by the measured σ_{df} (i.e., from triaxial tests) for different cutoff levels of 20, 30, 40, and 50 percent of the measured σ_{df}. It can be seen that, at the cutoff level of 50 percent, the estimated σ_{df} is reasonably close to the measured value (i.e., less than 15 percent difference). Hence, it was concluded that when the state of σ_d in a triaxial test reaches approximately 50 percent of σ_{df}, the hyperbolic relationship can be utilized to obtain the needed asymptotic value (i.e., σ_{df}).

The validation process to investigate the feasibility of FWD measurements to estimate the strength parameters was then continued by numerically simulating the FWD test using ILLI-PAVE software.[38] The FWD measurements acquired from experiment Nos. 1, 2, and 3 were also employed for the verification purpose and compared against the laboratory triaxial test results. In addition, the FWD measurements conducted at NAPTF and LanammeUCR were subsequently utilized.
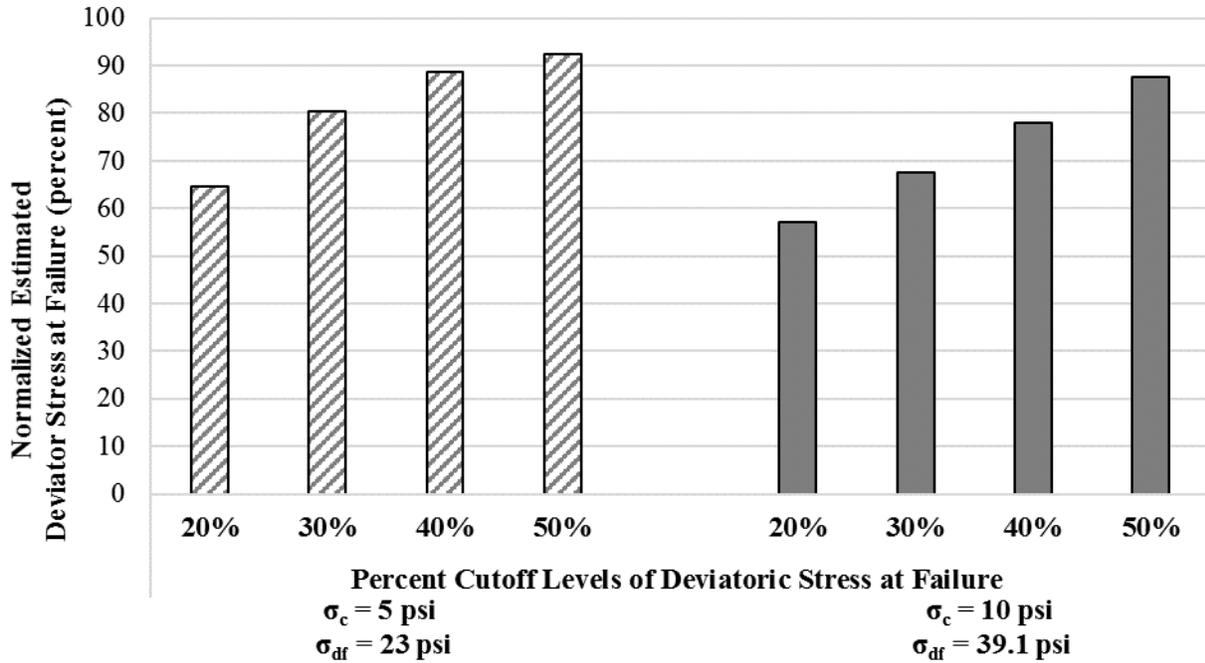
© 2018 UNR.

Figure 46. Bar chart. Normalized estimated σ_d using datasets at different cutoff levels of measured data for clayey sand with gravel.
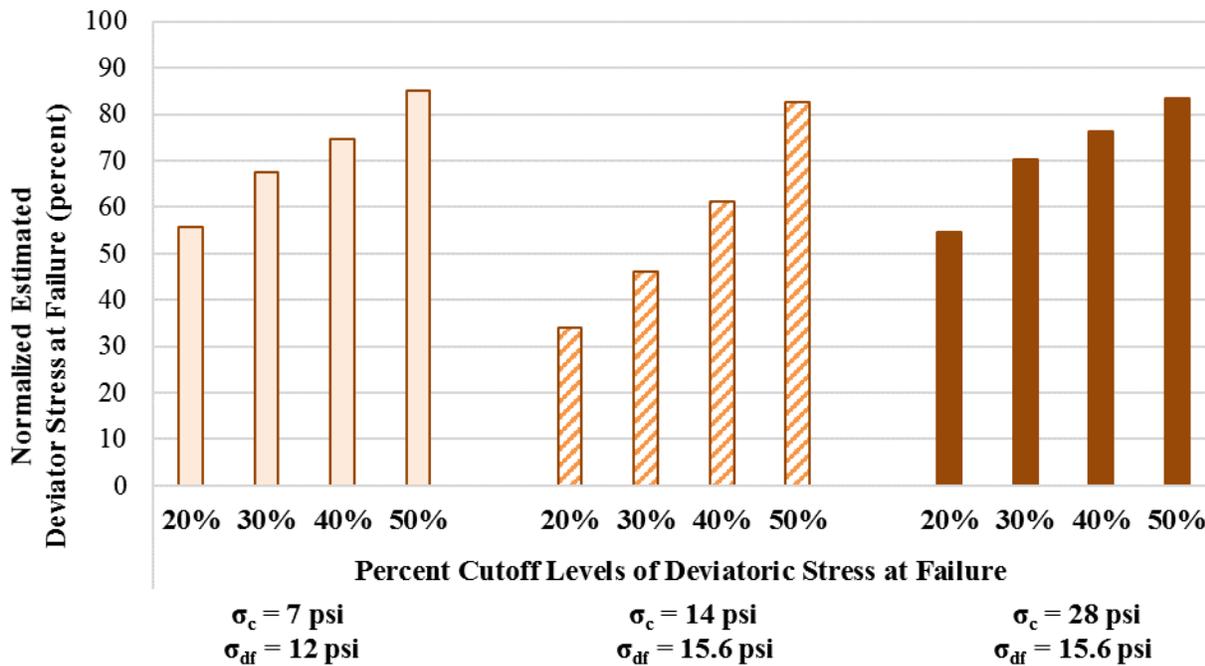
© 2018 UNR.

Figure 47. Bar chart. Normalized estimated σ_d using datasets at different cutoff levels of measured data for Dupont clay.

A detailed presentation of the verification process for unpaved and paved pavement structures can be found in Volume V: Appendix D.[4] Figure 48 represents the results of the verification

exercise, which compares the estimated τ_{max} properties using the FWD-based procedure with the measured ones. In summary, it was found that the proposed FWD-based methodology can reasonably estimate the τ_{max} properties (ϕ and c) of an SG layer with softening behavior. Such results were achieved when the highest induced σ_d level in the SG layer under the FWD loading was in excess of approximately 30 percent of the σ_{df} obtained with the proposed approach. It should be noted that the hardening behavior for an SG material at the FWD state of stress indicated by a negative slope of ε_1/σ_d versus ε_1 is recognized as a limitation of the proposed approach.
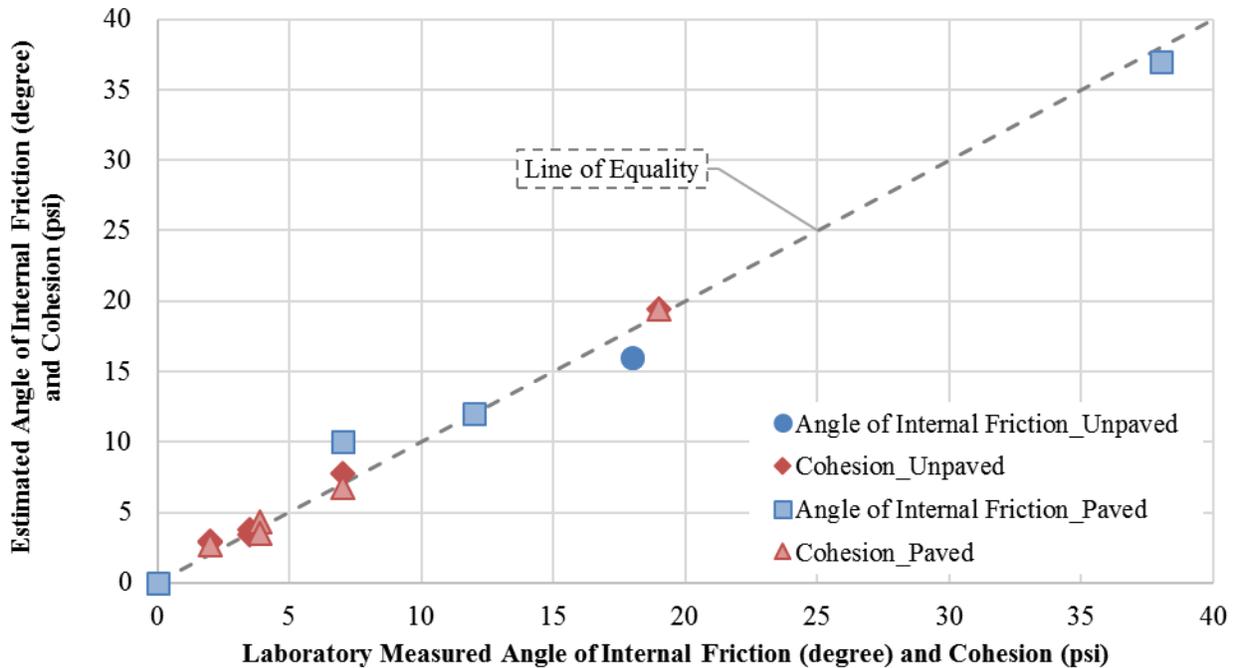
© 2018 UNR.

Figure 48. Graph. Estimated versus measured τ_{max} parameters.

3.2.3. Determination of $SAF_{Shoulder}$

As previously stated, the slope stability wedge method, which examines the sloped-shoulder failure, requires SHL vehicle–induced horizontal stresses at the location of the vertical plane of possible failure wedge. In this study, 3D-Move ENHANCED provides the load-induced stresses so that the horizontal deriving force due to a surcharge SHL-vehicle load is estimated.[11] The computed horizontal stresses, which are obtained assuming that the pavement layers extend laterally to infinity, are then modified using an $SAF_{Shoulder}$.

To determine the $SAF_{Shoulder}$, which accounts for the sloping soil domain (i.e., existence of sloped shoulder), large-scale experiments comprising a typical pavement structure with and without a sloped edge were designed and carried out. It is believed that a careful comparison between experiment No. 4 (which consisted of a sloped wedge) and experiment No. 3 (which was a control experiment and had no sloped pavement shoulder) can help to identify the role of a sloped edge in the stress distribution within a typical pavement structure.

Figure 49 and figure 50 illustrate the test setup for experiment No. 4. Detailed discussions regarding the construction and instrumentation plan can be found in Volume II: Appendix A.[1] Similar to experiment No. 3, the pavement structure consisted of 5 inches of AC on top of 6 inches of CAB and 66 inches of SG soil. However, the pavement structure in experiment No. 4 included a side slope of 1:1.5 (33.7 degrees with the horizontal), and the surface FWD loading at multiple levels was applied on top of the AC layer at three locations—12 inches (Loc12), 24 inches (Loc24), and 36 inches (Loc36)—from the edge of the slope. In this section, examples of experimental measurements and exercises conducted to determine the $SAF_{Shoulder}$ are presented. Detailed descriptions and extensive discussion are provided in Volume: VII Appendix F.[6]
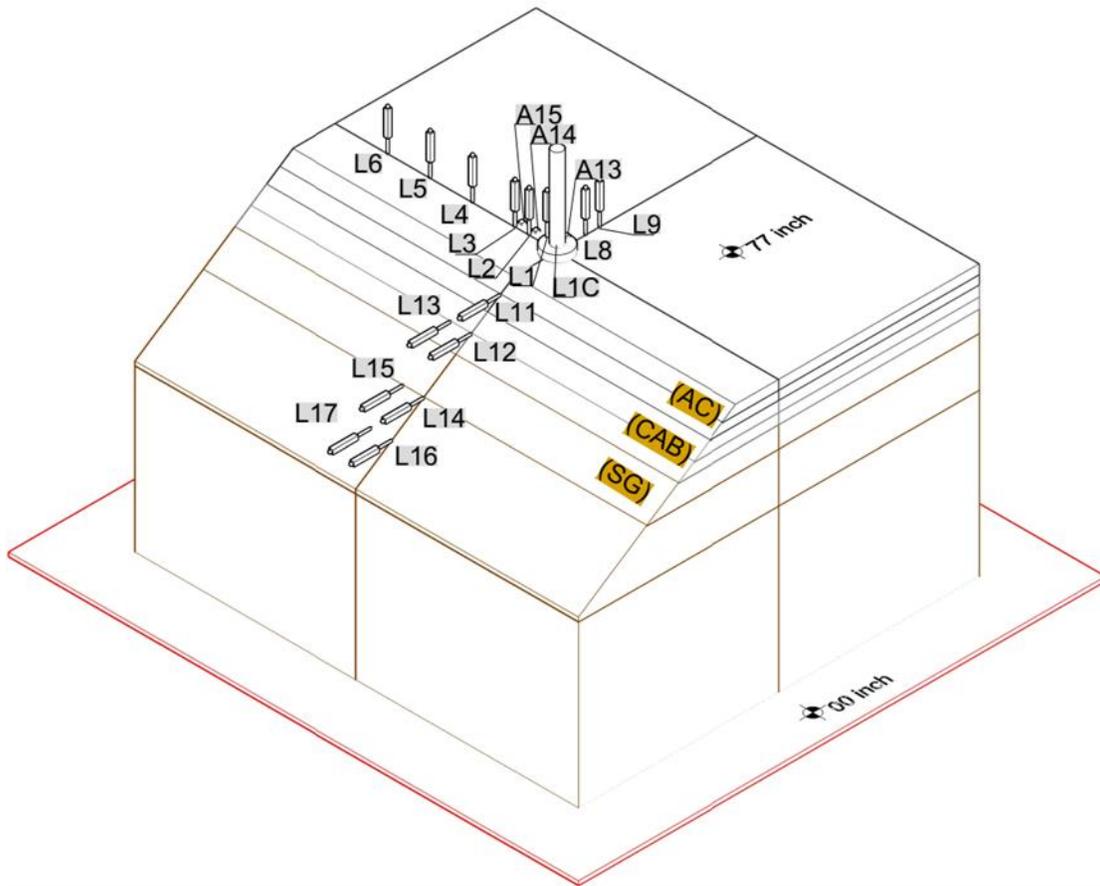
© 2018 UNR.
All dimensions are in inches; L = LVDT; P = total earth pressure cell; A = accelerometer; S = strain gauge.

Figure 49. Illustration. 3D view of large-scale box test setup for experiment No. 4.

© 2018 UNR.

Figure 50. Photo. Completed large-scale box test setup for experiment No. 4.

Figure 51 shows the measured σ_v in the SG on the nonslope side of the pavement structure with respect to the location of the surface-applied load. In comparison with the corresponding measured stresses in experiment No. 3, the stress distribution in the nonslope side of a pavement structure was not affected by the sloped edge.
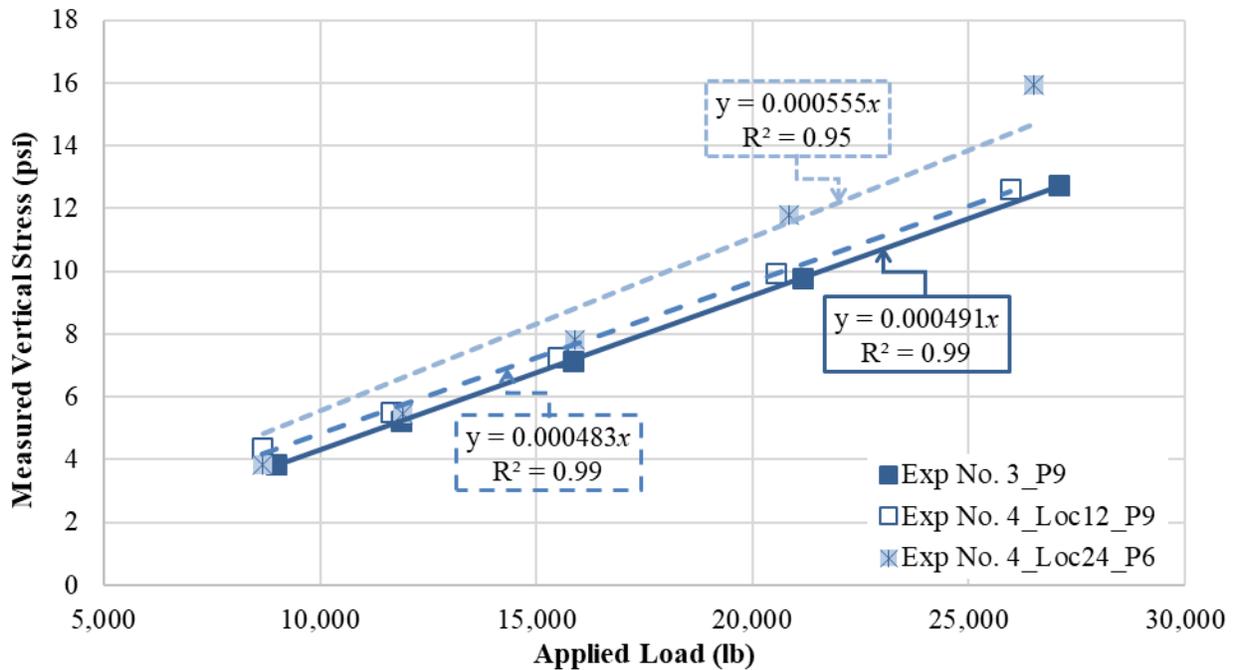
© 2018 UNR.

Figure 51. Graph. Comparison between measured σ_v in experiment No. 4 and experiment No. 3, nonslope side, 6 inches from SG surface, offset from the centerline of the load equal to 12 inches.

Figure 52 represents the load-induced σ_v measured by the TEPCs, which were installed exactly under the centerline of the load. A noticeable increase in the measured σ_v in experiment No. 4 compared to experiment No. 3 can be inferred from this figure.
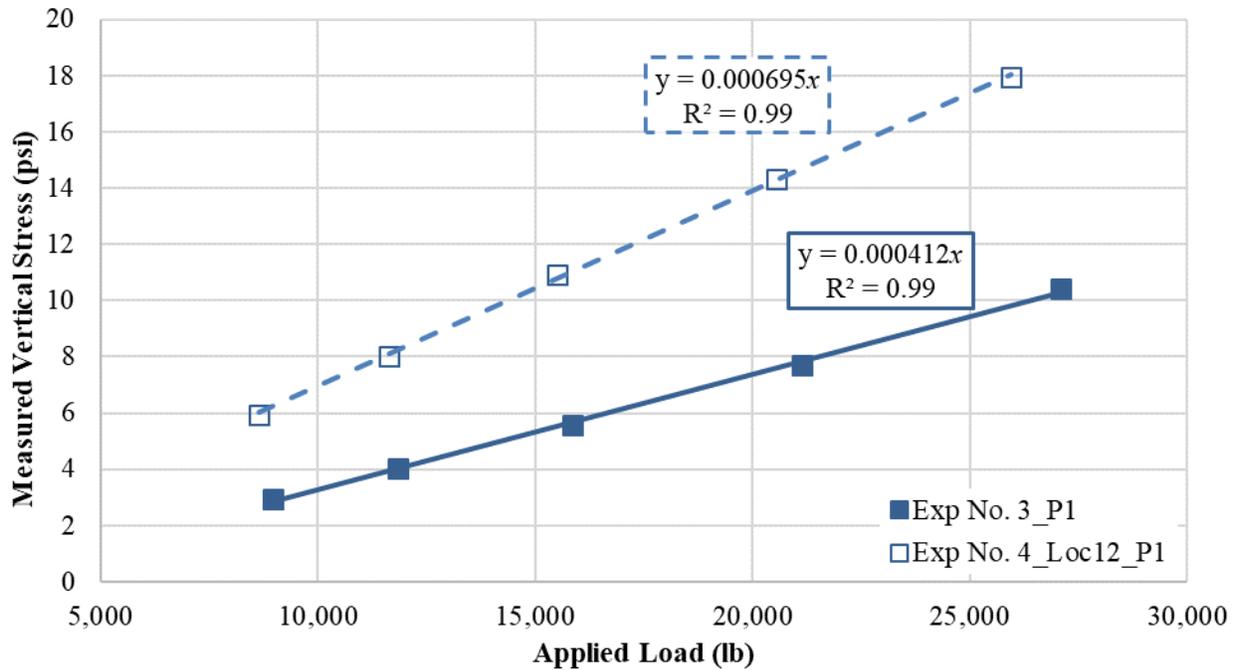
© 2018 UNR.

Figure 52. Graph. Comparison between measured σ_v in experiment No. 4 and experiment No. 3, 20 inches from SG surface, centerline of the load.

Figure 53 depicts the measured σ_v at the location of TEPCs where they were located in the slope side with respect to the applied surface load in experiment No. 4. In comparison to the matching locations in experiment No. 3, substantially higher stresses were induced by the surface load, which is attributed to the role of the sloped edge on the stress distribution. In summary, after comprehensively reviewing and comparing the σ_v recorded in experiment Nos. 3 and 4, it was concluded that the sloped shoulder plays a major role in the stress distribution within a pavement structure, particularly in the slope side.

$y = 0.000833x$
$R^2 = 0.99$

$y = 0.000807x$
$R^2 = 0.99$

$y = 0.000461x$
$R^2 = 0.99$

■ Exp No. 3_P9
□ Exp No. 4_Loc12_P9S
✕ Exp No. 4_Loc24_P10
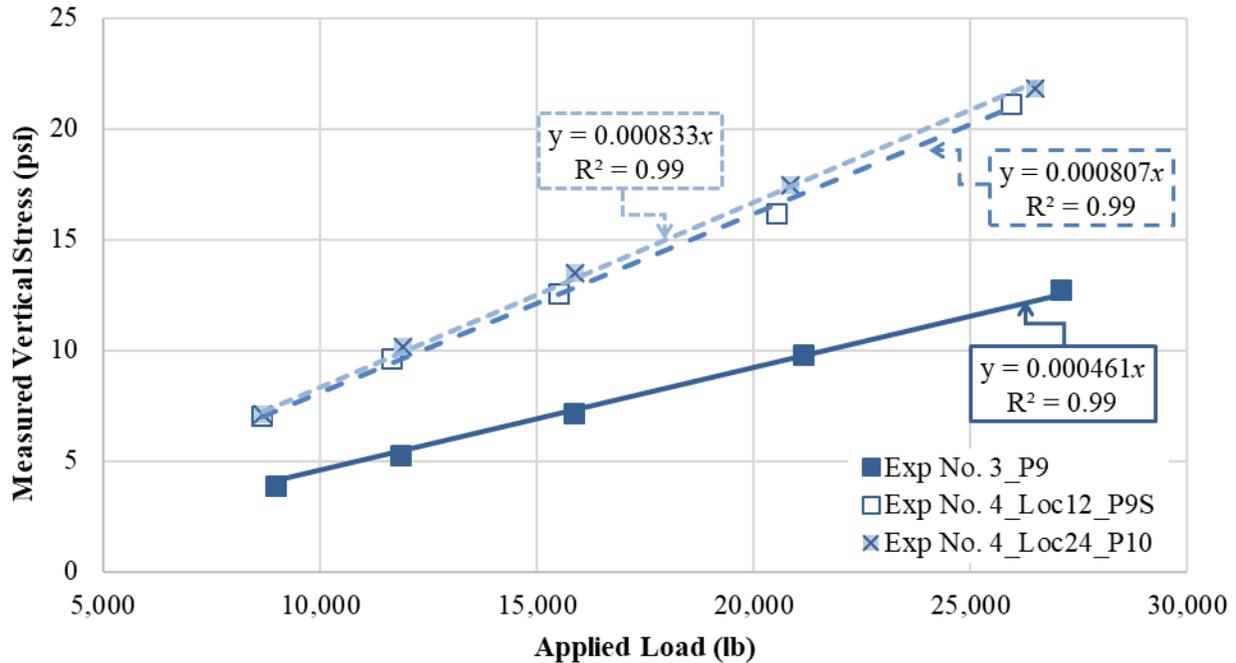
Figure 53. Graph. Comparison between measured σ_v in experiment No. 4 and experiment No. 3, slope side, 6 inches from SG surface, offset from the centerline of the load equal to 12 inches.

To determine an $SAF_{Shoulder}$, the measured σ_v at the location of TEPCs in experiment No. 4 were compared against the respective calculated stresses using 3D-Move ENHANCED along with the backcalculated moduli for the various layers from experiment No. 3.[11] Experiment No. 3 was intended to be a control experiment representing a pavement structure without any sloped shoulder (i.e., laterally extended to infinity).

A summary of the comparative exercise is represented in table 9. The data in the table show $SAF_{Shoulder}$ ranges between 1.4 and 1.8 (average of 1.63), depending on the depth within the SG and the location from the applied surface load. It is recommended that a single $SAF_{Shoulder}$ equal to 1.6 be applied to the computed horizontal stresses by 3D-Move ENHANCED when sloped shoulders are present.[11]

Table 9. Summary of comparison between stresses measured in experiment No. 4 and computed by 3D-Move Analysis software.

Pressure Cell	Depth From the SG Surface (Inches)	Surface-Load Location in Experiment No. 4	Offset From Centerline of the Load (Inches)	$SAF_{Shoulder}$
P1	20	Loc12	0	1.4
P10	6	Loc12	0	1.8
P1	20	Loc24	12	1.6
P1	20	Loc36	24	1.6
P9S	6	Loc12	12	1.6
P10	6	Loc24	12	1.6
P10	6	Loc36	24	1.8

3.2.4. Verification of Sloped-Shoulder Failure Analysis Procedure

To evaluate the applicability of the proposed slope stability analysis using the wedge method, the FOS of the sloping edge in experiment No. 4 was determined when the FWD loads were applied at three locations (i.e., Loc12, Loc24, and Loc36). Figure 54 shows an illustration of the pavement structure and loading locations in experiment No. 4. As shown in this figure, different failure wedges with horizontal and inclined slip surfaces were considered.
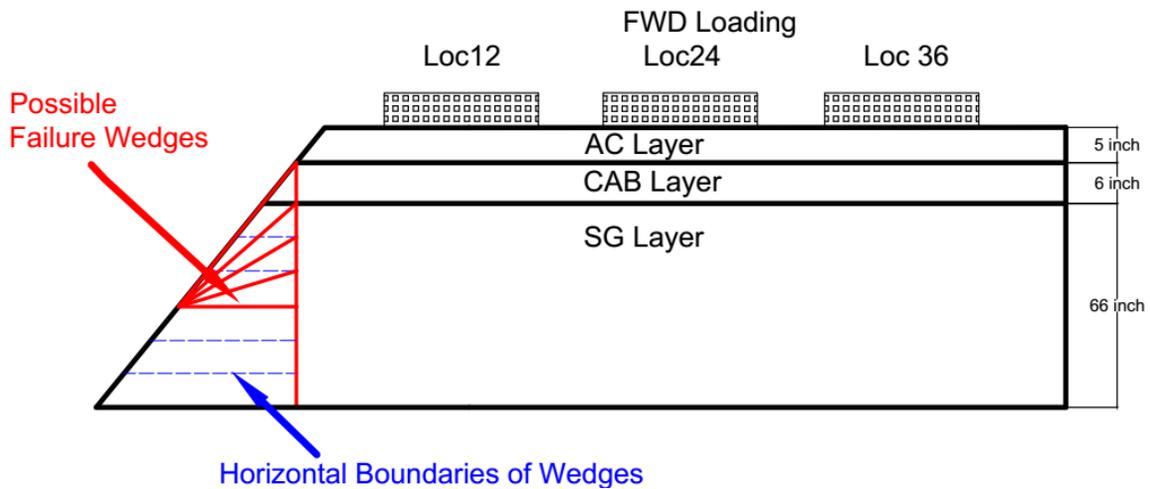
© 2018 UNR.

Figure 54. Illustration. Schematic of experiment No. 4.

The wedge method assumes plane strain condition for the slope stability analysis under the SHL vehicle since the length of SHL vehicles usually extends to a relatively large extent. However, in experiment No. 4, the FWD load was applied on the 11.9-inch circular plate, which means that the plane strain assumption does not hold true. Therefore, the wedge method was reformulated to account for the 3D domain present, which is described in Volume VII: Appendix F.[6] Figure 55 illustrates the possible 3D failure wedge as well as the force diagram in experiment No. 4 where the width of the wedge (B_{wedge}) equal to 11.9 inches (i.e., width of the FWD plate) was assumed.
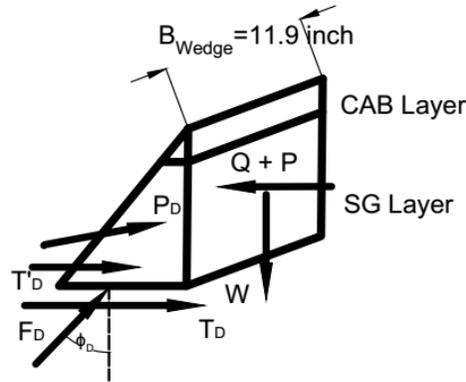
© 2018 UNR.

T'_D = developed resisting cohesion force resulting from mobilized cohesion acting on the side surfaces (i.e., front and back); P_D = resistive force from the side soil that makes an angle ϕ_D with the normal to the side surfaces (i.e., front and back).

Figure 55. Illustration. Force diagram applied on the possible failure wedge.

In this verification exercise, the highest FWD-load level (approximately 27,000 lb), which was applied at the aforementioned three locations, was considered. As for Loc12, a minimum FOS equal to 1.3 was determined for the possible failure wedge where the horizontal slip surface is located 3 inches from the SG surface (i.e., 14 inches from the pavement surface). When the FWD load was applied at Loc24 and Loc36, minimum FOS equal to 1.6 and 3.1, respectively, were determined. It should be mentioned that slope failure was not observed for the same loading cases in experiment No. 4, confirming that the proposed application of the wedge method is capable of assessing the stability of a sloping layered medium consisting of a typical pavement-layer configuration and properties.

3.2.5. Determination of $SAF_{Utility}$

Reliable risk analysis against failure of existing buried utilities due to an SHL-vehicle movement on a flexible pavement can only be achieved by appropriately assessing the SHL vehicle–induced stresses at the location of the buried utility. To this end, the computed σ_v by 3D-Move ENHANCED, in conjunction with the modification using $SAF_{Utility}$, was implemented.[11]

To determine the $SAF_{Utility}$ that accounts for the role of soil–structure interaction and discontinuities within the medium (i.e., existence of buried utilities), full-scale experiments comprising a typical pavement structure (i.e., experiment Nos. 3 and 5) were designed and carried out. As previously described, experiment No. 3 is considered the control experiment without any cavities (i.e., no buried utilities). Experiment No. 5 represents a similar pavement structure, including two types of buried utilities (flexible steel pipe and rigid concrete box culvert), which were installed in the SG (figure 56). Surface FWD loads at multiple intensities were applied directly above the centerlines of the buried utilities. Figure 57 and figure 58 illustrate the test setup for experiment No. 5. Detailed discussions regarding the construction and instrumentation plan are presented in Volume II: Appendix A.[1] In this section, the process to determine $SAF_{Utility}$ along with the important observations from experiment No. 5 are presented. Volume VII: Appendix F provides extensive discussion on this matter.[6]

Figure 56. Photo. Buried flexible steel pipe and rigid concrete box culvert in experiment No. 5.
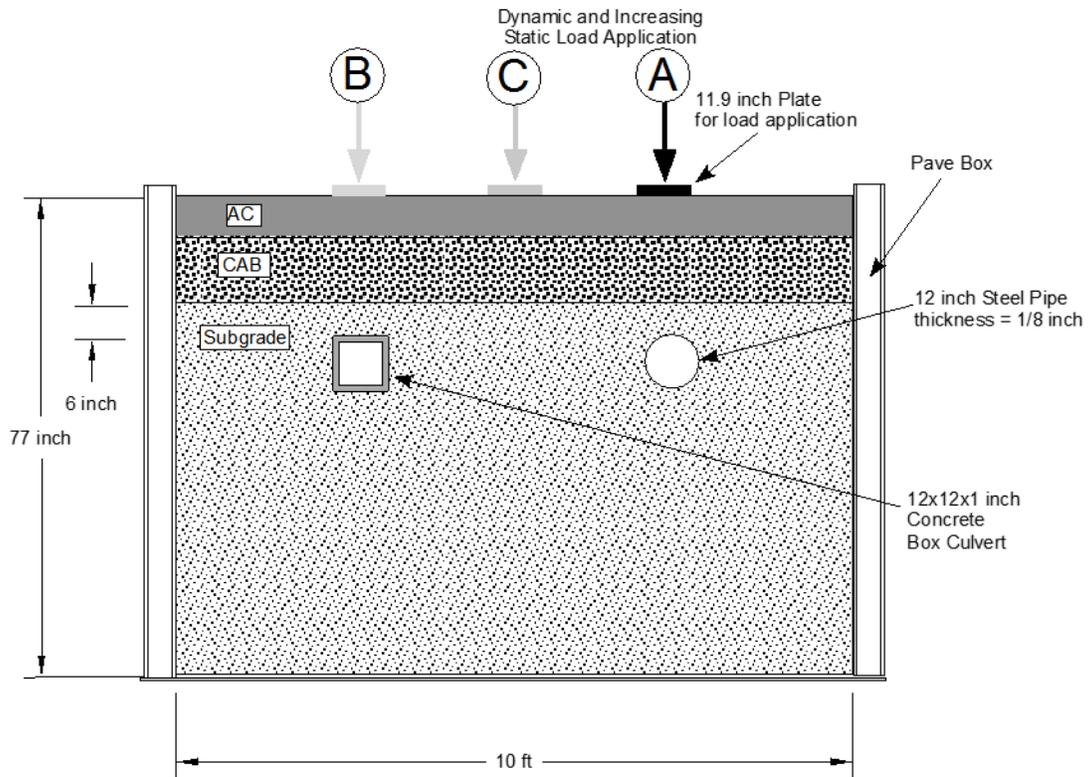
Figure 57. Illustration. Schematic of the test setup for experiment No. 5.
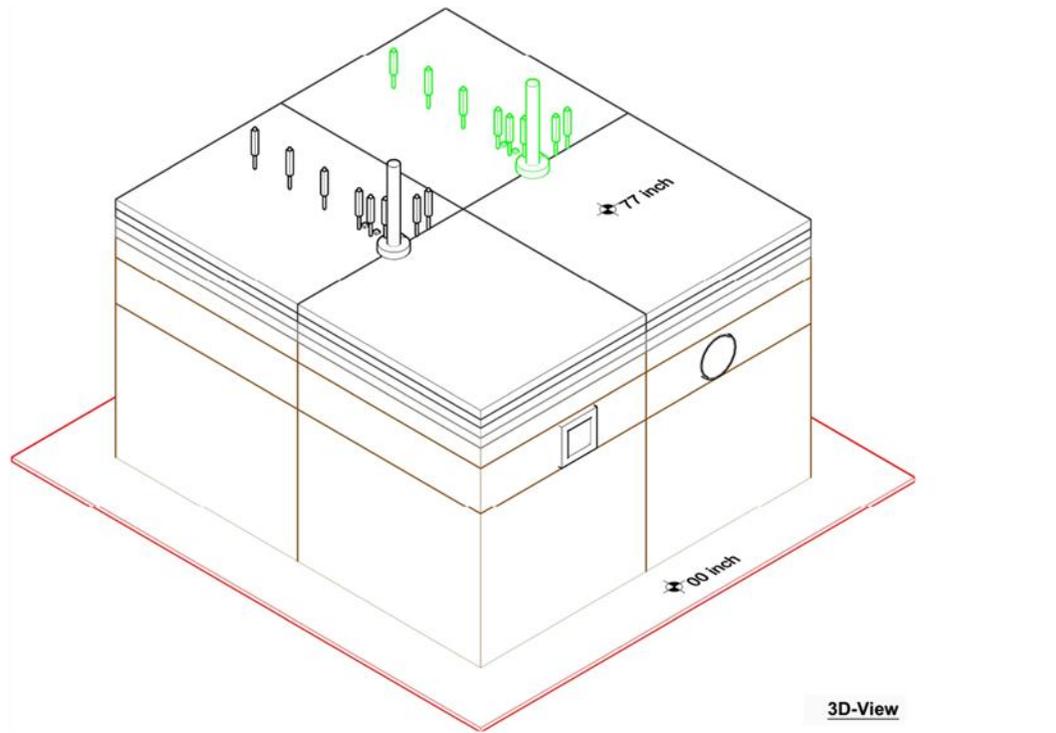
© 2018 UNR.

Figure 58. Illustration. 3D view of large-scale box test setup for experiment No. 5.

In experiment No. 5, TEPCs were installed at the top and bottom of the buried pipe and culvert to capture induced stresses due to surface loads. Data obtained from these TEPCs were compared with data obtained from TEPCs from experiment No. 3 installed at the same locations and depths.

Figure 59 shows the measured load-induced σ_v by the TEPCs installed at the top of the buried utilities when the FWD loads were applied at the centerline of the corresponding buried utility. As shown in this figure, the σ_v experienced by the flexible pipe are much lower than those stresses distributed in experiment No. 3 when buried utilities were not present. However, the load-induced σ_v in experiment No. 5 recorded at the top of the rigid culvert are higher than the measurements in experiment No. 3.

Figure 60 shows the measured σ_v by TEPCs installed at the bottom of the buried utilities in experiment No. 5 and the TEPCs located at the same depth and location in experiment No. 3 as a function of applied surface load. As shown, there is not much change in the stresses due to the presence of the flexible pipe. One possible explanation for this observation is that the presence of the flexible pipe redistributed the stresses and affected the stress flow near and around the pipe. However, substantially lower σ_v at the bottom of concrete culvert compared to the corresponding measurements in experiment No. 3 were observed. These observations can be attributed to the soil–structure interaction and higher rigidity (i.e., stiffness) of concrete culvert with respect to the surrounding SG soil.

55
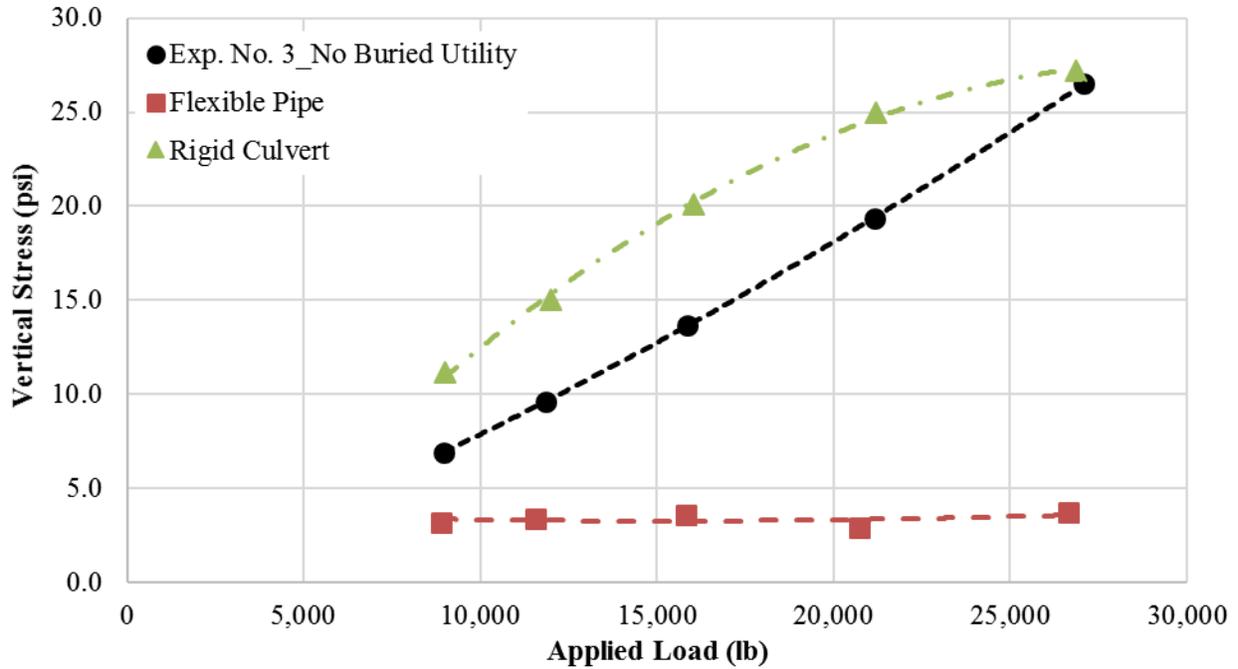
Figure 59. Graph. Measured σ_v in experiment No. 3 and top of buried utilities in experiment No. 5.
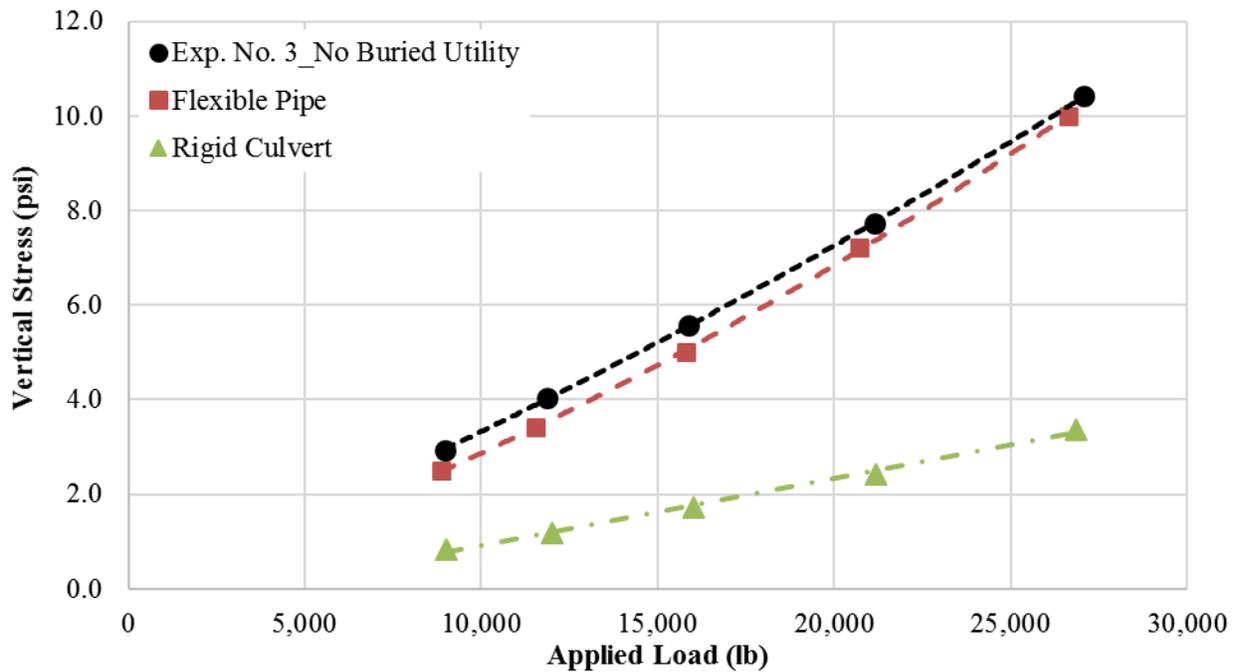
Figure 60. Graph. Measured σ_v in experiment No. 3 and bottom of buried utilities in experiment No. 5.

The aforementioned observations revealed that the existence of buried utilities in the pavement structure significantly influences the stress distribution within the pavement layers, indicating a

need for modification of computed σ_v using 3D-Move ENHANCED.[11] To this end, the measured stresses at the location of TEPCs in experiment No. 5 were compared against the respective computed stresses from 3D-Move ENHANCED. As before, the backcalculated moduli for the various layers from experiment No. 3 were used in 3D-Move simulations.

As depicted in figure 61, a linear fit with 0 A was imposed on datasets of σ_v, computed by 3D-Move ENHANCED, as well as on those measured at the top of buried utilities (i.e., flexible pipe and rigid culvert).[11] Although a linear fitting may not necessarily fit the measured data, it represents a convenient step. This figure implies that the computed σ_v are approximately four times higher than those the pipe actually experienced. Thus, an adjustment factor of 0.25 should be expected. However, such a substantial reduction in stress calculation cannot be recommended based solely on one experiment; therefore, it is recommended to retain the stress adjustment factor for flexible utilities ($SAF_{Flexible}$) for flexible pipe equal to 1. This recommendation is mainly to be on the conservative side until additional experimental testing and numerical investigations are carried out.

In the case of rigid concrete culvert, the measured σ_v on top of the box culvert are approximately 50 percent higher than those computed by 3D-Move ENHANCED.[11] According to these observations, a stress adjustment factor for rigid utilities (SAF_{Rigid}) equal to 1.5 is recommended. The examination of the data in figure 59 reveals a nonlinear behavior with respect to the response of the rigid culvert, which may skew its trend line. To eliminate the error due to nonlinearity, the data were limited to a surface load of approximately 21,000 lb.
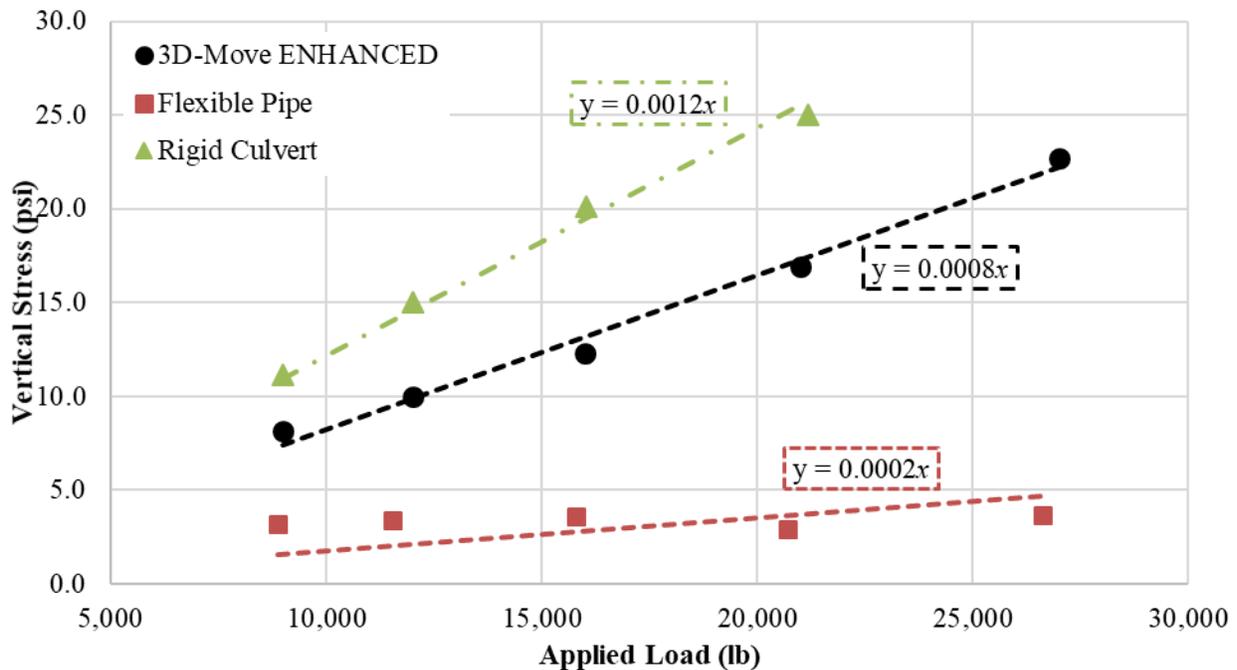
© 2018 UNR.

Figure 61. Graph. Comparison between measured and 3D-Move computed stresses at the crown of the pipe.

57

3.2.6. Verification of Buried Utility Risk Analysis Procedure

As previously noted, the analysis procedure to investigate the risk against the failure of existing buried utilities under an SHL-vehicle movement was adopted from existing well-established state of practices with a modification to stress distribution. Experiment No. 5 also provided insight into the behavior of the buried utilities under surface loading on a typical pavement structure.

In experiment No. 5, as demonstrated in figure 62, perpendicular LVDTs were installed inside the pipe under the centerline of the load to capture the horizontal and vertical deformation (change in pipe diameter). Figure 63 presents the vertical and horizontal deformations in the pipe cross section as a function of surface-load levels. The negative sign indicates that the deflection is inward, which means that the pipe diameter in the vertical direction was decreasing with load. As shown, the horizontal direction response is exactly the same but in opposite directions, leading to the conclusion that the pipe remained elastic during the load application (i.e., no yielding).

Data from the vertical LVDT were used to calculate pipe ovality, which is defined as the ratio of vertical deflection in the pipe cross section to the pipe diameter. As presented in figure 63, the maximum deflection was approximately 0.041 inch at a surface load of 26,631 lb. This translates to an ovality of 0.34 percent. Given the fact that some of the material properties associated with the flexible pipe (modulus of steel pipe, bedding factors, etc.) were assumed, the backcalculated σ_v of 1.3 psi at the crown of the pipe to cause such ovality is reasonably close to the measured stress of 3.7 psi.

© 2018 UNR.

Figure 62. Photo. Four LVDTs installed inside the buried steel pipe at the centerline of the pipe and 12 inches off the center of the pipe.
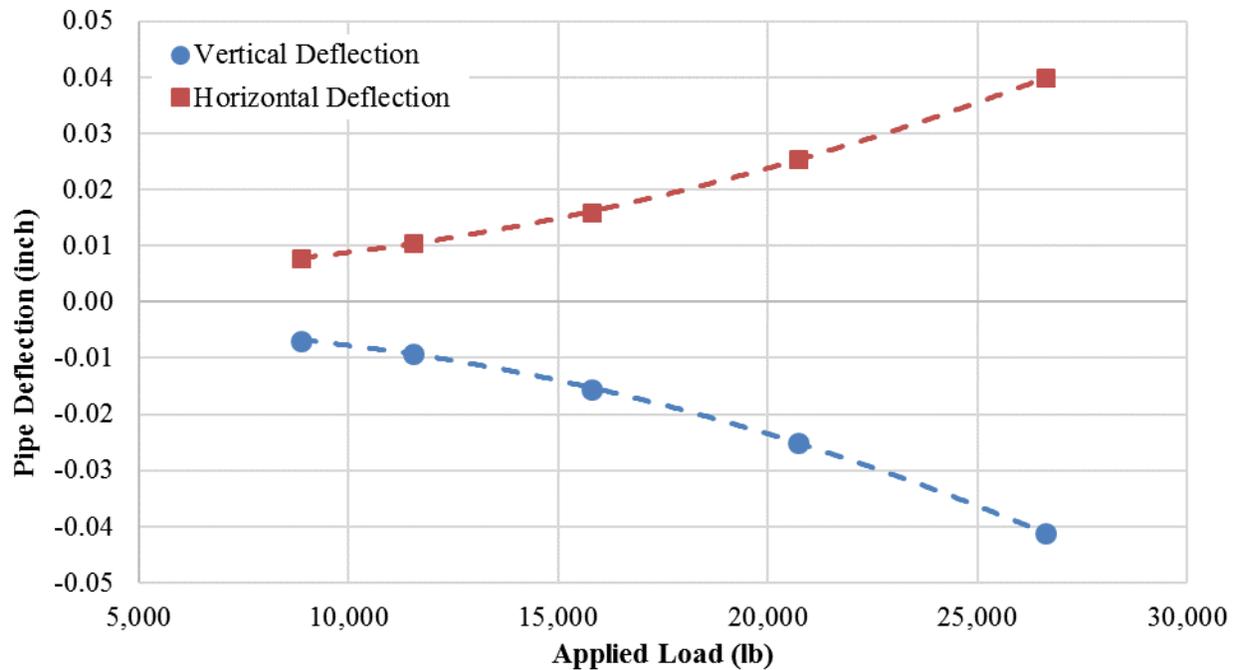
© 2018 UNR.

Figure 63. Graph. Vertical and horizontal deformations in pipe cross section.

To investigate the internal integrity of the buried concrete culvert in experiment No. 5, structural analysis was conducted with knowledge of the characteristics of the concrete culvert. The adjusted computed σ_v on top of the concrete culvert using 3D-Move ENHANCED was used.[11] Analyses of flexural strength, τ_{max}, and axial thrust for the members (i.e., top slab, bottom slab, and sidewalls) at different load levels revealed that the concrete culvert is structurally adequate at all FWD-load levels in terms of τ_{max} and axial thrust. However, at the highest FWD surface loading (i.e., 27,000 lb), the maximum induced moment (M_u) in the members is higher than their flexural capacity (i.e., factored flexural resistance ($\phi_f M_n$)), indicating a possibility of failure. Such an observation is consistent with the nonlinear behavior of rigid culvert response where the measured σ_v on top of the culvert at the highest FWD-load level of 27,000 lb indicated a visible skew in trend (figure 59). It should be noted that the concrete culvert was purposely designed in a way to experience distress at the high load levels of surface FWD loading.

CHAPTER 4. SHL CASE STUDIES

To demonstrate the developed methodology to evaluate SHL movements on flexible pavement, two SHL-vehicle configurations permitted by the Louisiana Department of Transportation and Development (LaDOTD) were investigated. The pavement structure at the APT facility in LanammeUCR was assumed for the two vehicles' route. For this flexible pavement structure, supplementary laboratory test results as well as FWD measurements were available. In this chapter, the analyses steps and a summary of the analysis results associated with the procedures developed are provided.

4.1. SHL ANALYSIS VEHICLES CONFIGURATIONS

The axle and tire configurations for the two SHL-vehicle cases under consideration (LA-12T-16, figure 2, and LA-8T-14, figure 1) are summarized in table 10. The LA-12T-16 SHL vehicle consisted of four identical dollies, and the spacing between the dollies was approximately 38 ft. The LA-8T-14 SHL vehicle consisted of 28 similar axles that were uniformly distributed at a spacing of 4 ft and 7 inches along the entire length of the SHL vehicle. A vehicle traveling speed of 10 mph was assumed for both cases.

Table 10. Summary of SHL-vehicle characteristics from Louisiana sample permits.

Load Case No.	GVW (lb)	Number of Axles	Number of Tires per Axle	Axle Width (Inches)	Center-to-Center Distance Between Adjacent Axles (Inches)	Tire Load (lb)
LA-12T-16	1,754,220	24	12	$209^{13}/_{16}$	$57^{1}/_{16}$	6,164
LA-8T-14	3,660,552	28	8	$209^{13}/_{16}$	$57^{1}/_{16}$	16,342

4.2. PAVEMENT STRUCTURE AND MATERIAL PROPERTIES

The thickness of the LanammeUCR pavement layers that were used in this exercise is shown in table 11. The viscoelastic properties of the AC layer, characterized using $E*$ laboratory data as a function of temperature and frequency, are presented in table 12 and table 13. It should be noted that $E*$ tests were conducted on the field-mixed laboratory-compacted specimens that are assumed to be representative of the AC-layer properties at the time of SHL movements. Knowing that the viscosity grading of the asphalt binder in the AC mixture was AC-30, the viscostiy–temperature susceptibility parameters (i.e., A and VTS) equal to 10.6316 and −3.548 were assumed, respectively.

Table 11. Flexible pavement structure: Layer thicknesses.

Layer	Thickness (Inch)
AC	5
Unbound CAB	9.5
Unbound subbase	12
SG	72

Table 12. *E* values for the AC layer in psi.

Temperature (°F)	0.1 Hz	0.5 Hz	1 Hz	5 Hz	10 Hz	25 Hz
40	1,176,000	1,514,000	1,670,000	2,027,000	2,186,000	2,398,000
70	312,800	510,800	614,300	910,000	1,057,000	1,263,000
100	57,600	117,800	15,4100	290,600	365,200	487,000
130	11,600	20,700	27,800	63,900	90,400	140,000

Table 13. Phase angle values for the AC layer in degrees.

Temperature (°F)	0.1 Hz	0.5 Hz	1 Hz	5 Hz	10 Hz	25 Hz
40	16.75	13.51	12.36	10.15	9.40	8.53
70	30.76	27.04	25.63	21.37	19.75	17.76
100	33.75	34.45	34.93	32.39	31.43	29.73
130	25.07	29.11	31.63	33.30	34.47	36.14

The backcalculated moduli of unbound materials using the available FWD measurements collected immediately after construction were utilized in this exercise. Figure 64 depicts the deflection measurements (i.e., deflection basins) at three target FWD-load levels of 9,000, 12,000, and 16,000 lb. It should be noted that, during the assessment of the methodology developed, FWD measurements at higher load levels were needed for given pavement structures to generate state of stresses comparable to those induced under an SHL vehicle.
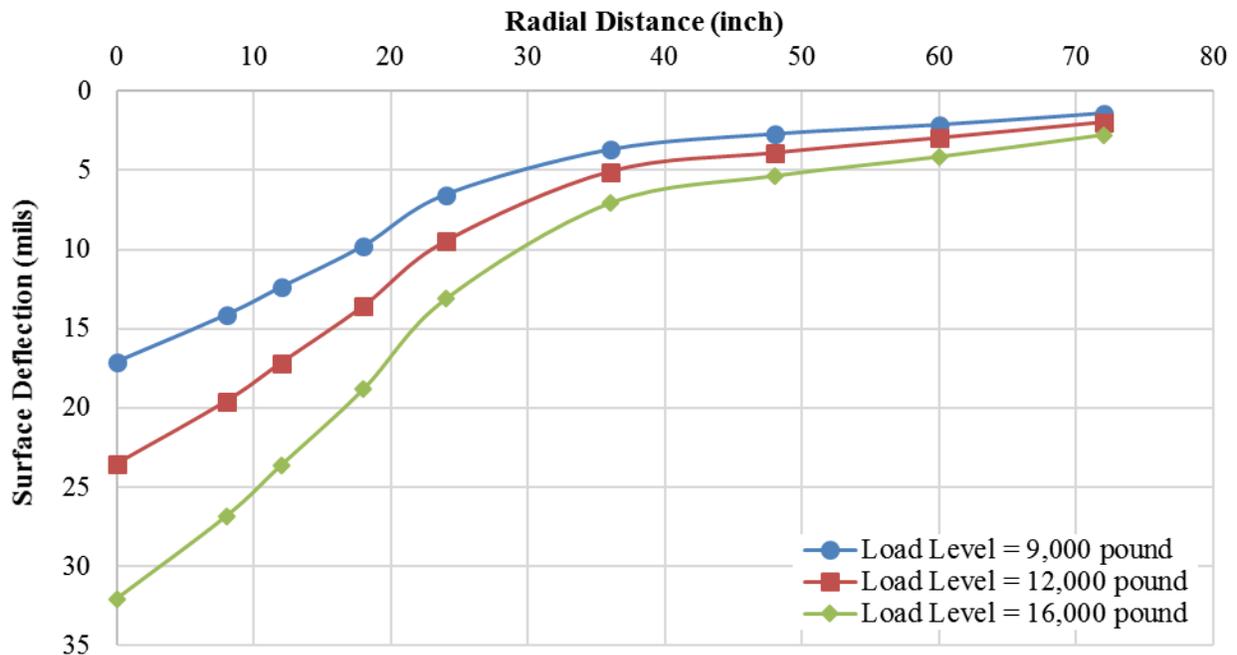
Figure 64. Graph. Vertical and horizontal deformations in pipe cross section.

To undertake the backcalculation process, BAKFAA open-source software was utilized.[39] Repeated attempts at the backcalculation process with many controls on the variability of the

elastic moduli values revealed that the SG layer should be subdivided into two sublayers using the Depth to an Apparent Rigid Layer Method.[40] Accordingly, the depth to the apparent rigid layer equal to 60 inches was determined. The results of the backcalculation exercise are summarized in table 14. It should be noted that the AC-layer temperature at the time of FWD testing was approximately 75 °F. A similar AC temperature was also assumed to be present at the time of SHL movement (i.e., analysis temperature).

As shown in table 14, the backcalculated moduli values for CAB and subbase do not exhibit significant load-level dependency. Therefore, uniform moduli equal to 21,500 and 13,500 psi were assumed for CAB and subbase, respectively. However, in the case of the SG layer, the backcalculated modulus of the top sublayer was assumed to be load dependent. Accordingly, the M_R relationship as a function of stress states was developed, which is expressed in figure 65, where θ is the bulk stress.

Table 14. Backcalculated moduli at different load levels.

FWD-Load Level (lb)	AC Modulus (psi)	Unbound CAB Modulus (psi)	Unbound Subbase Modulus (psi)	SG, Top Layer Modulus (psi)	Apparent SG Rigid Layer Modulus (psi)
9,001	603,734	21,397	14,547	11,677	30,000
11,733	588,853	21,777	12,988	10,211	30,000
15,260	571,604	21,419	12,135	9,315	30,000

$$M_R = 8883\theta^{0.72}\sigma_d^{-0.98}$$

Figure 65. Equation. M_R relationship for the SG layer.

The FWD measurements, in conjunction with the FWD-based procedure, were used to estimate the τ_{max} parameters (ϕ and c) of the SG layer. Consequently, ϕ equal to 10 and c equal to 4.3 psi were estimated. It should be noted that the estimated values are consistent with the laboratory triaxial test results, which were ϕ equal to 7 and c equal to 3.9 psi. It should be mentioned that the highest induced σ_d level in the SG, which was induced by the FWD-load level of 15,260 lb, is approximately 40 percent of the estimated σ_{df}. Even though the induced stress level is higher than the recommended value of 30 percent (see Volume V: Appendix D), for better estimation of the SG's τ_{max} parameters, additional FWD measurements at the higher load levels are recommended.[4]

4.3. AXLE GROUPING AND NUCLEUS OF SHL ANALYSIS VEHICLES

The LA-12T-16 SHL vehicle consisted of four individual dollies with similar axle and tire configurations, and it is modeled as having four individual axle groups. Therefore, there is a single nucleus for each of the four axle groups. As illustrated in figure 66 and figure 67, in both cases, the nucleus consisted of two additional tires in the travel direction (*x*-direction) and three tires in the transverse direction (*y*-direction). Subsequently, using the iterative process and knowing the M_R relationship for the SG layer (figure 65) and the nucleus for each SHL vehicle, representative SG moduli equal to 10,153 and 12,318 psi were determined for LA-12T-16 and LA-8T-14, respectively.
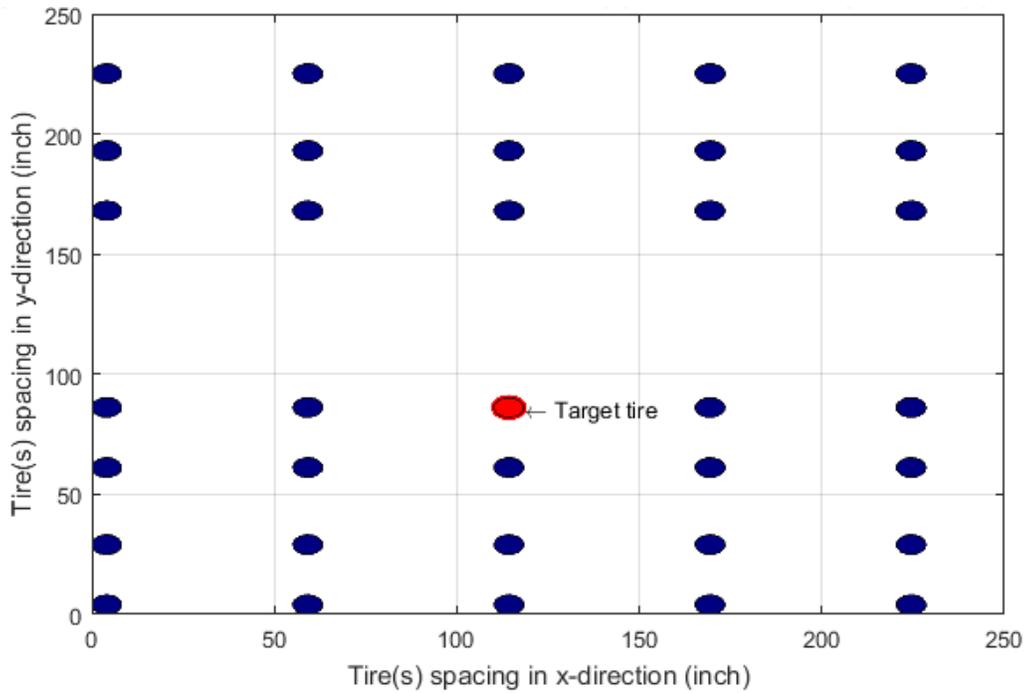
Figure 66. Graph. Representative nucleus for LA-12T-16 SHL vehicle.
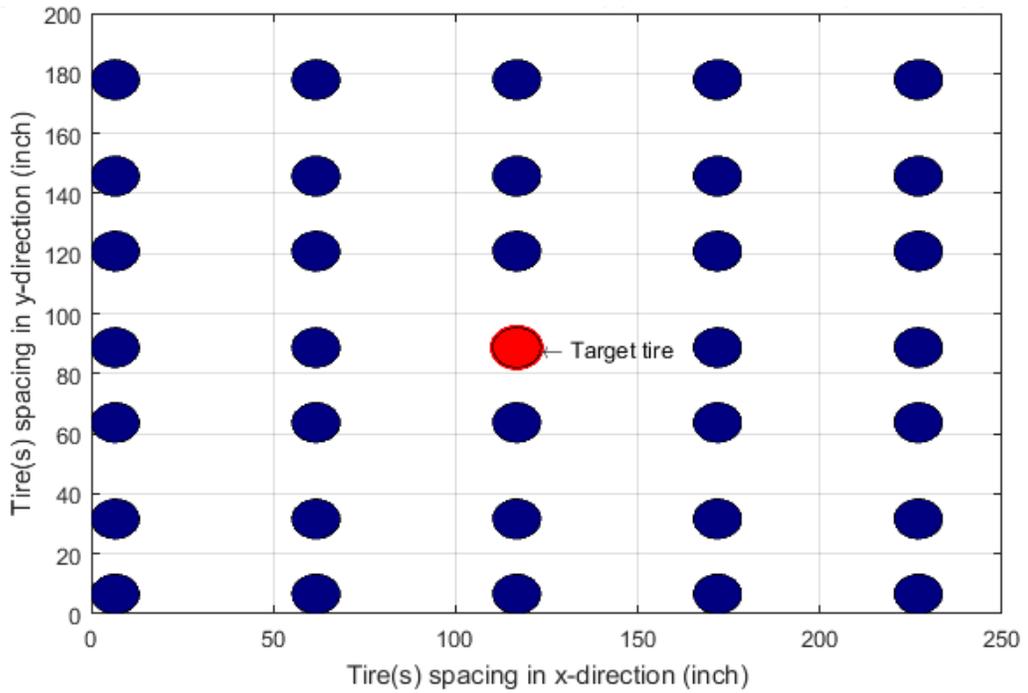
Figure 67. Graph. Representative nucleus for LA-8T-14 SHL vehicle.

64

4.4. ULTIMATE FAILURE ANALYSES UNDER SHL VEHICLES

4.4.1. SG Bearing Failure Analysis

The bearing capacity analysis investigates the likelihood of shear failure in the pavement SG layer. Figure 68 and figure 69 show the σ_v distribution on top of the SG where a maximum σ_v equal to 10.9 and 12.6 psi was computed for LA-12T-16 and LA-8T-14, respectively. The characteristics of σ_v distributions are different because they are affected by vehicle axle and tire configurations as well as tire loads.

Using the stress distribution surface plots, q_{ave} values equal to 10.5 psi and 11.0 psi were computed for LA-12T-16 and LA-8T-14, respectively. Meyerhof's general bearing capacity equation was used to estimate the bearing capacity of the SG soil. For the LA-12T-16 SHL vehicle, the bearing capacity investigation zone was for one of the four axle groups, and the axle groups were identical. The ultimate bearing capacity (q_u) was found to be 64.9 psi. Knowing that the average stress value, q_{ave}, is 10.5 psi, the FOS against bearing capacity failure is 6.2. For the LA-8T-14 SHL case, the bearing capacity investigation zone was the entire SHL vehicle because the whole vehicle represents one axle group. The q_u was found to be 59.2 psi. Knowing that the average stress value, q_{ave}, is 11 psi, the FOS against bearing capacity failure is 5.4.

Figure 68. Graph. Stress distribution on top of SG: LA-12T-16 SHL vehicle.
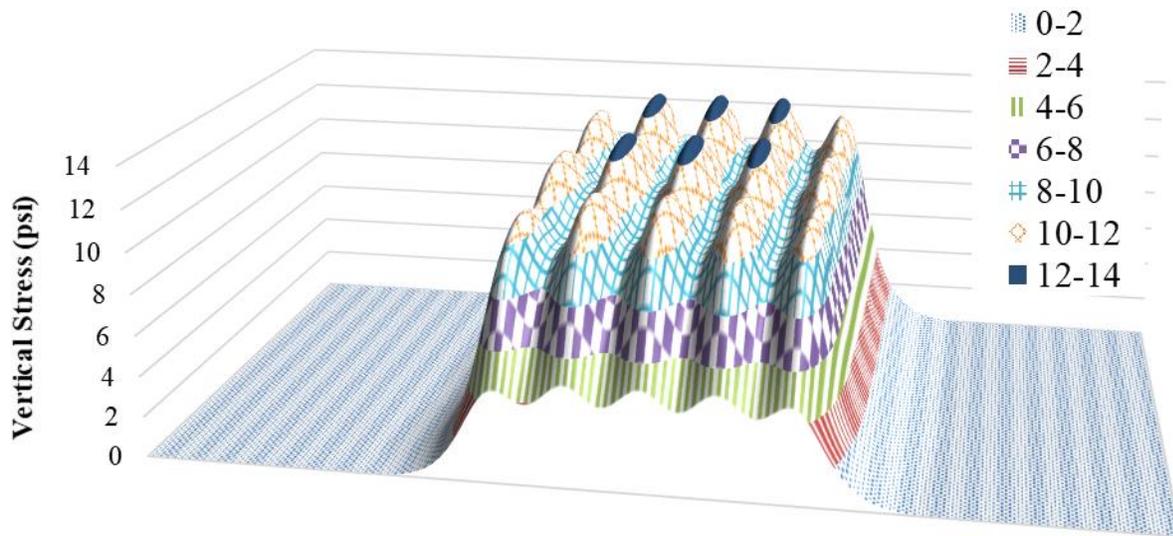
Figure 69. Graph. Stress distribution on top of SG: LA-8T-14 SHL vehicle.

4.4.2. Sloped-Shoulder Failure Analysis Under LA-8T-14

The sloped-shoulder failure analysis using the wedge method was undertaken for the SHL vehicle LA-8T-14, traveling on the selected pavement structure that includes a side slope of 1:1.5 (33.7 degrees with the horizontal). As shown in figure 70, the pavement layers are assumed to extend into the shoulder. In addition, the clearance between the edge of the most outer tire and sloped edge equal to 48 inches was assumed.
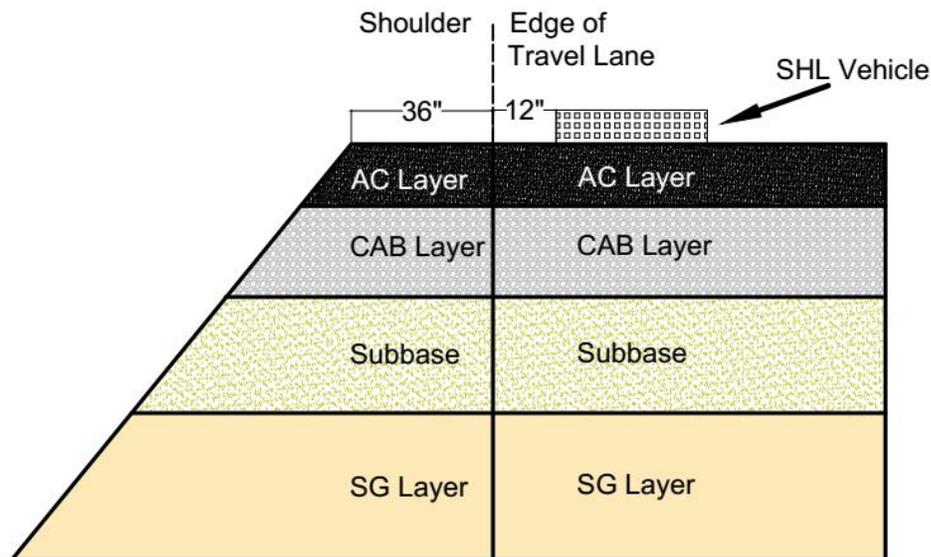
Figure 70. Illustration. Pavement structure with sloped pavement shoulder, side slope of 1:1.5.

The results of the analysis performed revealed that the horizontal deriving forces acting on the vertical plane, which is a summation of *Q* and *P*, are negative. This is attributed to the *c* of the SG when it is considered in the Rankine active pressure. Accordingly, it can be concluded that the disturbing force due to SHL-vehicle load is negligible, and thus, the sloped shoulder is deemed safe when subjected to the SHL-vehicle loading under consideration.

4.5. BURIED UTILITY RISK ANALYSIS UNDER LA-8T-14

Buried utility analysis was conducted for a rigid concrete culvert with the assumption that it is buried in the SG layer (figure 71) when the LA-8T-14 SHL vehicle was considered. To investigate the internal integrity of the buried culvert, structural analysis using the inputs represented in table 15 was conducted. A maximum modified SHL vehicle–induced stress of 18 psi on top of the concrete culvert was determined. This is calculated based on the maximum vertical load-induced stress computed using 3D-Move ENHANCED and the stress adjustment factor for rigid utilities, SAF_{Rigid} of 1.5.[11]
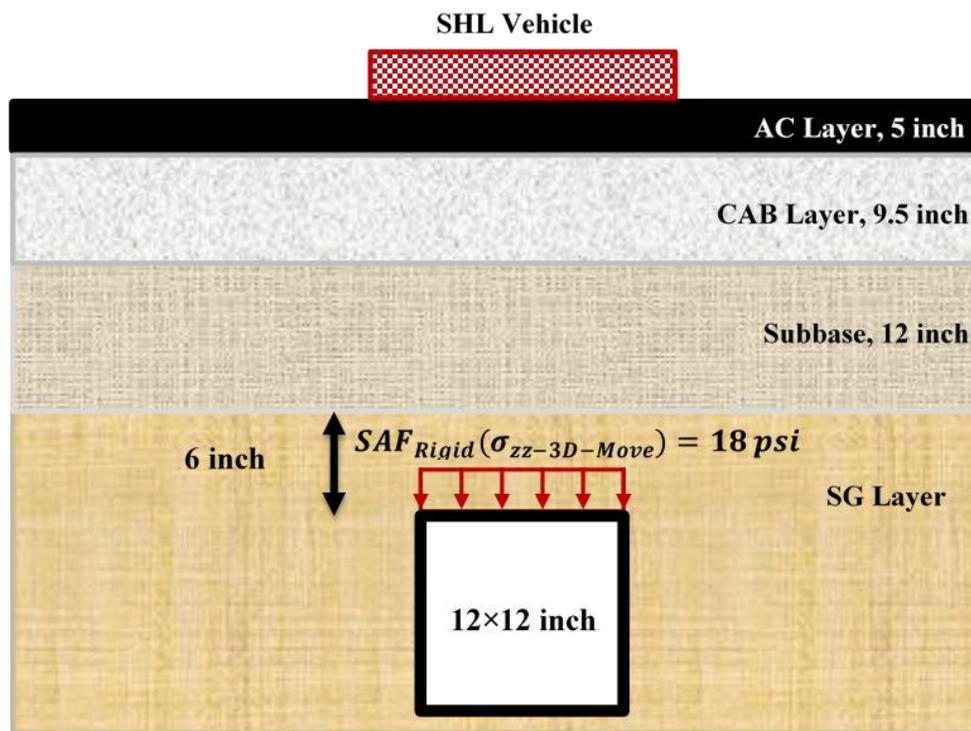
© 2018 UNR.

Figure 71. Illustration. Pavement structure with a buried rigid concrete culvert: LA-8T-14.

Table 15. Inputs for structural adequacy analysis of concrete culvert.

Properties	Value
AC unit weight (pcf)	150
Base unit weight (pcf)	138
Subbase unit weight (pcf)	120
SG unit weight (pcf)	110
SG ϕ (degrees)	10
Top slab and bottom slab width (inches)	12.00
Top slab and bottom slab thickness (inches)	1.00
Sidewall height (inches)	12.00
Sidewall thickness (inches)	1.00
Diameter of longitudinal reinforcement—all members (inches)	0.15
Spacing of longitudinal reinforcement—all members (inches)	4.00
Diameter of shear reinforcement—all members (inches)	0.15
Spacing of shear reinforcement—all members (inches)	4.00
Concrete cover on the reinforcements—all members (inches)	0.10
$f'c$ concrete (psi)	8,000
Yield strength of reinforcements (psi)	80,000

The analyses of flexural strength, τ_{max}, and axial thrust for the culvert's members (i.e., top slab, bottom slab, and sidewalls) are summarized in table 16. It can be seen that, in terms of τ_{max} and axial thrust, the concrete culvert is structurally adequate to withstand the load-induced stresses. However, the M_u in the sidewalls is higher than the corresponding flexural capacity, indicating a possibility of failure. Therefore, mitigation strategies are warranted.

Table 16. Risk analysis against buried utility: SHL vehicle LA-8T-14.

Member	Flexural Strength: $\phi_f M_n$ (lb×Inch)	Flexural Strength: M_u (lb×Inch)	τ_{max}: $\phi_s V_n$ (lb)	τ_{max}: V_u (lb)	Axial Thrust: $\phi_a P_n$ (lb)	Axial Thrust: P_u (lb)
Top slab	3,011	2,706	6,358	1,476	7,535	1,227
Bottom slab	3,011	2,741	6,358	1,496	7,535	1,249
Sidewall	3,011	3,731*	6,358	1,248	7,535	1,496

*Mitigation might be required.
P_u = maximum axial thrust; $\phi_s V_n$ = force factored shear resistance; V_u = maximum induced sheer; $\phi_a P_n$ = factored compressive axial resistance.

4.6. SERVICE LIMIT ANALYSES UNDER SHL VEHICLES

4.6.1. Localized Shear Failure Analysis Under SHL Vehicles

In the localized shear failure investigation, the focus is given to the possibility of failure on top of the SG. Figure 72 and figure 73 display surface plots of FOS against localized shear failure on top of the SG for LA-12T-16 and LA-8T-14, respectively. Correspondingly, minimum FOS values of 2.0 and 1.6 were determined for the analyzed SHL vehicles. This is consistent with the FOS against q_u failure (section 4.4.1).

FOS(minimum) = 2.0
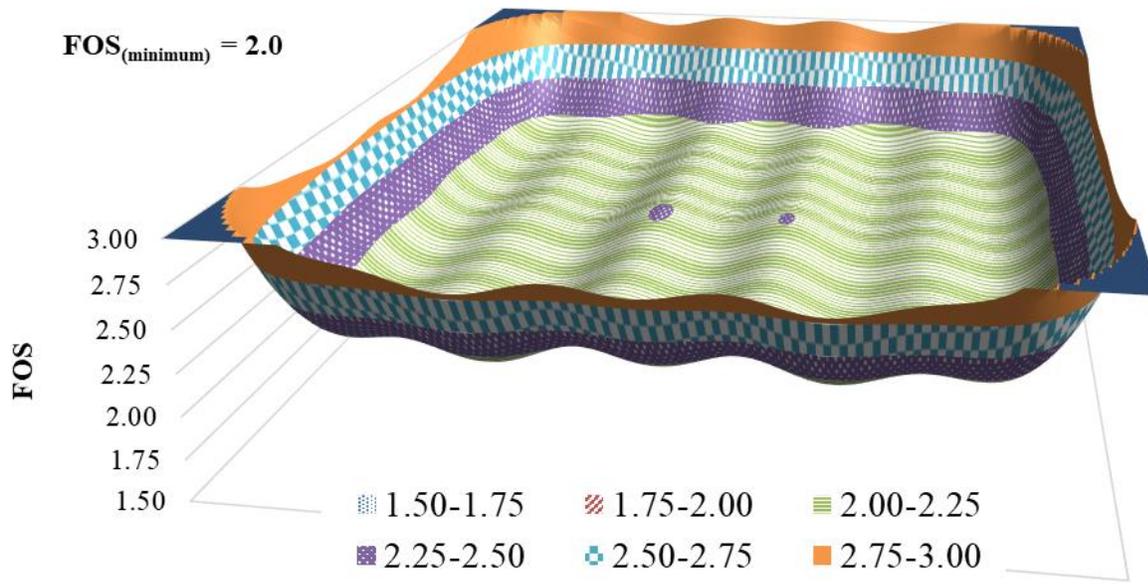
© 2018 UNR.

Figure 72. Graph. FOS against localized shear failure: LA-12T-16 SHL vehicle.

FOS(minimum) = 1.6
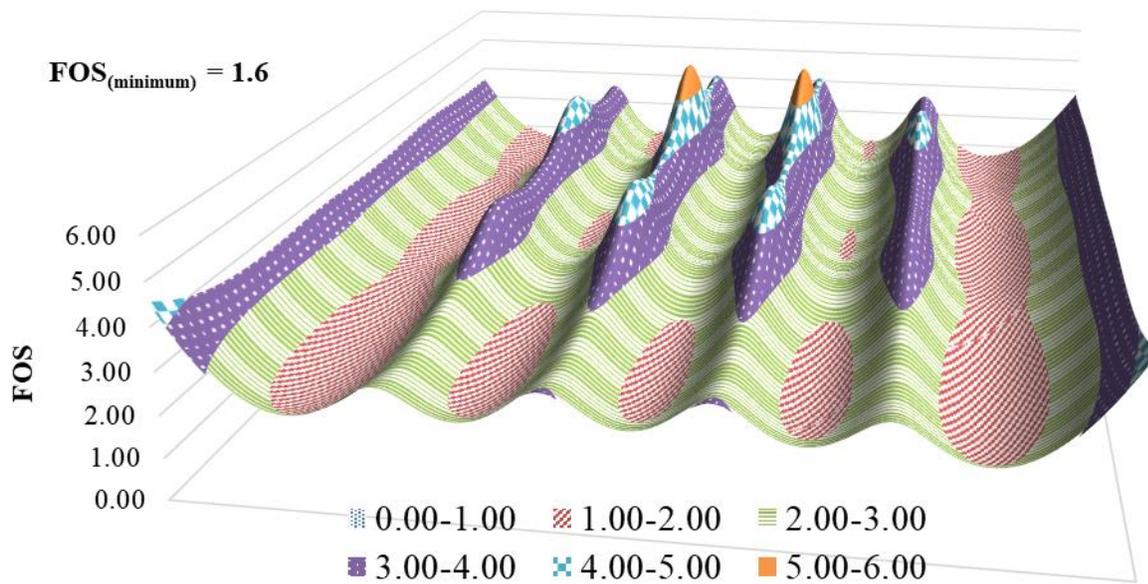
© 2018 UNR.

Figure 73. Graph. FOS against localized shear failure: LA-8T-14 SHL vehicle.

4.6.2. Deflection-Based Service Limit Analysis Under SHL Vehicles

The focus of the deflection-based service limit analysis is to avoid excessive surface deflections under the SHL analysis vehicle movements. This is achieved by checking the SHL vehicle–induced deflections against a certain allowable surface defection. As shown in figure 74 and

figure 75, maximum δ_{SHL} of 69.6 and 86.0 mils were determined under LA-12T-16 and LA-8T-14, respectively.
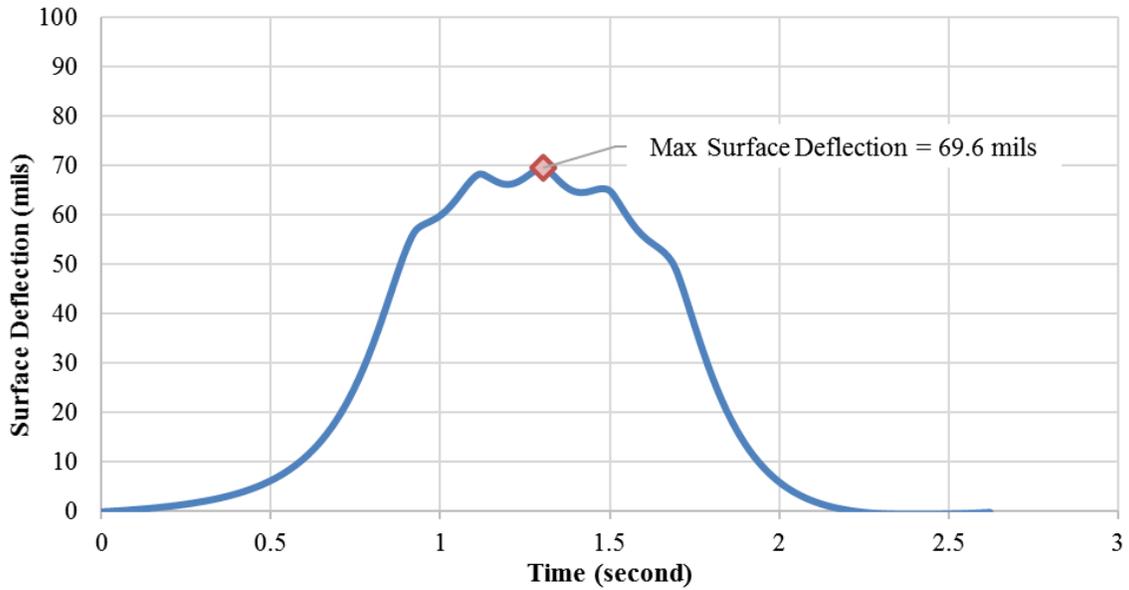
© 2018 UNR.

Figure 74. Graph. Induced surface deflection: LA-12T-16 SHL vehicle.
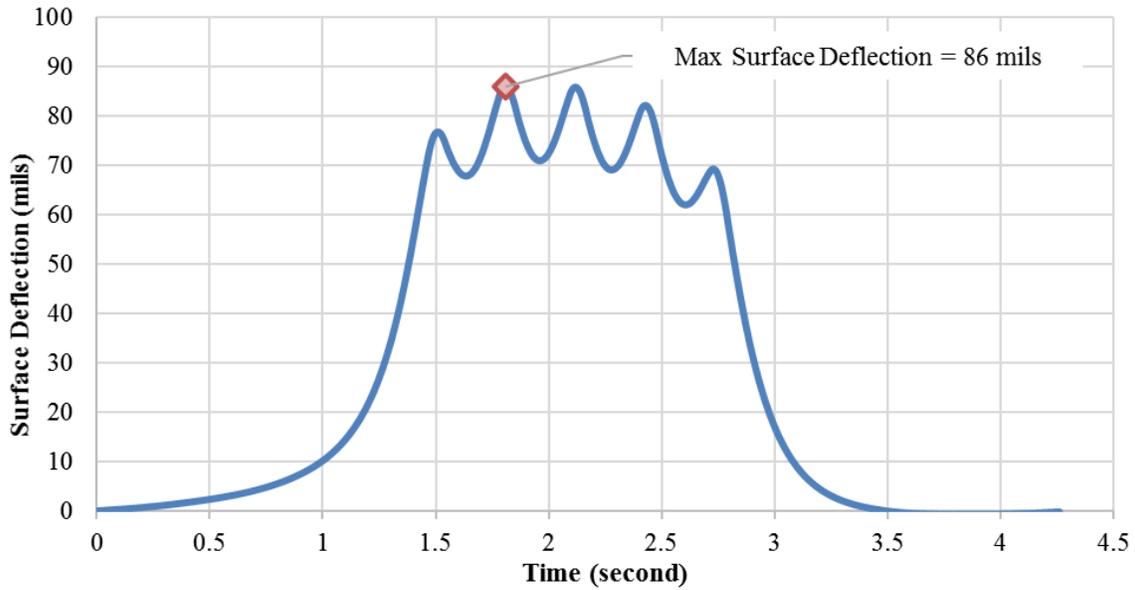
© 2018 UNR.

Figure 75. Graph. Induced surface deflection: LA-8T-14 SHL vehicle.

To determine the equivalent FWD_{equiv} that generates a D_0 equal to δ_{SHL}, the FWD load–deflection curve was developed using 3D-Move ENHANCED (figure 76).[11] It should be noted that the analysis temperature of 75 °F was assumed to be equal to the AC-layer temperature at the time of FWD testing. However, the measured FWD D_0 of 32 mils at the highest load level

70

(approximately 16,000 lb) was lower than the calculated δ_{SHL} values of 69.6 and 86 mils under the SHL vehicles. To extend the FWD deflections beyond the measured values, higher FWD-load levels (beyond 16,000 lb) were considered in the 3D-Move ENHANCED analysis. In these calculations, the backcalculated moduli of the pavement layers were used. In figure 65, the modulus of the top SG layer for each load level under consideration was iteratively estimated knowing the M_R relationship. As shown in figure 76, FWD_{equiv} equal to 31,000 and 37,500 lb for LA-12T-16 and LA-8T-14 were determined, respectively. These FWD-load levels correspond to the determined δ_{SHL} of 69.6 and 86.0 mils that were induced by SHL vehicles.

Similar steps were undertaken to determine the surface deflection under a typical 18-wheel truck with GVW of 80,000 lb, one steering axle weighing 12,000 lb, and two tandem axles each weighing 34,000 lb. Accordingly, a maximum surface deflection equal to 14.3 mils was determined under the tandem axle using 3D-Move ENHANCED.[11] As depicted in figure 76, this surface deflection corresponds to an FWD_{equiv} of 8,000 lb.

Using the FWD load–SSR curve (figure 77), an FWD_{allow} of 26,000 lb corresponding to an SSR of 0.7 was determined. The determined FWD_{equiv} values for both SHL vehicles were above 26,000 lb, indicating potential accumulation of unacceptable levels of permanent surface deformation. These observations reveal that mitigation strategies are warranted for both of the SHL analysis vehicles.
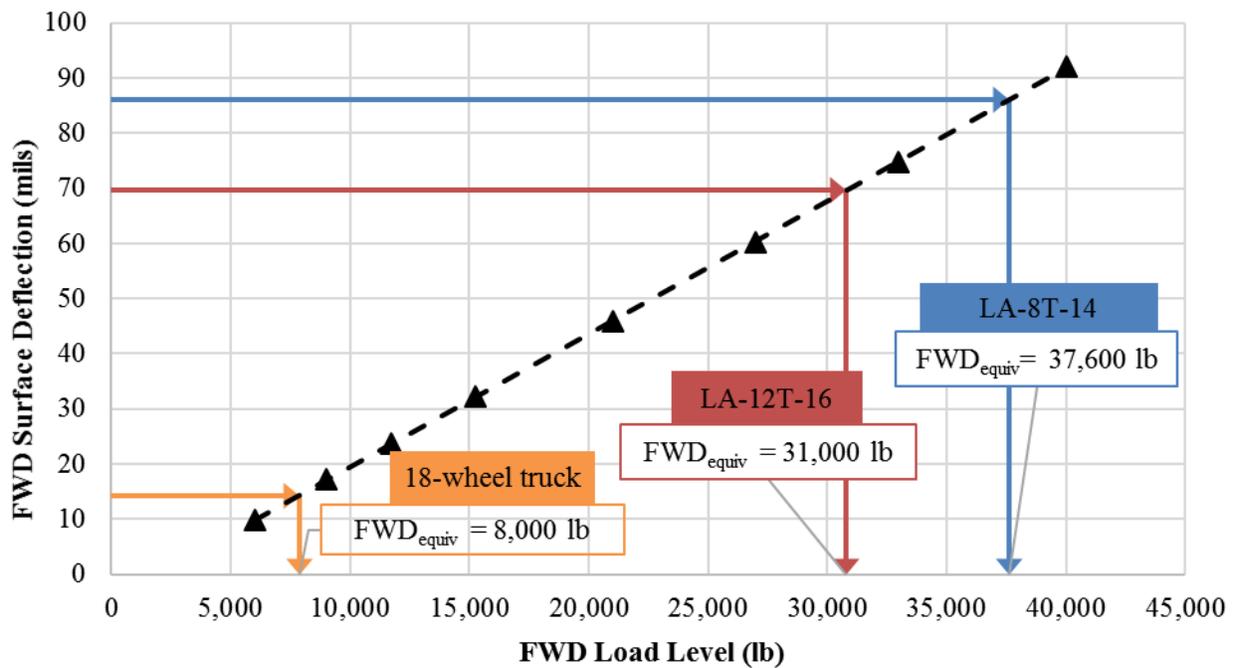
© 2018 UNR.

Figure 76. Graph. Developed FWD load–deflection curve.
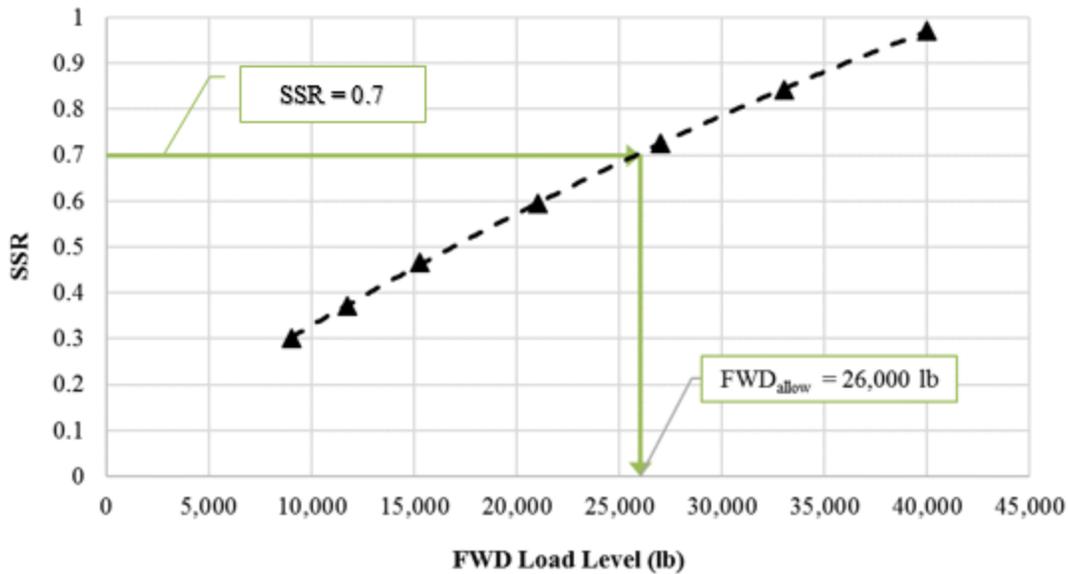
© 2018 UNR.

Figure 77. Graph. Developed FWD load–SSR curve.

4.7. COST ALLOCATION ANALYSIS: LA-12T-16 AND LA-8T-14

To conduct the cost analysis associated with pavement damage for the two analyzed SHL movements, the assumptions presented in table 17 were made. It needs to be noted that the analysis was conducted based on the MEPDG nationally calibrated factors for both AC permanent deformation and AC fatigue cracking. In addition, the 18-wheel truck defined for the deflection-based service limit analysis was used here as the reference vehicle.

Table 17. General analysis input information for cost allocation analysis.

Parameter	Input
AADTT	500
Number of reference vehicle passes prior to analysis vehicle movement	100,000
Pavement repair costs (dollars/lane-mile)	400,000
Discount rate (percent)	2

AADTT = annual average daily truck traffic.

In the case of LA-12T-16, the SHL vehicle consisted of four individual dollies with six axles each at identical spacings and configurations. Knowing that the nucleus of each axle group (every dolly consisted of a single axle group) involves five axles, each dolly is subsequently divided into 1.2 nuclei. Therefore, the LA-12T-16 corresponding to 4.8 repetitions of the nucleus (4 dollies times 1.2 nuclei per dolly) was used in the cost allocation analysis. The LA-8T-14 SHL vehicle with 28 continuous axles was treated as one axle group with a nucleus that includes 5 axles. Therefore, the LA-8T-14 corresponding to 5.6 repetitions of the nucleus (28 axles divided by 5 axles per nucleus) was used in the cost allocation analysis.

Figure 78 and figure 79 present the estimated distress damage curves corresponding to the SHL vehicle LA-12T-16. Figure 80 presents PDAC output results in dollars per lane-mile based on

the remaining service life (RSL) of the analysis pavement section. The PDAC values based on AC permanent deformation were greater than the AC fatigue cracking-based values.
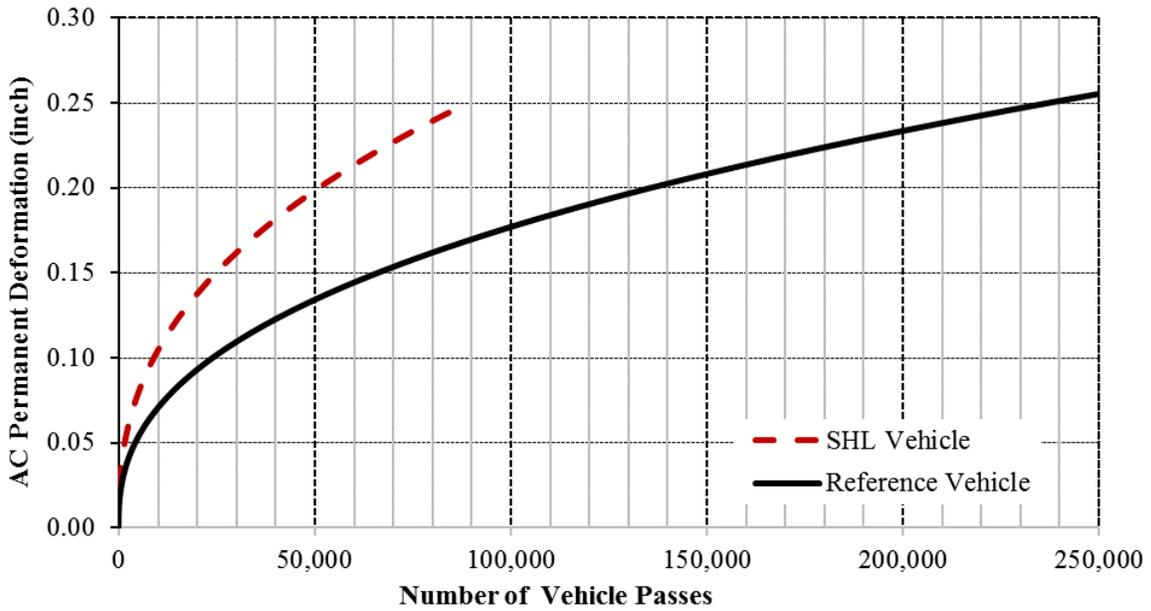
© 2018 UNR.

Figure 78. Graph. Estimated AC permanent deformation: LA-12T-16 SHL vehicle.
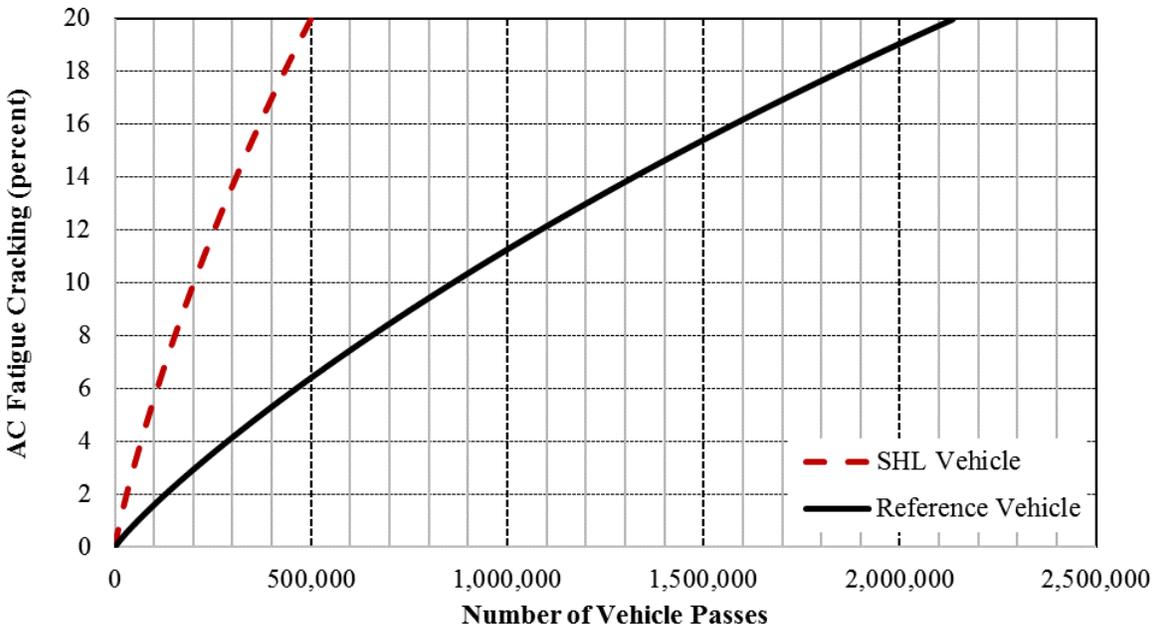
© 2018 UNR.

Figure 79. Graph. Estimated AC fatigue cracking deformation: LA-12T-16 SHL vehicle.

73
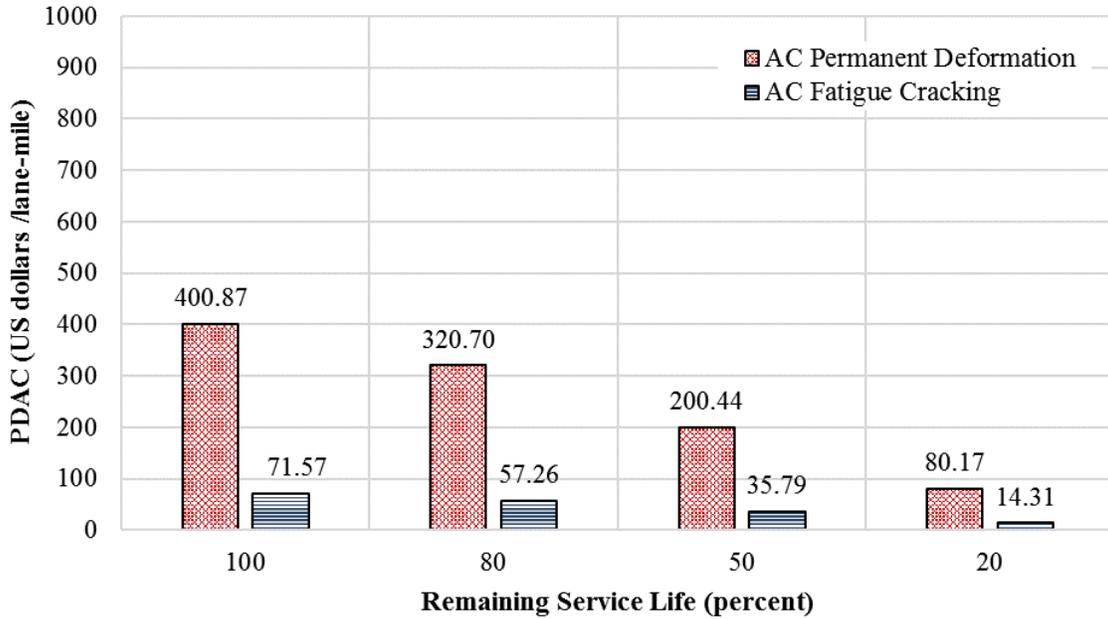
© 2018 UNR.

Figure 80. Bar chart. PDAC for the LA-12T-16 SHL vehicle.

The estimated distress damage curves corresponding to LA-8T-14 are depicted in figure 81 and figure 82. Figure 83 shows PDAC output results in dollars per lane-mile based on the RSL of the analysis pavement section. The PDAC values based on AC permanent deformation were greater than the AC fatigue cracking-based values.
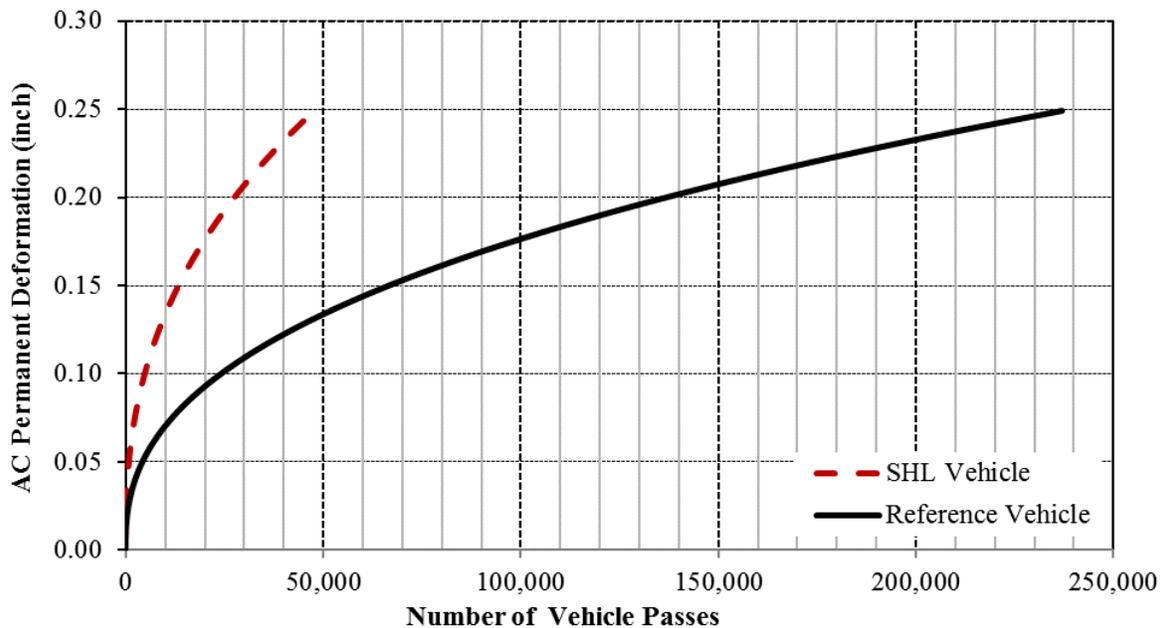
© 2018 UNR.

Figure 81. Graph. Estimated AC permanent deformation: LA-8T-14 SHL vehicle.

74
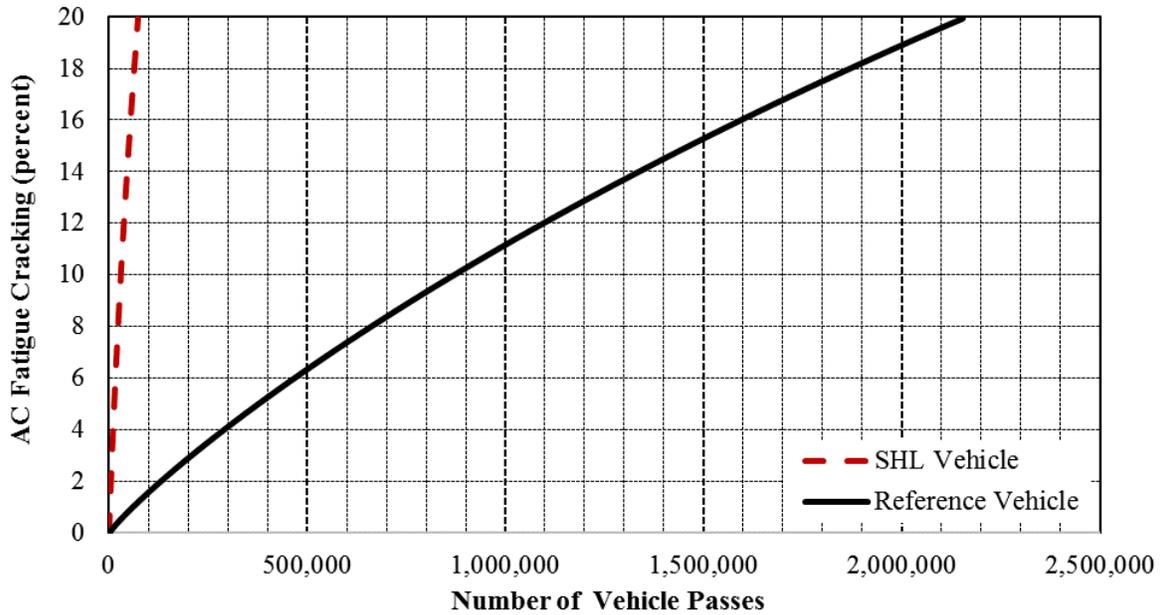
© 2018 UNR.

Figure 82. Graph. Estimated AC fatigue cracking deformation: LA-8T-14 SHL vehicle.
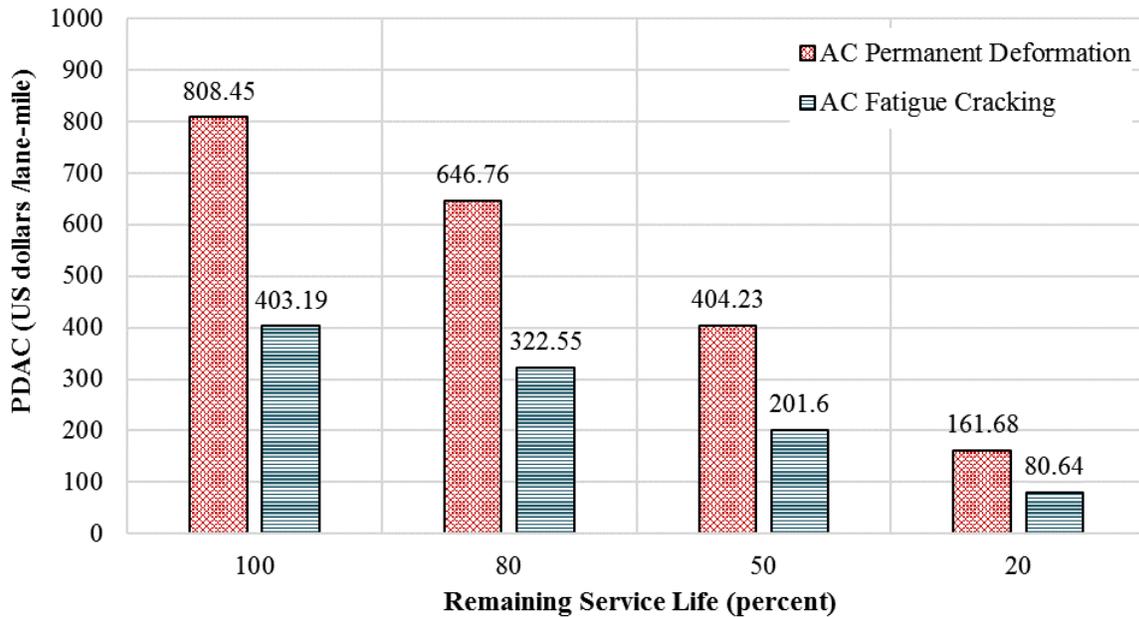
© 2018 UNR.

Figure 83. Bar chart. PDAC for the LA-8T-14 SHL vehicle.

Although the same pavement structure is used in both analyses, the LA-8T-14 resulted in significantly higher PDAC values than those obtained under the LA-12T-16. This is mainly attributed to the difference in the characteristics of the axle and tire configurations and loadings.

75

4.8. SUMMARY

In this chapter, the analysis procedures developed to evaluate SHL movements on flexible pavement were demonstrated. Two SHL-vehicle movements (LA-12T-16 and LA-8T-14) permitted by LaDOTD were considered for the same existing pavement structure along the vehicles route. The LA-12T-16 consisted of four identical dollies with a spacing between the dollies of approximately 38 ft. This LA-12T-16 configuration was considered as four individual axle groups. For this case, the GVW was over 1.7 million lb with a tire load of 6,164 lb. On the other hand, LA-8T-14 consisted of 28 similar axles that are uniformly spaced at 4 ft and $9^1/_{16}$ inches along the entire length of the SHL vehicle. Accordingly, this SHL-vehicle configuration was viewed as one axle group. In this case, the GVW was in excess of 3.6 million lb with a tire load of 16,342 lb. The results associated with the analysis procedures of the developed methodology for both SHL-vehicle movements are summarized in table 18.

As shown in table 18, in both cases, the nucleus consisted of two additional tires in the travel direction and three tires in the transverse direction. The results of the SG bearing failure analysis indicated that the likelihood for ultimate shear failure under the two SHL vehicles is small.

The investigation associated with the sloped-shoulder failure analysis under LA-8T-14 revealed that the pavement shoulder was stable. The risk analysis against buried utility failure for an existing rigid concrete culvert indicated the need for a mitigation strategy (the M_u in the culvert's sidewall was higher than the $\phi_f M_n$).

Regarding service limit analysis, FOS against localized shear failure of 2.0 and 1.6 were determined for LA-12T-16 and LA-8T-14, respectively. These results indicate the pavement structure under consideration is adequate to withstand the SHL-vehicle movements without experiencing localized shear failure, assuming an acceptable FOS of 1.5. However, the results from the deflection-based service limit analysis indicated the possibility of excessive surface deflections leading to potential accumulation of permanent surface deformations. Thus, there is a need for a mitigation strategy for each of the SHL-vehicle movements.

PDAC results in dollars per lane-mile based on RSL for both SHL vehicles were presented. It was noted that, whereas the same pavement structure was used in both analyses, the LA-8T-14 resulted in significantly higher PDAC values, which were mainly attributed to the difference in the characteristics of the axle and tire configurations and loadings. In the case of the LA-12T-16, AC permanent deformation was more critical with a PDAC value of $200.44 per lane-mi at 50 percent RSL. In the case of LA-8T-14, the PDAC based on AC permanent deformation was $404.23 per lane-mi at 50 percent RSL.

Table 18. Summary of case studies: LA-12T-16 SHL vehicle and LA-8T-14 SHL vehicle.

Analysis	LA-12T-16	LA-8T-14
Axle grouping and nucleus of SHL vehicle	• Four axle groups. • Two tires in travel direction (x-direction). • Three tires in transverse direction (y-direction).	• One axle group. • Two tires in travel direction (x-direction). • Three tires in transverse direction (y-direction).
SG bearing failure analysis	• q_{ave} = 10.5 psi. • q_u = 64.9 psi. • FOS = 6.2.	• q_{ave} = 11.0 psi. • q_u = 59.2 psi. • FOS = 5.4.
Sloped-shoulder failure analysis	• Not considered.	• No possible failure.
Buried utility risk analysis	• Not considered.	• Possible flexural failure in the culvert's sidewall. • M_u = 3,731 lb×inch. • $\phi_f M_n$ = 3,011 lb×inch. • Mitigation is required.
Localized shear failure analysis	• FOS = 2.0.	• FOS = 1.6.
Deflection-based service limit analysis	• δ_{SHL} = 69.6 mils. • FWD_{equiv} = 31,000 lb. • FWD_{allow} = 26,000 lb. • Mitigation is required.	• δ_{SHL} = 86.0 mils. • FWD_{equiv} = 37,600 lb. • FWD_{allow} = 26,000 lb. • Mitigation is required.
Cost allocation analysis	• Number of nucleus repetitions = 1.2. • AC permanent deformation-based PDAC is critical. • PDAC at 50 percent RSL = $200.44 per lane-mi.	• Number of nucleus repetition = 4.8. • AC permanent deformation-based PDAC is critical. • PDAC at 50 percent RSL = $404.23 per lane-mi.

CHAPTER 5. IMPLEMENTATION: SUPERPACK

Calculations associated with the analysis procedures developed are complex and sometimes require employing an iterative process. Furthermore, load-induced pavement responses are needed for all the aforementioned analyses. Therefore, as part of this project, a comprehensive user-friendly software package capable of conducting a variety of analyses that include preprocessing and postprocessing to evaluate the impact of SHL movements on flexible pavement was developed. The software is called SuperPACK and comprises three main components: preanalysis, analysis, and analysis engine. These components are briefly described in this chapter; detailed discussions are presented in Volume X: Appendix I.[9]

Figure 84 illustrates the SuperPACK main window.[9] In this figure, the preanalysis and analysis sections are presented. The section allocated to the initial information needed for 3D-Move ENHANCED analysis is also shown.[11] The preanalysis modules use this information as well as certain pavement responses to obtain inputs, which may be needed later for analysis modules.
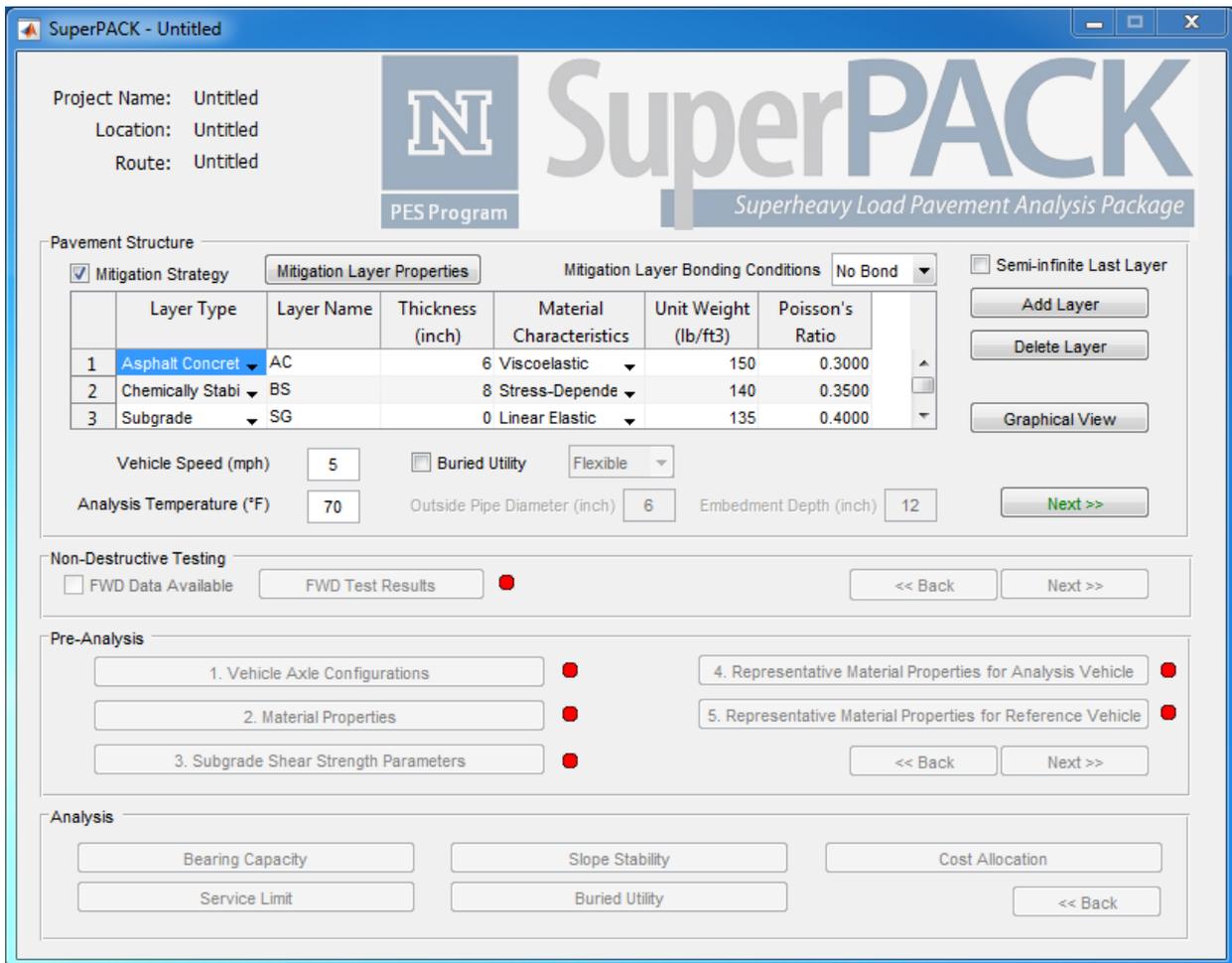
© 2018 UNR.

Figure 84. Screenshot. SuperPACK main window.[9]

As illustrated in figure 84, there are five preanalysis and five analysis modules, all of which are described later in this chapter (see section 5.2 and section 5.3). The preanalysis and analysis modules are accessed from the SuperPACK main window.[9] The preanalysis modules are prerequisite to proceed to the analysis modules. Information needed for calculating pavement responses (e.g., pavement structure, material types) should be entered by the SuperPACK user in the main window. Pavement response(s) needed for a particular preanalysis or analysis module is provided by 3D-Move ENHANCED. Each time a module requires a pavement response for its assigned calculations, it has to make a connection to 3D-Move ENHANCED and request the response type and depth (or point) of interest. In addition to inputs provided by 3D-Move ENHANCED (i.e., pavement responses), each of the preanalysis and analysis modules has an individual graphical user interface (GUI) to input SuperPACK user data for that specific module. Additionally, some modules may need data from other modules. For instance, a specific analysis module may use the information provided by certain preanalysis module(s). Likewise, a preanalysis module may need information provided by the SuperPACK user in the main window. Figure 85 schematically presents different SuperPACK components and their interactions.
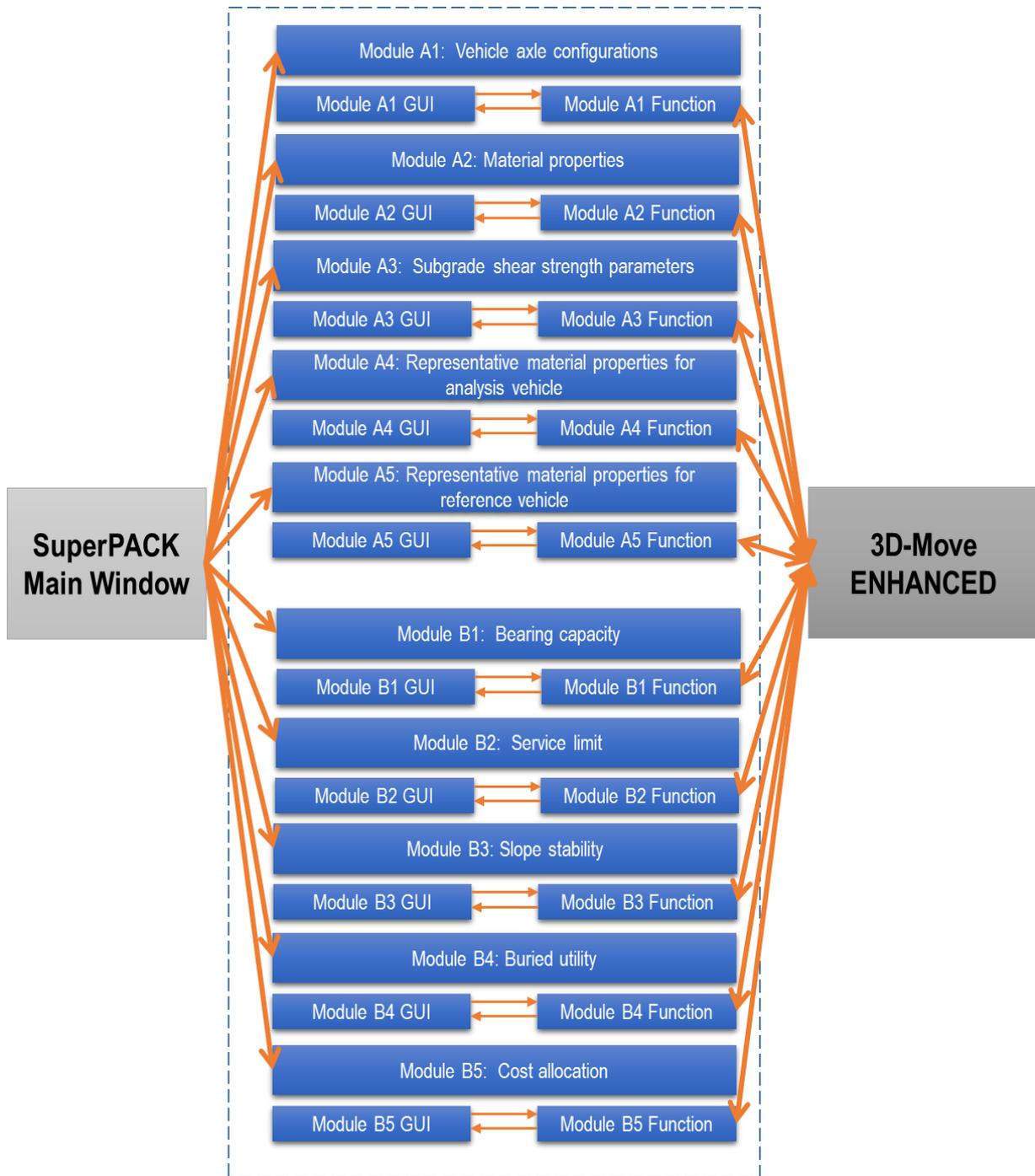
© 2018 UNR.

Figure 85. Illustration. SuperPACK components interaction.[9]

5.1.   ANALYSIS ENGINE: 3D-MOVE ENHANCED

Reliable estimation of pavement responses is important when pavement mechanistic models are to be used. For an SHL-vehicle movement, the pavement performance and serviceability can be a concern when compared to a conventional pavement analysis under a standard (or reference) vehicle.

Early pavement mechanical analysis models were based on Multilayer Linear Elastic Theory (MLET). For instance, VESYS, BISAR, and KENLAYER are among the popular software packages that use such a method.[41–43] One of the advantages of these software packages is that they are computationally efficient because their formulation is based on the presence of axisymmetric surface loads. A notable shortcoming is their inability to model noncircular moving load, nonuniform contact stress distribution (normal and shear), and viscoelastic material characterization. The finite element method (FEM) has been employed to overcome some of the shortcomings associated with MLET. In this regard, ILLIPAVE, MICH-PAVE, etc., are software packages developed based on FEM.[38,44] Although some of the shortcomings of MLET can be resolved using FEM, many specific issues, such as influence of external boundaries, incorporation of damping, and element discretization, remain.

Therefore, 3D-Move ENHANCED was developed as a robust pavement response analysis model for evaluation of a specific SHL-vehicle movement case.[11] 3D-Move ENHANCED, which is part of SuperPACK software, avoids many limitations associated with MLET and FEM.[9] The original formulation of 3D-Move was developed by Siddharthan et al., and a number of enhancements were introduced to the original formulation to make it suitable for use with SuperPACK.[45,9]

The family of 3D-Move models uses the finite layer approach and accounts for viscoelastic material characterization.[12] Furthermore, the models are capable of analyzing a moving load at constant speed with nonuniform and/or noncircular tire loads. Surface shear stresses in both longitudinal (i.e., vehicle moving direction) and transverse directions can be modeled independently with no limitation such as symmetry. This is very important when analysis of interface shear stresses from vehicle breaking is to be investigated.

The pavement layers can be divided into many sublayers as needed and each of the sublayers assigned one set of material properties. For brevity, figure 86 shows only the SG divided into sublayers. If the material properties are the same, there is no need for finer subdivision of layers because the solution technique adopted directly uses the solutions of the differential equations for displacements of the layers for each of the wave components. There are three types of boundary conditions for each of the wave components: surface boundary, interface boundaries, and bottom boundary. At the surface boundary, the conditions are dictated by the stress distributions from vertical normal stress and longitudinal and transverse shear stresses. At the interfaces between layers (or sublayers), the conditions are in terms of all three displacements, stress distributions from vertical normal stress, and longitudinal and transverse shear stresses. At the bottom rigid boundary, there are no displacements. The 3D-Move family of pavement response evaluation programs provides solutions to the differential equations that govern the pavement responses subject to these boundary conditions. More details on the solution technique are presented in Siddharthan et al.[45]
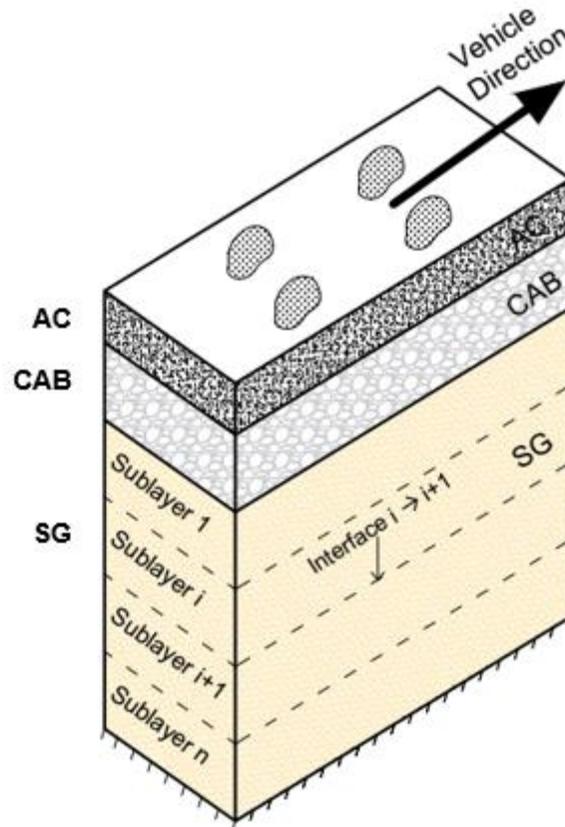
Figure 86. Illustration. Loading, boundary, and interface conditions.

3D-Move ENHANCED is capable of providing a 3D surface plot for a specific pavement response at any given depth where the response distribution is needed.[11] Layer interface conditions such as debonding or slippage can be modeled using 3D-Move ENHANCED. Runtime improvement is also an added important feature. These unique features make 3D-Move ENHANCED a robust pavement response analysis model that is ideally appropriate for incorporation with SuperPACK. Detailed presentation of 3D-Move ENHANCED formulation is provided in Volume X: Appendix I.[9] A number of enhancements were incorporated into this formulation, and they are summarized in this section.

5.2. SURFACE PLOTS

In the original 3D-Move formulation, load-induced pavement responses were calculated at a specific point within the pavement structure by summing the responses from all the decomposed waves.[45] However, in the 3D-Move ENHANCED formulation, inverse Fourier transformation was employed to obtain surface plots for pavement responses at a specific depth.[11] In this method, the corresponding response for each wave is first calculated in the frequency domain. Then, the response is transformed into the spatial domain using inverse Fourier algorithm. These methods can be applied for all 15 responses (i.e., 3 displacements, 6 stresses, and 6 strains). The surface plot of responses at selected depths can be generated for a particular time of analysis. As an example, the top and perspective views for a sample superheavy quad axle are presented in

figure 87 and figure 88. The vertical surface displacement under this SHL-vehicle quad axle traveling at a low constant speed is presented in figure 89 as a 3D surface plot.
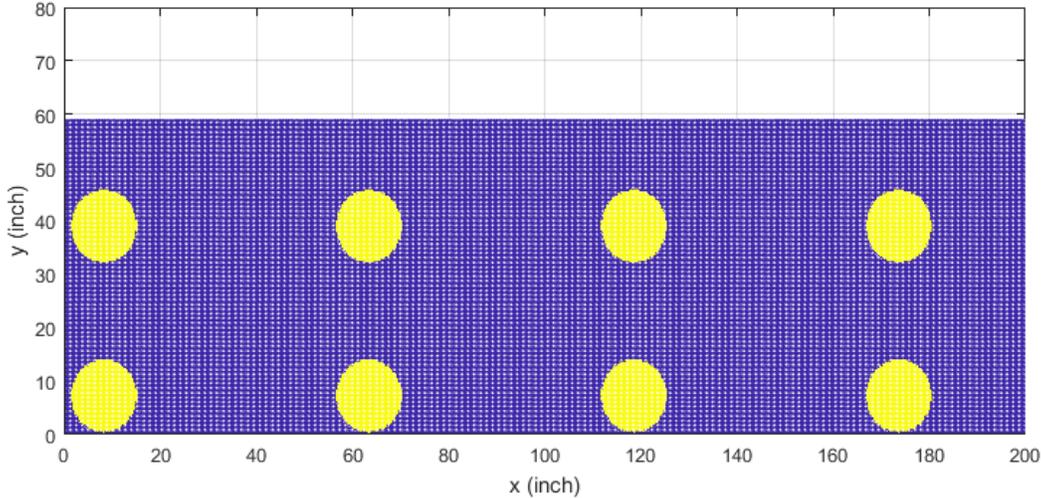
Figure 87. Graph. A sample quad SHL-vehicle quad axle (top view).
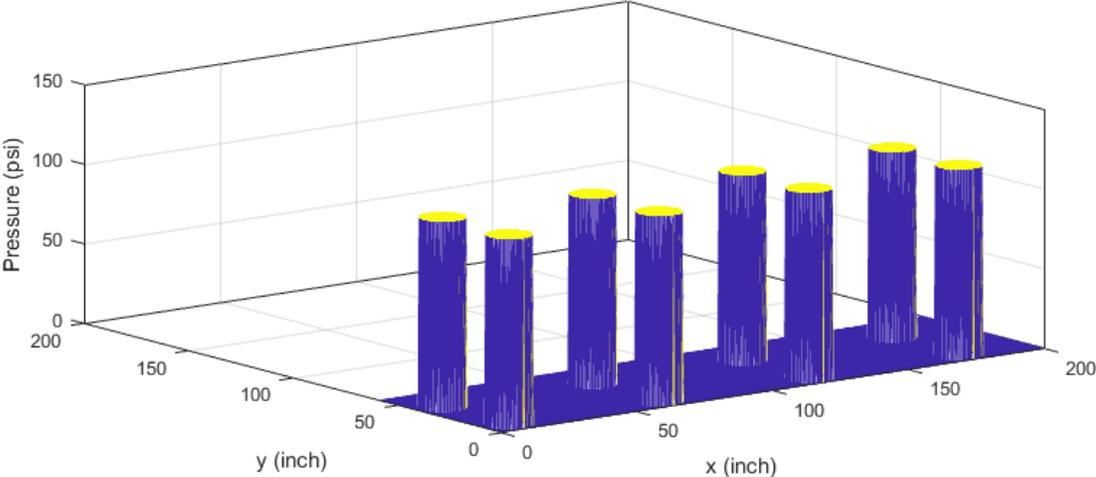
Figure 88. Graph. Sample quad SHL-vehicle quad axle (perspective view).
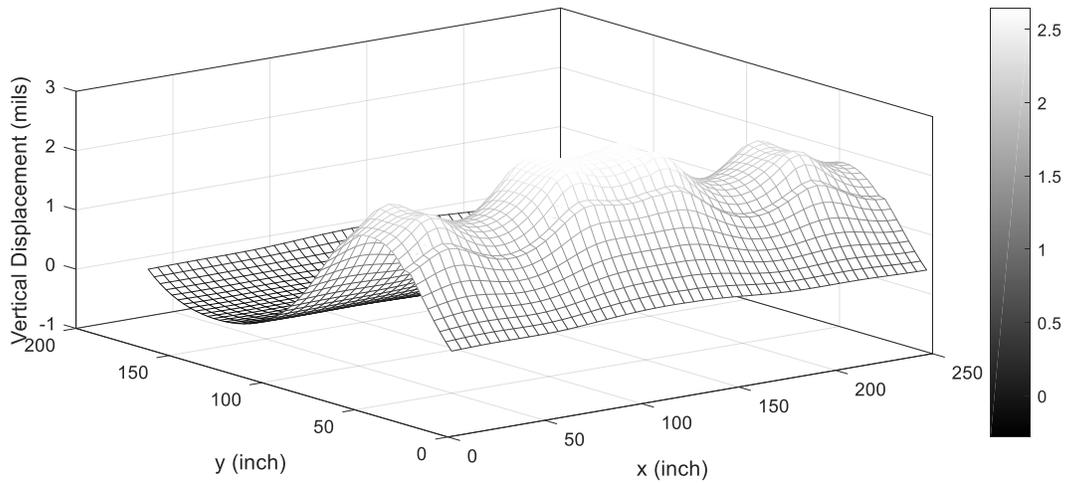
© 2018 UNR.

Figure 89. Graph. Surface plot for vertical displacement at pavement surface under a sample SHL-vehicle quad axle.

5.3. INTERFACE BOND CONDITIONS

Interface debonding is a significant issue in pavement remediation (i.e., mitigation), which involves layer-to-layer interaction at the interface. This issue can be critical for pavements subjected to large loading, such as SHL vehicles and aircrafts. Sometimes mitigation strategies such as steel plates are used to decrease the detrimental effects of an SHL-vehicle movement. In this case, the steel plates and existing pavement surface layer do not represent fully bonded conditions. Therefore, proper modeling of the layer bond condition is essential for flexible pavements experiencing SHL movement. Layer interface debonding was incorporated into SuperPACK through 3D-Move ENHANCED.[9,11]

The analytical approach adopted in 3D-Move ENHANCED, particularly the formulation of interface boundary conditions, allows for effective incorporation of various interface bond condition models.[11] There have been several methods suggested in the literature to model slippage or debonding at layer interfaces. However, a modified version of the slippage model developed by Maina et al. was used to model interface bond conditions.[46] The modified equations for interface layer boundary conditions are presented in figure 90 and figure 91 for *x*- and *y*-directions, respectively.

$$u_1^-(H_i) - \tilde{u}_1^+(0) = \frac{\tau_{xz}^i(H_i)}{K_{xx}}$$

Figure 90. Equation. Modified layer interface boundary conditions to include interface bond conditions in *x*-direction.

$$u_2^-(H_i) - \tilde{u}_2^+(0) = \frac{\tau_{yz}^i(H_i)}{K_{yy}}$$

Figure 91. Equation. Modified layer interface boundary conditions to include interface bond conditions in *y*-direction.

85

In these equations, the formulation is provided for the interface of layers i and $(i + 1)$, where i refers to the layer number. The layer closest to the pavement surface is numbered as 1, and the layer number increases with increasing depth. Also, K_{xx} and K_{yy} are shear slippage stiffness in the x- and y-directions, respectively; $u_1^-(H_i$ and $u_2^-(H_i)$ are displacements in the x- and y-directions, respectively, at the bottom of layer i; $\tilde{u}_1^+(0)$ and $\tilde{u}_2^+(0$ are displacements in the x- and y-directions, respectively, on top of layer $(i + 1)$; and $\tau_{xz}^i(H_i)$ and $\tau_{yz}^i(H_i)$ are longitudinal and lateral shear stresses, respectively, at the interface of layers i and $(i + 1)$.

5.4.   RUNTIME IMPROVEMENT

From a computer programming perspective, the formulation of 3D-Move ENHANCED is complex to be implemented as a single computer module.[11] For instance, the formulation contains two-dimensional (2D) forward and inverse Fourier transform as well as substantial matrix calculations. Thus, a number of different computer programming languages were scrutinized to evaluate whether they supported such features, as well as other requirements such as stand-alone execution, GUI, and capability to support convenient connection between SuperPACK components, in particular the connection between 3D-Move ENHANCED and preanalysis/analysis components.[9,11] MATLAB was selected because it supports 2D Fourier transformation and handles large matrix manipulations efficiently. Moreover, MATLAB facilitates the development of GUI programs, which can be implemented as individual functions. These features are ideally suited in the development of SuperPACK because they help reliably link different SuperPACK components together and with the SuperPACK main window. In addition to these MATLAB features, MATLAB code can be compiled and published as a stand-alone software package. This latter feature enabled SuperPACK as stand-alone software so that it can be made available to all interested users to download and run on their personal computers. A MATLAB complier runtime is needed to run SuperPACK, which is freely available online to download.

Most of the processing time for different SuperPACK modules is consumed in computing pavement responses.[9] In this respect, employing inverse Fourier transform was found to help with a significant decrease in runtime compared to the original approach for computing response points using summation of all responses from all waves. Furthermore, not only is the new approach substantially quicker than the original approach, it also generates surface plots for different response types.

Another mechanism used to improve runtime was parallel processing. In fact, formulation of 3D-Move ENHANCED allows for using parallel processing because the waves are processed independently.[11] Therefore, values for response(s) of interest could be determined by assigning waves to different processing units. Finally, responses in frequency domain are collected from all the processing units and assembled. Pavement responses are transformed into the space domain using inverse Fourier transform. The speed-up factor was close to 3 for a quad processor (75 percent increase in speed-up factor), showing that the parallel process can efficiently improve 3D-Move ENHACNED runtime.

5.5.   PREANALYSIS MODULES (A MODULES)

The preanalysis modules (A modules) include the following items:

- Vehicle axle configurations (module A1).
- Material properties (module A2).
- SG τ_{max} parameters (module A3).
- Representative material properties for analysis vehicle (module A4).
- Representative material properties for reference vehicle (module A5).

To illustrate how preanalysis modules work, the inputs and outputs associated with the modules are presented in table 19 through table 23 for modules A1 to A5, respectively. All five preanalysis modules (A modules) should be processed by the user to proceed to analysis modules (B modules).

5.6.   ANALYSIS MODULES (B MODULES)

The analysis modules (B modules) include the following items:

- Bearing capacity (module B1).
- Service limit (module B2).
- Slope stability (module B3).
- Buried utility (module B4).
- Cost allocation (module B5).

The analysis modules (B modules) can be accessed through the SuperPACK main window (figure 84).[9] Analysis modules will be enabled after all the preanalysis modules (A modules) are completed by the SuperPACK user. To illustrate how an analysis module works, table 24 through table 28 present the inputs and outputs of analysis modules for Module B1 through Module B5, respectively.

Table 19. Inputs and outputs for preanalysis module A1: Vehicle axle configurations.

Inputs	Outputs
1. Pavement structure. 2. Total number of axles. 3. Axle loads. 4. Spacing between the axles. 5. Number of tires for each axle. 6. Spacing between the tires for each axle.	1. Axle groups.

Table 20. Inputs and outputs for preanalysis module A2: Material properties.

Inputs	Outputs
1. Pavement structure.	1. Field damage E^* master curve for existing AC-layer mixture.
2. FWD plate's diameter.	
3. Applied FWD-load levels.	2. M_r relationship for the base.
4. Backcalculated layers' moduli at different load levels.	3. M_r relationship for the SG.
5. Layers' unit weight.	
6. V_a content of existing AC-layer mixture.	
7. V_{beff} of existing AC-layer mixture.	
8. Cumulative percent retained on the ¾ sieve of existing AC-layer mixture.	
9. Cumulative percent retained on the ⅜ sieve of existing AC-layer mixture.	
10. Cumulative percent retained on the No. 4 sieve of existing AC-layer mixture.	
11. Percent passing the No. 200 sieve of existing AC-layer mixture.	
12. Binder shear modulus at multiple temperatures.	
13. Binder phase angle at multiple temperatures.	
14. Temperature in Rankine at which the viscosity was estimated.	

V_a = air void; V_{beff} = effective binder content.

Table 21. Inputs and outputs for preanalysis module A3: Subgrade τ_{max} parameters.

Inputs	Outputs
1. Pavement structure.	1. Stress dependency using load-response characteristic method.
2. FWD plate's diameter.	
3. Applied FWD-load levels.	2. Stress dependency using deflection ratio method.
4. Radial distances for FWD measurements.	3. Estimation of the SG τ_{max} parameters.
5. Surface deflection at different radial distances.	
6. Backcalculated layers' moduli at different load levels.	
7. Layers' unit weight.	
8. Representative range for the SG friction angle.	

Table 22. Inputs and outputs for preanalysis module A4: Representative material properties for analysis vehicle.

Inputs	Outputs

1. Pavement structure.
2. FWD plate's diameter.
3. Applied FWD-load levels.
4. Backcalculated layers' moduli at different load levels.
5. Layers' unit weight.
6. Standard truck axle configuration.
    6.1. Axle spacing.
    6.2. Tire spacing.
    6.3. Tire pressure.
    6.4. Tire loading.
7. Standard truck speed.
8. Field damage E^* master curve for existing AC-layer mixture.
9. Analysis temperature.
10. M_r relationship for the base.
11. M_r relationship for the SG.
	1. Representative material properties under standard truck.
	    1.1. M_R of the base layer.
	    1.2. M_R of the SG layer.

Table 23. Inputs and outputs for preanalysis module A5: Representative material properties for reference vehicle.

Inputs	Outputs

Pavement structure.
1. Layers' unit weight.
2. SHL-vehicle axle configuration.
    9.1. Axle spacing.
    9.2. Tire spacing.
    9.3. Tire pressure.
    9.4. Tire loading.
3. SHL truck speed.
4. Field damage E^* master curve of existing AC-layer mixture.
5. Analysis temperature.
6. M_r relationship for the base.
7. M_r relationship for the SG.
8. Material properties under standard truck.
    8.1. M_R of the base layer.
    8.2. M_R of the SG layer.
9. Depth of interest for identifying the nucleus.
	1. Influential number of tires in the x-direction.
	2. Influential number of tires in the y-direction.
	3. Representative nucleus of axle load configuration.
	4. Representative material properties under the SHL-vehicle nucleus.
	    4.1. M_R of the base layer.
	    4.2. M_R of the SG layer.

Table 24. Inputs and outputs for analysis module B1: Bearing capacity.

Inputs	Outputs

1. Pavement structure.
2. Representative nucleus of SHL-vehicle configuration.
   2.1. Axle spacing.
   2.2. Tire spacing.
   2.3. Tire pressure.
   2.4. Tire loading.
3. SHL truck speed.
4. Field damage E^* master curve of existing AC-layer mixture.
5. Analysis temperature.
6. Material properties under SHL truck.
   6.1. M_R of the base layer.
   6.2. M_R of the SG layer.
7. Estimated τ_{max} parameters of the SG.
	1. Maximum average stress on top of the SG using representative nucleus of SHL-vehicle configuration.
	2. q_u of the SG layer.
	3. FOS against general bearing capacity failure of the SG layer and the need for mitigation strategy.

Table 25. Inputs and outputs for analysis module B2: Service limit.

Inputs	Outputs

1. Pavement structure.
2. Representative nucleus of SHL-vehicle configuration.
   2.1. Axle spacing.
   2.2. Tire spacing.
   2.3. Tire pressure.
   2.4. Tire loading.
3. SHL truck speed.
4. Field damage E^* master curve of existing AC-layer mixture.
5. Analysis temperature.
6. Material properties under SHL truck.
   6.1. M_R of the base layer.
   6.2. M_R of the SG layer.
7. Estimated τ_{max} parameters of the SG.
8. Standard truck axle configuration.
   8.1. Axle spacing.
   8.2. Tire spacing.
   8.3. Tire pressure.
   8.4. Tire loading.
9. Standard truck speed.
10. Material properties under standard truck.
   10.1. M_R of the base layer.
   10.2. M_R of the SG layer.
11. FWD plate's diameter.
12. Applied FWD-load levels.
13. Backcalculated moduli at different load levels.
14. Surface deflection at center of loading plate.
15. Layers' unit weight.
	1. Equivalent triaxial state of stresses under nucleus of SHL-vehicle configuration at the top of SG.
	2. FOS against the localized shear failure and the need for mitigation strategy.
	3. Stress level under FWD loading and the nucleus of SHL-vehicle configuration at the top of SG.
	4. FWD_{equiv} corresponding to the SHL using the computed stress level.
	5. Surface deflection under the nucleus of SHL-vehicle configuration.
	6. Comparison of the surface deflection under the nucleus of SHL configuration with FWD measurements.
	7. FWD_{equiv} corresponding to the SHL-vehicle using computed surface displacement.
	8. Need for any mitigation strategy based on the determined FWD_{equiv}.

Table 26. Inputs and outputs for analysis module B3: Service limit.

Inputs	Outputs

1. Pavement structure.
2. Representative nucleus of SHL-vehicle configuration.
   2.1. Axle spacing.
   2.2. Tire spacing.
   2.3. Tire pressure.
   2.4. Tire loading.
3. SHL truck speed.
4. Field damage E^* master curve of existing AC-layer mixture.
5. Analysis temperature.
6. Material properties under SHL truck.
   6.1. M_R of base layer.
   6.2. M_R of SG layer.
7. Estimated τ_{max} parameters of SG.
	1. Investigation of the failure development in the sloped shoulder.
	2. Need for any mitigation strategy based on slope stability analysis.

Table 27. Inputs and outputs for analysis module B4: Buried utility.

Inputs	Outputs

1. Pavement structure.
2. Representative nucleus of SHL-vehicle configuration
   2.1. Axle spacing.
   2.2. Tire spacing.
   2.3. Tire pressure.
   2.4. Tire loading.
3. SHL truck speed.
4. Field damage E^* master curve of existing AC-layer mixture.
5. Analysis temperature.
6. Material properties under SHL truck.
   6.1. M_R of base layer.
   6.2. M_R of SG layer.
	1. FOS against circumferential stress failure.
	2. Check for pipe ovality.
	3. Check for ring buckling stress.
	4. Check for wall crushing stress.
	5. Need for any mitigation strategy based on buried utility analysis.

Table 28. Inputs and outputs for analysis module B5: Cost allocation.

Inputs	Outputs

1. Pavement structure.
2. Standard truck axle configuration.
   2.1. Axle spacing.
   2.2. Tire spacing.
   2.3. Tire pressure.
   2.4. Tire loading.
3. Standard truck speed.
4. Representative nucleus of SHL-vehicle configuration.
   4.1. Axle spacing.
   4.2. Tire spacing.
   4.3. Tire pressure.
   4.4. Tire loading.
5. SHL truck speed.
6. Field damage E^* master curve of existing AC-layer mixture.
7. Analysis temperature.
8. Material properties under standard truck.
   8.1. M_R of base layer.
   8.2. M_R of SG layer.
9. Material properties under SHL truck.
   9.1. M_R of base layer.
   9.2. M_R of SG layer.
10. Allowable AC distress before rehabilitation at desired reliability.
   10.1. Allowable AC permanent deformation.
   10.2. Allowable AC bottom-up fatigue cracking.
11. AADTT for pavement section.
12. Discount rate for present value calculation.
13. Maintenance/rehabilitation activity repair cost.
14. Performance models' local calibration factors.
   14.1. AC permanent deformation: K_1, K_2, K_3, B_{r1}, B_{r2}, B_{r3}.
   14.2. AC bottom-up fatigue cracking: K_1, K_2, K_3, B_{f1}, B_{f2}, B_{f3}.
   14.3. Base permanent deformation: B1.
   14.4. SG permanent deformation: B1.
15. Estimation of the number of standard trucks prior to the pass of the SHL truck pass.
16. Estimation of E^* value at the specific pavement temperature and SHL truck operational speed.
	1. Cost associated with the AC permanent deformation.
	2. Cost associated with the AC bottom-up fatigue cracking.
	3. Cost associated with the base permanent deformation.
	4. Cost associated with the SG permanent deformation.

AADTT = annual average daily truck traffic.

5.7. SUMMARY

In this chapter, the SHL pavement analysis software package (SuperPACK) was illustrated.[9] SuperPACK incorporates the various analysis procedures developed in this study to evaluate the impact of SHL movements on flexible pavements. This analysis package was developed in MATLAB as a stand-alone software with the following three main components: preanalysis modules, analysis modules, and analysis engine. The analysis engine is called 3D-Move ENHANCED, which is based on the formulation of 3D-Move Analysis software. The

enhancements included 3D surface plots for a specific pavement response at a desired depth, layer interface conditions such as debonding or slippage, and runtime improvement.

The SuperPACK main window contains general information about the project as well as basic information needed for 3D-Move ENHANCED analysis (e.g., layer thicknesses, material types).[9,11] The preanalysis and analysis modules could be accessed through the SuperPACK main window. Each of these modules has a function and a GUI specifically developed for that module. The GUI developed for each module inputs specific information needed to execute that module. Additionally, 3D-Move ENHANCED provides the module with necessary pavement responses when requested. Preanalysis modules are prerequisite to proceed to analysis modules.

CHAPTER 6. SUMMARY AND SUGGESTED RESEARCH

6.1. SUMMARY AND VALIDATION OF DEVELOPED APPROACH

The number of SHL-vehicle movements on the Nation's highways has grown significantly during the past decade. Many of these superheavy components are very large in size and weight, often requiring specialized trailers and hauling units. The SHL vehicles are mostly oversized and exceed legal GVW, axle load, and tire load limits, warranting the need for single-trip permits. Accordingly, a full pavement analysis is needed to ensure that the pavement is structurally adequate to sustain the SHL movement. Consequently, the evaluation of SHL movements on flexible pavements should be cognizant of the following important factors:

- Nonconventional SHL-vehicle axle and tire loadings and configurations.

- Slow-moving nature of SHL vehicle in relation to viscoelastic properties of AC layer.

- Role of higher magnitude stress states induced by an SHL-vehicle movement on stress-dependent behavior of unbound materials.

- Likelihood of ultimate and localized shear failure in the influenced zone of the SG layer.

- Likelihood of excessive pavement surface deflections.

- Role of SHL-vehicle movement on the stability of a sloped pavement shoulder.

- Impact of SHL vehicle on the integrity of existing buried utilities.

- PDACs attributable to SHL-vehicle movement.

A comprehensive mechanistic-based analysis methodology seeking to address these factors associated with SHL movement on flexible pavements was developed. In general, the methodology consists of the following four major components:

- Ultimate failure analyses.
- Buried utility risk analysis.
- Service limit analyses.
- Cost allocation analysis.

It should be noted that mitigation strategies to attenuate the SHL vehicle–induced distresses and damage may be needed at any stage of the evaluation process when the analysis results fail to meet the imposed respective requirements.

One of the major tasks in this project was to estimate pavement responses (i.e., stress, strain, and deflections) under SHL-vehicle movements. Focus is to be given to understanding the role of governing factors such as nonstandard vehicle loading (e.g., tire configuration, tire loading, and inflation pressure), lower SHL-vehicle speed compared to normal truck, and pavement-layer material properties that are consistent with SHL vehicle.

To model SHL-vehicle movements on flexible pavements while considering the nonstandard axle and tire configurations, a novel approach to identify element(s) of the SHL-vehicle configuration that can be regarded as representative of the entire SHL vehicle (referred to as nucleus) was presented. The σ_v distribution (or any other pavement response) under the entire SHL-vehicle configuration can be estimated by superimposing the stresses calculated under the nucleus, hence eliminating the need to model the entire SHL vehicle.

A critical input for the analysis of an SHL-vehicle movement when using numerical models is the material properties of the existing pavement layers, including the SG. These properties should appropriately represent the characteristics of the materials that exist at the time of the SHL movement. The role of lower SHL-vehicle speed in the pavement analysis was addressed using the $E*$ master curve for the existing AC layer. An approach to estimate field damaged $E*$ master curve that considers the reduction in the AC-layer stiffness was presented. On the other hand, the stiffness of unbound layers, such as the CAB and SG, is affected by the load-induced stresses. The FWD backcalculated moduli for unbound materials can be viewed as a representative stiffness in the pavement analysis when standard truck traffic is of concern. However, in the case of an SHL vehicle, higher state of stresses, especially from overlapping of closely spaced wheel loads, compared to those observed under a common FWD-load level, are expected. Consequently, the FWD-based backcalculated modulus of an unbound layer may not represent the stiffness of the layer expected under an SHL-vehicle movement. Accordingly, an iterative approach incorporating the nonlinear stress-dependent M_R relationship and the existing state of stresses in the unbound layers was employed in this project.

The ϕ and c of the SG layer contained within the loaded influence zone (i.e., contributing pavement SG layer) are necessary inputs for assessing the risk of instantaneous shear failure under SHL movement of flexible pavements. These SG τ_{max} parameters are also critical inputs for the stability analysis of a sloped pavement shoulder under an SHL movement. In this study, an innovative methodology to estimate in situ τ_{max} parameters of the pavement SG layer based on nondestructive FWD testing undertaken at multiple load levels has been developed. The validity of the developed approach was explored using numerical simulation of FWD measurements and FWD data collected from large-scale experiments on full-scale pavement structures as well as APT facilities. A variety of unpaved and paved pavement structures were utilized in the verification process.

The SHL vehicle can render a critical condition (distress modes) of instantaneous ultimate shear failure, localized shear failure, or excessive surface deflection. To examine the risk of instantaneous shear failure, Meyerhof's general bearing capacity equation was used. The distributed σ_v on the top of the SG induced by an SHL vehicle in comparison with the bearing capacity of the SG layer were used to identify the possibility of ultimate shear failure in the pavement structure. The ultimate failure analysis focused on the SG layer as it is generally the weakest layer in pavement structures. It should be noted that a modified bearing capacity approach was applied in the case of a sloping pavement shoulder.

Once bearing capacity investigation confirms the adequacy of pavement structure to withstand the general shear failure, the possibility for localized shear failure needs to be evaluated. Such analysis is conducted by computing the load-induced stress level on top of the SG layer using

96

Drucker–Prager failure criterion. A stress level closer to τ_{max} indicates likelihood of localized failure (yield criterion) and a need for mitigation strategies.

Although shear analyses (i.e., ultimate and localized) are viewed as a check for failure condition, they do not provide any information regarding surface displacement (i.e., deflection) under SHL movement. In other words, though the shear failure analyses may indicate that the pavement structure is capable of sustaining the SHL movement without experiencing any shear failure, excessive surface deflections resulting from SHL-vehicle loading can give rise to a rapid deterioration of pavement structure and development of premature surface distresses (e.g., permanent deformation). Accordingly, the δ_{SHL} should be limited to an allowable surface deflection. An FWD_{equiv} to generate D_0 equivalent to the surface deflection computed under the SHL vehicle is determined and compared to FWD_{allow} . The concept of SSR is employed to determine FWD_{allow}. An FWD_{equiv} higher than the FWD_{allow} indicates the potential accumulation of unacceptable levels of permanent surface deformation.

SHL vehicles are usually moved under traffic control so that it is often possible to keep the SHL vehicle away from the pavement edge and shoulder. It is recommended that the vehicle stay away from the pavement edge, particularly on routes where there is an unpaved shoulder and/or a deep slope. It is not always possible to keep the SHL vehicle far from the pavement edge (e.g., narrow lanes and/or wide SHL vehicle). Therefore, it is necessary to investigate the stability of a sloped pavement shoulder under the SHL-vehicle movement.

In this study, the wedge method, which is a well-accepted slope stability analysis methodology in geotechnical practice, was modified so that the stability of a sloping layered medium consisting of pavement layers with distinct properties can be evaluated under SHL movements. Resultant horizontal force due to the SHL vehicle is the major component of the horizontal deriving force leading to the instability of failure wedge. The 3D-Move ENHANCED was used to compute these horizontal stresses on the vertical face of the sliding wedge. However, the 3D-Move ENHANCED computed stresses were modified to account for the role of the sloping shoulder near the edge of the pavement since this software assumes that pavement layers extend laterally to infinity. A SAF to adjust the calculated stresses in the presence of the sloped shoulder was identified based on the results obtained from two full-scale experiments with similar pavement structures (with and without sloped pavement shoulder). The validity of the approach was verified using measurements obtained from a full-scale pavement structure with a sloping shoulder.

An approach to analyze the risk against buried structures due to SHL movement on flexible pavements was presented. The approach was based on widely accepted and available buried utility (flexible and rigid) design procedures. For flexible pipes, a hybrid step-by-step evaluation procedure, provided in ALA and CEPA reports, was implemented. The procedure is divided into four general checks: (1) Assess FOS against pipe circumferential stress failure; (2) check ovality of pipe cross section; (3) check ring buckling stress; and (4) check wall crushing stress. In the case of rigid concrete culvert, the stability was investigated by analyzing the flexural strength, τ_{max}, and axial thrust in the culvert members (i.e., top slab, bottom slab, and sidewalls) in accordance with *AASHTO LRFD Bridge Design Specifications*.[31]

Fair assessment of the induced stresses from the SHL vehicle is required to reliably analyze the internal integrity of a buried utility. Though the existing state-of-practice methodologies provide recommendations with respect to the load distribution, they are limited when assessing the risk of buried utilities under an SHL-vehicle movement. Considering only a standard truck (mostly HS20) as a live load and simulating it as a point load or over a rectangular loaded area that is statically applied directly at the surface of unpaved roads (i.e., neglecting the AC and CAB layer) are the significant limitations.

Therefore, the 3D-Move ENHANCED was adopted to realistically simulate pavement structure and SHL vehicle (e.g., viscoelastic properties of the AC layer, moving load). However, the 3D-Move ENHANCED computed stresses were modified to account for the role of buried utilities and the soil–structure interaction. SAFs to adjust the calculated stresses in the presence of buried utility (flexible and rigid) were also identified based on the results obtained from two full-scale experiments with similar pavement structures (with and without buried utilities). The validity of the approach was verified using measurements obtained from a full-scale pavement structure with buried utilities.

After completing and satisfying the ultimate failure analyses, buried utility risk analysis, and service limit failure analyses, the cost allocation attributable to pavement damage under an SHL vehicle is conducted. The approach employs input information that is commonly accessible to highway agencies and implements an ME-based analysis that considers the determination of critical pavement responses associated with different types of pavement distresses. This cost allocation approach estimates pavement damage costs based on vehicle axle loading and configuration and considers the predicted pavement life reduction due to a single pass of the evaluated SHL vehicle. With this method, different pavement distress models, pavement repair options, and any axle configuration can be considered. The NPV of repairing costs and VMT are also needed inputs of the process. The approach considers the current condition of the pavement at the time of the SHL movement. Consequently, lower PDAC will be estimated for an SHL movement occurring on a pavement section with lower remaining life (i.e., a pavement section that has already been subjected to a percentage of its original design traffic). Factors such as pavement temperature, SHL-vehicle operational speed, rehabilitation threshold value, and pavement structure were found to influence PDAC.

A comprehensive user-friendly software package incorporating the 3D-Move ENHANCED analysis engine in conjunction with the implementation of developed analysis procedures was developed to evaluate the impact of SHL movements on flexible pavements. SuperPACK comprises three main components: preanalysis, analysis, and analysis engine.[9] The preanalysis modules include the respective procedures for axle grouping and nucleus of SHL analysis vehicle, material characterization, estimation of SG τ_{max} parameters, and representative material properties for SHL-vehicle analysis. The analysis modules include the assessment of bearing capacity failure, service limit, slope stability, buried utility, and cost allocation under an SHL-vehicle movement. The 3D-Move ENHANCED analysis engine allows for the determination of pavement responses under an SHL-vehicle loading at any depth within the pavement structure within a reasonable amount of run time.

The analysis procedures developed to evaluate SHL movements on flexible pavement were demonstrated using two SHL-vehicle movement cases. These two cases represented actual SHL

vehicles with different characteristics that consisted of fragmented and continuous axle configurations with a GVW of 1.7 and 3.6 million lb. The findings from this exercise revealed that the methodology was able to capture various aspects of the impact of the two SHL movements analyzed. Similar case studies should be conducted to cover a variety of SHL-movement scenarios (vehicles types, pavement structures and materials, existing pavement condition, etc.). The various aspects (in situ material characterization, pavement distresses, cost allocation, etc.) of the developed methodology should be evaluated and verified by highway agencies using past and future permit data. Such efforts will serve as feedback to improve and calibrate the various components of the developed methodology (e.g., estimated pavement damage cost allocation attributable to SHL-vehicle movement).

To familiarize highway agencies' personnel with the methodology developed and the use of SuperPACK, training and workshop activities are needed.[9] This can be achieved by first conducting a webinar on the overall methodology developed, assumptions, limitations, etc., followed by hands-on training on the use of SuperPACK, which includes preanalysis, analysis, and postprocessing of the results.

6.2. SUGGESTED RESEARCH

The comprehensive mechanistic-based analysis methodology developed addressed several factors governing the assessment of the impact of SHL movement on flexible pavements. The methodology was based on well-accepted and available analysis and evaluation procedures. Simplified yet reasonable assumptions such as those related to the type of tire, characterization of the tire–pavement interaction stresses, and pavement material characterization were utilized in the analysis procedures.

The following are suggested future developments and enhancements of the developed methodology:

- Constant tire pressure with a circular tire–pavement contact area was utilized. However, 3D-Move ENHANCED is capable of handling nonuniform contact pressure of any shape (not necessarily circular), including stress distributions from wide-base tires that can be an attractive option for SHL vehicles. Such cases can be readily investigated using the methodology developed.

- The SHL vehicle was assumed moving under constant speed conditions. However, 3D-Move ENHANCED allows for modeling vehicle loading under braking and turning conditions as well as sloping pavement grade (uphill or downhill). Thus, the impact of tire-induced shear stresses exerted on the pavement surface under such circumstances can be addressed and incorporated in the developed methodology.

- The backcalculation analysis to determine the moduli of the existing pavement layers should be undertaken independently from the developed analysis procedures. A potential improvement is the incorporation of the backcalculation process as a part of the developed methodology.

- The estimate of in situ τ_{max} parameters of the pavement SG layer is based on nondestructive FWD testing undertaken at multiple load levels. The range of the FWD-load levels should result in a state of stresses in the pavement structure that are consistent with the anticipated stresses induced by an SHL-vehicle movement. A practical consideration is the development of a procedure to identify the desired FWD-load levels as part of SHL-movement investigation/analysis.

- SAFs were determined for sloped pavement shoulders and buried utilities based on test results from three full-scale pavement experiments. Further investigation by conducting complementary experiments and additional numerical analyses is recommended to extend the findings to other case scenarios. Such investigations should consider, in the case of sloped pavement shoulders, various scenarios of flexible pavement structures and materials, slope angles, distance of the surface load from the edge of the slope, etc. In the case of buried utilities, the investigation should also consider various scenarios of depth of cover, buried utility dimensions and characteristics, interaction between adjacent utilities, etc.

- SuperPACK was established in MATLAB as a stand-alone software program to implement the various aspects of the developed methodology.[9] A Web-based next generation of the software can be developed so that authorities in highway agencies and engineers dealing with SHL movement can readily use SuperPACK online. The new version should incorporate enhancements and improvements, such as the ones previously suggested, to the developed methodology. The analysis associated with the mitigation strategies can also be integrated within the new version of the SuperPACK framework.

- The overall procedures developed in this study for failure investigation under an SHL-vehicle movement are general in nature, and they require the estimation of select critical pavement responses. In cases involving rigid pavements, appropriate techniques to estimate needed responses can be potentially used to investigate applicable failure modes. Such an investigation should account for factors specifically related to rigid pavements (e.g., longitudinal and transverse joints characteristics, curling and warping conditions).

REFERENCES

1. Nimeri, M., Nabizadeh, H., Hajj, E.Y., Siddharthan, R.V., Elfass, S, and Piratheepan, M. (2018). *Analysis Procedures for Evaluating Superheavy Load Movement on Flexible Pavements, Volume II: Appendix A, Experimental Program*, Report No. FHWA-HRT-18-050, Federal Highway Administration, Washington, DC.

2. Nimeri, M., Nabizadeh, H., Hajj, E.Y., Siddharthan, R.V., and Elfass, S. (2018). *Analysis Procedures for Evaluating Superheavy Load Movement on Flexible Pavements, Volume III: Appendix B, Superheavy Load Configurations and Nucleus of Analysis Vehicle*, Report No. FHWA-HRT-18-051, Federal Highway Administration, Washington, DC.

3. Nabizadeh, H., Hajj, E.Y., Siddharthan, R.V., and Elfass, S. (2018). *Analysis Procedures for Evaluating Superheavy Load Movement on Flexible Pavements, Volume IV: Appendix C, Material Characterization for Superheavy Load Movement Analysis*, Report No. FHWA-HRT-18-052, Federal Highway Administration, Washington, DC.

4. Nabizadeh, H., Hajj, E. Y., Siddharthan, R. V., Nimeri, M., Elfass, S., and Piratheepan, M. (2018). *Analysis Procedures for Evaluating Superheavy Load Movement on Flexible Pavements, Volume V: Appendix D, Estimation of Subgrade Shear Strength Parameters Using Falling Weigh Deflectometer*, FHWA-HRT-18-053, Federal Highway Administration, Washington, DC.

5. Nabizadeh, H., Nimeri, M., Hajj, E.Y., Siddharthan, R.V., Elfass, S., and Piratheepan, M. (2018). *Analysis Procedures for Evaluating Superheavy Load Movement on Flexible Pavements, Volume VI: Appendix E, Ultimate and Service Limit Analyses*, Report No. FHWA-HRT-18-054, Federal Highway Administration, Washington, DC.

6. Nabizadeh, H., Siddharthan, R.V., Elfass, S., and Hajj, E.Y. (2018). *Analysis Procedures for Evaluating Superheavy Load Movement on Flexible Pavements, Volume VII: Appendix F, Failure Analysis of Sloped Pavement Shoulders*, Report No. FHWA-HRT-18-055, Federal Highway Administration, Washington, DC.

7. Nabizadeh, H., Elfass, S., Hajj, E.Y., Siddharthan, R.V., Nimeri, M., and Piratheepan, M. (2018). *Analysis Procedures for Evaluating Superheavy Load Movement on Flexible Pavements, Volume VIII: Appendix G, Risk Analysis of Buried Utilities Under Superheavy Load Vehicle Movements*, Report No. FHWA-HRT-18-056, Federal Highway Administration, Washington, DC.

8. Batioja-Alvarez, D.D., Hajj, E.Y., and Siddharthan, R.V. (2018). *Analysis Procedures for Evaluating Superheavy Load Movement on Flexible Pavements, Volume IX: Appendix H, Analysis of Cost Allocation Associated with Pavement Damage Under a Superheavy Load Vehicle Movement*, Report No. FHWA-HRT-18-057, Federal Highway Administration, Washington, DC.

9. Kazemi, S.F., Nabizadeh, H., Nimeri, M., Batioja-Alvarez, D.D., Hajj, E.Y., Siddharthan, R.V., and Hand, A.J.T. (2018). *Analysis Procedures for Evaluating Superheavy Load Movement on Flexible Pavements, Volume X: Appendix I, Analysis Package for Superheavy Load Vehicle Movement on Flexible Pavement (SuperPACK)*, Report No. FHWA-HRT-18-058, Federal Highway Administration, Washington, DC.

10. National Cooperative Highway Research Program. (2008). *State Highway Cost Allocation Studies, NCHRP Synthesis 378*, National Cooperative Highway Research Program, Transportation Research Board, National Research Council, Washington, DC.

11. Seyed-Farzan, K. (2018). "3D-FAST: Three-Dimensional Fourier Analysis of Pavement Structures Under Transient Loading." (dissertation) Department of Civil and Environmental Engineering, University of Nevada, Reno, NV.

12. 3D-Move Analysis software v2.1. (2013). Developed by University of Nevada, Reno, NV. Available online: http://www.arc.unr.edu/Software.html#3DMove, last accessed September 19, 2017.

13. Rada, G.R., Nazarian, S., Visintine, B.A., Siddharthan, R., and Thyagarajan, S. (2016). *Pavement Structural Evaluation at the Network Level*, Report No. FHWA-HRT-15-074, Federal Highway Administration, Washington, DC.

14. National Cooperative Highway Research Program. (2004). *Guide for Mechanistic–Empirical Design of New and Rehabilitated Pavement Structures*, Transportation Research Board, Washington, DC.

15. AASHTO T 319. (2015). *Standard Method of Test for Quantitative Extraction and Recovery of Asphalt Binder From Asphalt Mixtures*, American Association of State Highway and Transportation Officials, Washington, DC.

16. AASHTO T 315-12. (2016). *Standard Method of Test for Determining the Rheological Properties of Asphalt Binder Using a Dynamic Shear Rheometer (DSR)*, American Association of State Highway and Transportation Officials, Washington, DC.

17. AASHTO T 378-17. (2017). *Standard Method of Test for Determining the Dynamic Modulus and Flow Number for Asphalt Mixtures Using the Asphalt Mixture Performance Tester (AMPT)*, American Association of State Highway and Transportation Officials, Washington, DC.

18. AASHTO T 166-16. (2016). *Standard Method of Test for Bulk Specific Gravity (Gmb) of Compacted Hot Mix Asphalt (HMA) Using Saturated Surface-Dry Specimens*, American Association of State Highway and Transportation Officials, Washington, DC.

19. AASHTO T 209-12. (Revised 2016). *Standard Method of Test for Theoretical Maximum Specific Gravity (Gmm) and Density of Hot-Mix Asphalt*, American Association of State Highway and Transportation Officials, Washington, DC.

20. AASHTO T 30-15. (2015). *Standard Method of Test for Mechanical Analysis of Extracted Aggregate*, American Association of State Highway and Transportation Officials, Washington, DC.

21. Groeger, J. L., Rada, G. R., and Lopez, A. (2003). "AASHTO T 307-Background and Discussion," Resilient Modulus Testing for Pavement Components, Report No. ASTM STP 1437, ASTM, West Conshohocken, PA.

22. AASHTO T 307-99. (2017). *Standard Method of Test for Determining the Resilient Modulus of Soils and Aggregate Materials*, American Association of State Highway and Transportation Officials, Washington, DC.

23. Nabizadeh, H., Hajj, E.Y., Siddharthan, R., Elfass, S., and Nimeri, N. (2017). "Application of Falling Weight Deflectometer for the Estimation of In Situ Shear Strength Parameters of Subgrade Layer." *Bearing Capacity of Roads, Railways, and Airfields*, pp. 743–749, Taylor & Francis Group, Milton Park, Didcot, United Kingdom.

24. Nabizadeh, H., Hajj, E.Y., Siddharthan, R., Elfass, S., and Sebaaly, P.E. (2016). "Estimation of In Situ Shear Strength Parameters for Subgrade Layer Using Non-destructive Testing." *The Roles of Accelerated Pavement Testing in Pavement Sustainability*, pp. 525–538, Springer, Cham, Switzerland.

25. Kondner, R.L. (1963). "Hyperbolic Stress-Strain Response: Cohesive Soils." *Journal of the Soil Mechanics and Foundations Division*, *89*(1), pp. 115–144, American Society of Civil Engineers, Reston, VA.

26. Duncan, J.M. and Chang, C.Y. (1970). "Nonlinear Analysis of Stress and Strain in Soils." *Journal of the Soil Mechanics and Foundations Division*, *96*(5), pp. 1,629–1,653, American Society of Civil Engineers, Reston, VA.

27. Das, B.M. and Sobhan, K. (2014). *Principles of Geotechnical Engineering*, Cengage Learning, Stamford, CT.

28. U.S. Army Corps of Engineers. (2003). *Slope Stability*, Department of the Army, Washington, DC.

29. American Lifelines Alliance. (2001). *Guidelines for the Design of Buried Steel Pipe*, American Society of Civil Engineers, Reston, VA.

30. Warman, D.J., Hart, J.D., and Francini, R.B. (2009). *Development of a Pipeline Surface Loading Screening Process and Assessment of Surface Load Dispersing Methods*, Report No. 05-44R1, Canadian Energy Pipeline Association, Worthington, OH.

31. AASHTO. (2012). *AASHTO LRFD Bridge Construction Specifications*, Sixth Edition, American Association of State Highway and Transportation Officials, Washington, DC.

32. Drucker, D.C. and Prager, W. (1952). "Soil Mechanics and Plastic Analysis or Limit Design." *Quarterly of Applied Mathematics*, *10*(2), pp. 157–165, Brown University, Providence, RI.

33. Chow, L.C., Mishra, D., and Tutumluer, E. (2014). "Framework for Development of an Improved Unbound Aggregate Base Rutting Model for Mechanistic–Empirical Pavement Design." *Transportation Research Record*, *2401*, pp. 11–21, Transportation Research Board, Washington, DC.

34. Kazmee, H. and Tutumluer, E. (2015). *Evaluation of Aggregate Subgrade Materials Used as Pavement Subgrade/Granular Subbase*, Report No. FHWA-ICT-15-013, Federal Highway Administration, Washington, DC.

35. Seyhan, U. and Tutumluer, E. (2002). "Anisotropic Modular Ratios as Unbound Aggregate Performance Indicators." *Journal of Materials in Civil Engineering*, *14*(5), pp. 409–416, American Society of Civil Engineers, Reston, VA.

36. Tutumluer, E., Kim, I.T., and Santoni, R.L. (2004). "Modulus Anisotropy and Shear Stability of Geofiber-Stabilized Sands." *Transportation Research Record*, *1874*, pp. 125–135, Transportation Research Board, Washington, DC.

37. Tirado, C., Carrasco, C., Mares, J.M., Gharaibeh, N., Nazarian, S., and Bendana, J. (2010). "Process to Estimate Permit Costs for Movement of Heavy Trucks on Flexible Pavements," *Transportation Research Record*, *2154*, pp. 187–196, Transportation Research Board, Washington, DC.

38. Raad, L. and Figueroa, J.L. (1980). "Load Response of Transportation Support Systems." *Journal of Transportation Engineering*, *106*(1), pp. 111–128, American Society of Civil Engineers, Reston, VA.

39. BAKFAA V2.0. (2012). Backcalculation software, Federal Aviation Administration, Washington, DC.

40. Rohde, G.T. and Scullion, T. (1990). *MODULUS 4.0: Expansion and Validation of the MODULUS Backcalculation System*, Report No. FHWA/TX-91/1123-3, Texas Transportation Institute, College Station, TX.

41. Kenis, W.J. (1978). *Predictive Design Procedures, VESYS User's Manual: An Interim Design Method for Flexible Pavements Using the VESYS Structural Subsystem*, Report No. FHWA-RD-77-154, Pavement System Group, Structures and Applied Mechanics Division, Federal Highway Administration, Washington, DC.

42. DeJong, D.L., Pentz, M.G.F., and Korswagen, A.R. (1973). *Computer Program BISAR*, Koninklijke/Shell-Laboratorium, Amsterdam, Netherlands.

43. Huang, Y.H. (2004). *Pavement Analysis and Design*, Pearson Education, Cranbury, NJ.

44. Harichandran, R.S., Yeh, M.S., and Baladi, G.Y. (1990). "MICH-PAVE: A Nonlinear Finite Element Program for Analysis of Flexible Pavements." *Transportation Research Record*, *1286*, pp. 123–131, Transportation Research Board, Washington, DC.

45. Siddharthan, R.V., Yao, J., and Sebaaly, P.E. (1998). "Pavement Strain From Moving Dynamic 3D Load Distribution." *Journal of Transportation Engineering*, *124*(6), pp. 557–566, American Society of Civil Engineers, Reston, VA.

46. Maina, J.W., De Beer, M., and Matsui, K. (2007). "Effects of Layer Interface Slip on the Response and Performance of Elastic Multi-Layered Flexible Airport Pavement Systems." International Conference on Maintenance and Rehabilitation of Pavements and Technological Control (MAIREPAV5), Fifth Proceedings, pp. 145–150, University of Iowa, Iowa City, IA.